TURBULENT PIPE FLOW WITH ROUGH AND POROUS WALLS

by
R.J. Muñoz Goma and L.W. Gelhar

HYDRODYNAMICS LABORATORY
Report No. 109

Prepared Under
National Science Foundation
Engineering Division
Grant No. GK-114.1

April 1968

MIT

DEPARTMENT
OF
CIVIL
ENGINEERING

SCHOOL OF ENGINEERING
MASSACHUSETTS INSTITUTE OF TECHNOLOGY
Cambridge, Massachusetts 02139

R68-14

HYDRODYNAMICS LABORATORY

Department of Civil Engineering
Massachusetts Institute of Technology

TURBULENT PIPE FLOW WITH ROUGH AND POROUS WALLS

by

Roberto J. Muñoz Goma

and

Lynn W. Gelhar

April, 1968

Report No. 109

Prepared Under

National Science Foundation
Engineering Division
Grant No. GK-114.1

ABSTRACT

The characteristics of turbulence in shear flow near rough and porous walls are investigated theoretically and experimentally. Flows of this nature are present, for instance, in the case of a erodible particulate streambed.

The fluctuating flow generated in the porous wall by the external turbulent flow is analyzed using a macroscopic, linearized equation of motion, with the boundary condition at the surface defined by a pressure distribution of the same form as that observed at smooth walls. Two different specifications for the wall pressure are applied, one as a random function of space and time and the other as a sinusoidal wave. The intensity of the longitudinal velocity fluctuations at the wall surface, normalized with respect to shear velocity, is shown to approach an asymptotic value of 0.38 as the permeability increases, whereas the fraction of the total energy dissipation that occurs within the porous medium has a maximum for a characteristic dimensionless combination of permeability, viscosity and external velocity. The Reynolds stress is identically zero throughout the porous medium.

Experiments were conducted in two pipes, 10" in diameter, one with 1/8" spherical roughness elements and the other with a 1.20" thick porous lining, for Reynolds numbers between 10^5 and 5×10^5. The rough pipe behavior with respect to friction factor and mean velocity distribution is in good agreement with classical experiments for sand roughness. The porous pipe has very high friction factors, between 0.06 and 0.08, which increase with Reynolds number. Both friction factor and the displacement of mean velocity profile with respect to the smooth law indicate an equivalent relative roughness of the order of 0.10. A value of 0.40 for Karman constant κ is consistent with the observations, but deviations from the logarithmic velocity law occur at a distance from the wall less than 10% of the radius. Both the eddy viscosity and the velocity defect distributions show systematic variations in the core region depending on the nature of the wall.

Measurements of turbulence intensity in the longitudinal and radial directions made with hot wire anemometers show a universal distribution, in agreement with smooth wall results, when normalized with respect to shear

velocity. However, the intensities relative to the local velocity increase with the effective roughness of the wall. The ratio between the radial and longitudinal intensities agrees with the smooth wall distribution throughout most of the pipe, except very close to the wall where it remains at a constant level of 0.6 for the rough and porous cases. Energy spectra for both components of turbulence indicate a definite change with distance to the wall. In normalized form, the spectral measurements for both rough and porous walls are in substantial agreement with previous smooth wall measurements.

ACKNOWLEDGEMENTS

The present investigation was sponsored by the National Science Foundation under grant No. GK-114.1, administered by the M.I.T. Division of Sponsored Research under project No. DSR 74528. The computation work was done at the M.I.T. Computation Center.

This report is essentially a reproduction of the thesis submitted by the senior author in May 1968 in partial fulfillment of the requirements for the degree of Doctor of Science. Dr. Lynn W. Gelhar, Assistant Professor of Civil Engineering, served as thesis advisor.

Mr. Muñoz Goma received financial support from the University of Chile, which granted him a leave of absence, and from the Organization of American States during the early portion of his doctoral program.

The colaboration of all the staff of the Hydrodynamics Laboratory is gratefully acknowledged. Mr. Edward McCaffrey, electronic technician, provided special assistance in the operation of the instrumentation. Messrs. Charles D. Howard and David D. Moran, Research Assistants at that time, contributed substantial work in the early phases of the project.

TABLE OF CONTENTS

CHAPTER I

INTRODUCTION

The theory of sediment transportation by streams is one of the most difficult problems encountered by the hydraulic engineer. In spite of its practical importance, very little progress has been made in its theoretical formulation, no doubt because of the complexity of the interaction that takes place at the surface of the bed between a highly turbulent shear flow and an irregular and moving solid matrix made up of the bed grains.

The past attempts to deal with the problem have, of necessity, involved gross over-simplifications, because of the lack of adequate information concerning the structure of the turbulence in the neighborhood of the bed. Reviews of the current theories have been presented by Leliavsky (1959) and by Raudkivi (1967). They show that most formulations ultimately reduce to an evaluation of the drag and/or lift forces in terms of the velocity at some representative level. In the most refined methods, as by Kalinske (1947) or Einstein (1950), statistical features are introduced in the form of a normally distributed velocity fluctuation superposed onto a mean velocity defined by the classical law of the wall. The same concepts have been used by Yalin (1963) to compute the trajectories of the particle and obtain in this way the solid discharge.

Rather than attempting to reformulate the problem along the same lines of thought, the present investigation is oriented towards a basic examination of the characteristics of the turbulence near a sediment bed. This is a long range purpose and only modest goals could be defined for the first stage of the project reported here. Attention is focused on the effects induced by the porosity of the bed on the turbulent shear flow characteristics. The reasons to select this aspect of the problem are simple. As an impervious boundary is approached, the intensity of the turbulent fluctuations must vanish. However, if the boundary is porous, these fluctuations may remain significant at elevations well below the top layer of particles. Another way in which the porosity of the head may affect the particles motion, as pointed out by Raudkivi, is through local pressure

gradients developing in connection with the turbulent flow in or near the porous medium.

Turbulent flow along porous walls with suction or injection has been extensively studied because of its importance in chemical processes. Olson and Eckert (1965) report considerable distortion in the shear and eddy viscosity distributions in a circular tube, even at very moderate rates of injection. No similar study has been made for the case of a porous wall without suction or injection. Murray (1965) has shown that such a boundary may produce significant effects on the flow. He considered the damping of gravity waves moving over a permeable sand bed. In particular, the damping can be greatly augmented if the bed comes close to a state of fluidization, because then the porosity becomes much larger.

In view of the scarcity of information on the subject, the present study is aimed at the theoretical and experimental evaluation of the major characteristics of turbulent flow along porous boundaries. No further reference is made to the theory of sediment transport, the problem being approached as a basic fluid mechanics question whose solution may prove useful for a variety of purposes. In particular, the porous wall is defined as fixed in space, since an erodible-particulate bed would interfere with the necessary turbulence measurements. In principle, any type of wall shear flow could be selected for the present purpose. Pipe flow was chosen for experimental convenience and because of the fairly complete information available in regard to its characteristics for smooth and rough walls.

A brief outline of the contents of this report is as follows. The existing experimental knowledge about pipe flow is analyzed from the phenomenological point of view and some prediction is attempted as to the kind of effects that may be induced by the presence of a porous wall. A mathematical model of the flow in the porous wall is developed, using an extension of Darcy's law with a fluctuating pressure imposed at the bed surface by the external pipe flow. The results of this analysis cannot be extended to the evaluation of the resulting pipe flow, and therefore the latter is treated only in an experimental way. Comparative

experiments were conducted with air flow in two circular pipes of 10" diameter, using spherical roughness elements in one of them and a thick porous lining in the other. The reported measurements include friction factor, distribution of mean velocity and eddy viscosity, Reynolds stress, intensity of turbulence in the axial and radial directions and the corresponding energy spectra, all the turbulence measurements being made with hot wire anemometers.

CHAPTER 2

ANALYSIS OF TURBULENT PIPE FLOW

Despite much work being done in the statistical theory of turbulence, still highly complex situations like wall turbulence must be approached through the semiempirical methods usually designated as phenomenological theories. Essentially, the method is a search for significant gross parameters that exhibit a universal behavior, and as such, it must rely entirely on experimentation. Once a universal parameter is found, some analytical expression can be assumed to represent it, and then, a tool is available to predict the flow pattern under different conditions.

Obviously, the method is not satisfactory; it is, however, the only one available. A major objection comes from the fact that universal behavior cannot be extrapolated beyond the realm of actual observations. Therefore, the theory does not exist for entirely new situations. Within this context, the present investigation can be looked upon as a test of how well the current models for turbulent pipe flow apply under rather radical changes in the flow conditions. The introduction of a highly porous wall is not intended to represent in a precise way an actual model of a sediment bed but rather to give a qualitative description of the main features to be expected in such a case. From another point of view, the physical characteristics of the wall can be considered as the input to a system, whose mode of operation is unknown. However, by observation of the changes in such outputs as mean velocity or turbulence distributions, some insight into the significant mechanisms can be gained.

The purpose of this chapter is to review the current description of turbulent pipe flow; to discuss the conceptual models constructed upon it and the available evidence in support or contradiction of them; and, finally, to discuss the various alternatives for the reformulation of the problem in terms of a porous wall.

2.1 Turbulent Pipe Flow with Smooth and Rough Walls

There are many detailed presentations of turbulent pipe flow, such as Clauser (1956), Hinze (1959) and Rotta (1962). Only the factors essential

to the discussion will be reviewed here.

The mean flow is assumed to be in the x-direction, coincident with the axis of the pipe, and uniform. The local mean velocity is U. Turbulent components are u, v, w in the axial, radial and circumferential directions. The respective intensities of turbulence are $u' = \sqrt{\overline{u^2}}$, $v' = \sqrt{\overline{v^2}}$, $w' = \sqrt{\overline{w^2}}$. The radius of the pipe is R, the distance from the centerline is r and the radial distance to the wall is y. The shear stress is τ, at the wall is τ_o and the shear velocity is $u_* = \sqrt{\tau_o/\rho}$. Properties of the fluid are: ρ, density; μ, dynamic viscosity; $\nu = \frac{\mu}{\rho}$, kinematic viscosity.

With regard to the mean velocity distribution, two distinct regions are recognized. Closest to the wall, where the shear stress is essentially constant and equal to τ_o, the relevant factors for similarity are shear velocity u_* and viscosity ν. Defining as reference velocity u_* and as reference length $\frac{\nu}{u_*}$, the velocity is given by an expression of the form

$$\frac{U}{u_*} = f\left(\frac{u_* y}{\nu}\right) \tag{2-1}$$

In fact, experiments in smooth pipes show that

$$\frac{U}{u_*} = A \log \frac{u_* y}{\nu} + B \tag{2-2}$$

where A and B are, to a first approximation, universal constants. There is some disagreement concerning the values for A and B. Proposals for A range from 5.6 to 5.75 and for B, from 4.9 to 5.85.

When y approaches zero, (2-2) obviously cannot remain valid. Measurements very close to the wall are scarce and inaccurate, but they show significant departures from (2-2) for $\frac{u_* y}{\nu} < 15$. This behavior is explained by assuming the existence of a viscous sublayer, where the shear stress is essentially determined by the viscous force $\mu \frac{dU}{dy}$. Thus,

$$\tau = \tau_o = \rho u_*^2 = \mu \frac{dU}{dy}$$

which leads to

$$\frac{U}{u_*} = \frac{u_* y}{\nu} \quad . \tag{2-3}$$

Observations indicate that some turbulence is present throughout this layer, which is not laminar as (2-3) implies. This corresponds to the fact that mean velocity measurements approach (2-3) asymptotically. In the case of rough walls, the experimental evidence indicates that the same law applies, except for a change in the constant B, which now becomes dependent on the roughness height, k_s,

$$\frac{U}{u_*} = A \log \frac{u_* y}{\nu} + C\left(\frac{u_* k_s}{\nu}\right). \tag{2-4}$$

For very large roughnesses, the fully rough regime is established, and C is found to be related to k_s by

$$C = -A \log \frac{u_* k_s}{\nu} - D_k \tag{2-5}$$

where D_k depends only on the type of roughness. For fully rough flow, introduction of (2-5) into (2-4) leads to

$$\frac{U}{u_*} = A \log \frac{y}{k_s} - D_k. \tag{2-6}$$

Another form of (2-4) is in terms of its deviation from the smooth law, (2-2),

$$\frac{U}{u_*} = A \log \frac{u_* y}{\nu} + B - \frac{\Delta U}{u_*} \quad . \tag{2-7}$$

It is seen that

$$\frac{\Delta U}{u_*} = B - C\left(\frac{u_* k_s}{\nu}\right) \tag{2-8}$$

and for the fully rough case

$$\frac{\Delta U}{u_*} = A \log \frac{u_* k_s}{\nu} + B - D_k. \qquad (2\text{-}9)$$

Experimental evidence of this formulation is presented in the references mentioned above.

A second region is recognized in the central portion, or core, of the pipe. Here the flow is defined mostly in terms of geometric position. Assuming that the maximum velocity U_{max} at the centerline includes the dependence on wall conditions, a velocity-defect law is found to exist:

$$\frac{U - U_{max}}{u_*} = f\left(\frac{y}{R}\right). \qquad (2\text{-}10)$$

Experimental measurements can also be fitted to a logarithmic form of $f\left(\frac{y}{R}\right)$, although not as clearly defined as in the wall region:

$$\frac{U - U_{max}}{u_*} = A \log \frac{y}{R} \qquad (2\text{-}11)$$

where A is the same constant found in the law of the wall. Sometimes, correction factors are introduced in (2-11), giving

$$\frac{U - U_{max}}{u_*} = A \log \frac{y}{R} + B_1 + h\left(\frac{y}{R}\right).$$

Values of these corrections may be found in Hinze (1959).

There are a number of ways to justify the above relations, which up to now have been presented only on an empirical basis. First of all, the logarithmic character of the velocity distribution can be established just from very general functional considerations, assuming that there is an overlapping layer where both (2-1) and (2-10) apply (Millikan, 1938). The argument leads to the expressions (2-2) and (2-11), with the same constant A. More insight into what actually happens can be gained by introducing the concepts of the mixing length ℓ and scalar eddy viscosity ε. These are

defined by

$$-\overline{uv} = \ell^2 \frac{dU}{dy}\left|\frac{dU}{dy}\right| \tag{2-12}$$

$$-\overline{uv} = \varepsilon \frac{dU}{dy} \tag{2-13}$$

where $-\overline{uv}$ is the mean product of the turbulent components u and v. In fact, equilibrium requires:

$$\frac{\tau}{\rho} = \nu \frac{dU}{dy} - \overline{uv} \tag{2-14}$$

but, except very close to the wall, the viscosity term is negligible and $-\overline{uv} = \frac{\tau}{\rho}$. As the shear stress τ in a pipe is given by

$$\tau = \tau_o \left(1 - \frac{y}{R}\right)$$

it follows from (2-12) and (2-13) that

$$\frac{\varepsilon}{u_*} = \ell \sqrt{1 - \frac{y}{R}} \ . \tag{2-15}$$

Therefore, for pipe flow, any formulation in terms of mixing length can be converted by (2-15) into an expression in terms of eddy viscosity and vice versa. The eddy viscosity concept was introduced by Boussinesq in the last century, without leading to much success. In order to produce an explicit expression for ε, Prandtl reformulated the concept as a mixing length, which he assumed through intuitive consideration to be, in the region close to a wall, of the form

$$\ell = \kappa y \tag{2-16}$$

where κ should be a universal constant (afterwards named after von Kármán). By further assuming the shear stress to be constant and equal to the wall shear, Prandtl was able to derive the logarithmic law (2-2), with $A = \frac{1}{\kappa}$.

Prandtl's approach has been repeatedly criticized, mainly on the grounds that the turbulent momentum transfer function $\overline{uv}$ cannot be determined solely by the local conditions, as it is implied in (2-12), but must be a function of the overall flow pattern. Another form of the same argument is to say that, in fact, the computed values of the mixing length are much too large to warrant Prandtl's considerations of infinitesimal disturbances. In order to clarify the point, it is necessary to distinguish between two different interpretations of l. One is a purely mathematical function, defined by equation (2-12), or equivalently by (2-13) in terms of eddy viscosity. Given an experimental distribution of mean velocity $U(y)$, l is completely defined, and therefore, is a valid function to use. As it depends on the derivative of the velocity, it can be a more sensitive characterization of the flow than the velocity profile itself. A quite different concept is the definition of l as a measure of the turbulent mixing process; however, the proposition that such a measure should satisfy (2-12) or (2-13) cannot be supported by purely theoretical considerations. The fact remains, however, that experimental observations have shown that l and ε have a fairly universal behavior, and even if this behavior cannot be explained in terms of proper mechanical laws, at least it can be described by analytic expressions and applied to a variety of situations. Going along with the objection relative to the dependence of $\overline{uv}$ on overall conditions, one might say that, in (2-12), l is a kind of integral factor which takes account of everything else; if there are regions where l is found to be a function of position only, then it must be concluded that the flow in those regions is hardly affected by the rest of the flow, and conversely, a definite variation of l with Reynolds number indicates interaction between regions far apart in the flow.

Keeping the first, merely descriptive, interpretation of the mixing length (which he calls more properly the "characteristic length-scale of turbulence"), Lettau (1961) has shown that every proposed formula for the velocity distribution in pipes can be derived from an explicitly or implicitly assumed analytical expression for l. In particular, the logarithmic law (2-2) results from:

$$\frac{\tau}{\rho} = \frac{\tau_o}{\rho}\left(1 - \frac{y}{R}\right)$$

and

$$\ell = \kappa y \sqrt{1 - \frac{y}{R}} \,. \tag{2-17}$$

Lettau compares a number of alternative expressions for ℓ by deriving the velocity distribution corresponding to each one and normalizing in terms of the average velocity given by the integration of the profile. In this way, the constant κ, whose numerical value is uncertain, does not appear in the final result. Rather than comparing the velocities themselves with experimental observations, he compares the deviations with respect to the logarithmic law, which is a more sensitive procedure, and finds that the best fit is obtained by assuming

$$\ell = \frac{\kappa y}{1 + 2\left(\frac{y}{R}\right)^{3/2}} \tag{2-18}$$

which gives, with $\xi = 1 - \frac{y}{R} = \frac{r}{R}$,

$$\kappa \frac{U_{max} - U}{u_*} = \ln \frac{1 + \sqrt{\xi}}{1 - \sqrt{\xi}} - 2\sqrt{\xi} + \left(\xi - \frac{1}{2}\right)\sqrt{\xi - \xi^2} + \frac{1}{2} \sin^{-1}\sqrt{\xi} \,. \tag{2-19}$$

An essential feature of all the expressions for ℓ compared by Lettau, including his own (2-18), is that

$$\lim_{y \to 0} \frac{d\ell}{dy} = \kappa \tag{2-20}$$

which shows the physical significance of κ, as well as assures that the velocity distribution will approach the logarithmic law (2-2) close to the wall. This is a common feature to all velocity-defect expressions, where the implicit assumption is that the nature of the wall enters the final result only as an additive constant representing the boundary condition for the differential equation at y = 0. In order to extend the analysis

to cover the relationship between the value of this constant and the wall roughness characteristics, many attempts have been made to modify the basic mixing length expression (2-16) in the immediate neighborhood of the wall. Rotta (1962) lists a number of these propositions, mostly intended to predict the existence of a viscous sublayer by requiring that l tends to zero as y approaches δ_v rather than zero, where δ_v is the thickness of the viscous sublayer. Typical of the approach is the expression proposed by Rotta himself (1950), which gives

$$\left.\begin{aligned} l &= 0 \quad \text{for } y < \delta_v \\ l &= \kappa(y - \delta_v) \quad \text{for } y > \delta_v \end{aligned}\right\} \tag{2-21}$$

where $\frac{u_* \delta_v}{\nu} = 6.8$. Furthermore, the complete expression for the shear (2-14) is used, instead of assuming $\tau = -\rho \overline{uv}$. It is beyond the scope of this discussion to examine the detailed format of all these various propositions, especially since they have been constructed in a rather arbitrary way in order to fit empirical data. The agreement is good, indeed, including the value of the constant B in equation (2-2). More important is the handling of the boundary conditions, because they provide the adjustment for the model to cover the case of rough walls.

Before going into the proposed law for rough walls, it is necessary to discuss the position of the origin of distances normal to the wall. Very often, the wall is conceived as a flat plate, to which individual roughness elements are attached. Distances are measured from the plate. Such a method provides an unambiguous definition of the origin, but it is clearly arbitrary and it is not applicable to a natural roughness. Clauser (1956) has indicated that the origin should be found by trial-and-error, so as to obtain the best fit of the measured velocities to a semi-logarithmic straight line. As he says, "no evidence has come to light of a case where such an origin does not lie between the top and bottom of the roughness elements or where the origin of a given roughness pattern shifts with changes in the roughness Reynolds number". Implicit is the idea that the

semi-logarithmic profile extends down to the top of the roughness elements, where "it blurrs into indistinctness". Clauser's definition of the origin y = 0 is expedient (even when fairly ambiguous in practice, as will be discussed later), but its physical interpretation is confusing. The custom is to think of y = 0 as that point where U = 0. Such a concept is meaningless in a rough wall. But it has been found from experiments that, away from the roughness elements, the velocity is a function of position. It is reasonable to expect the same functional dependence as in the case of smooth walls, and therefore, an arbitrary origin y = 0 can be defined such that the velocity profile will become semi-logarithmic in all the region close to the wall.

Within this context, Rotta's approach (1950) may be explained in the following way. With reference to fig. 2-1, let y be the distance to the wall measured from the top of the roughness elements. At y = 0, the mixing length is not zero, since there is considerable turbulence in the roughness interstices, and it may be written

$$l = l_o + \kappa y$$

or

$$l = \kappa(y_o + y) = \kappa y_B \qquad (2\text{-}22)$$

where $l_o = \kappa y_o$ is a constant that depends on the nature of the wall.

By introducing (2-22) into (2-12) and (2-14), the same result is obtained as for a smooth wall, except for a different constant of integration, which is given as a function of y_o. Rotta has computed y_o from Nikuradse's experiments and he found it linearly dependent on the sand roughness height k_s. When this relationship is introduced into his equation for the velocity profile, an expression similar to (2-6) results, which is in good agreement with experimental observations. The modification of the mixing length postulated in (2-22) is, therefore, valid. It is interesting to note that the coordinate y_B proposed by Rotta in (2-22) is exactly the same found by the trial-and-error adjustment of the origin to fit the observations to a semi-logarithmic straight line. For, if the points fit a straight line in terms of an arbitrary coordinate y_B, then:

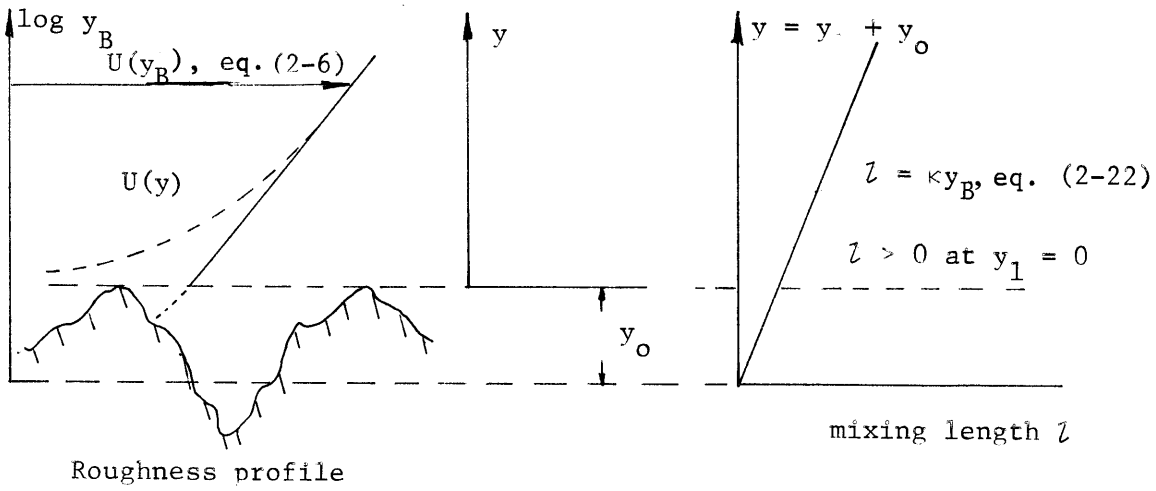

Fig. 2-1 Definition sketch for the mixing length in rough wall flow.

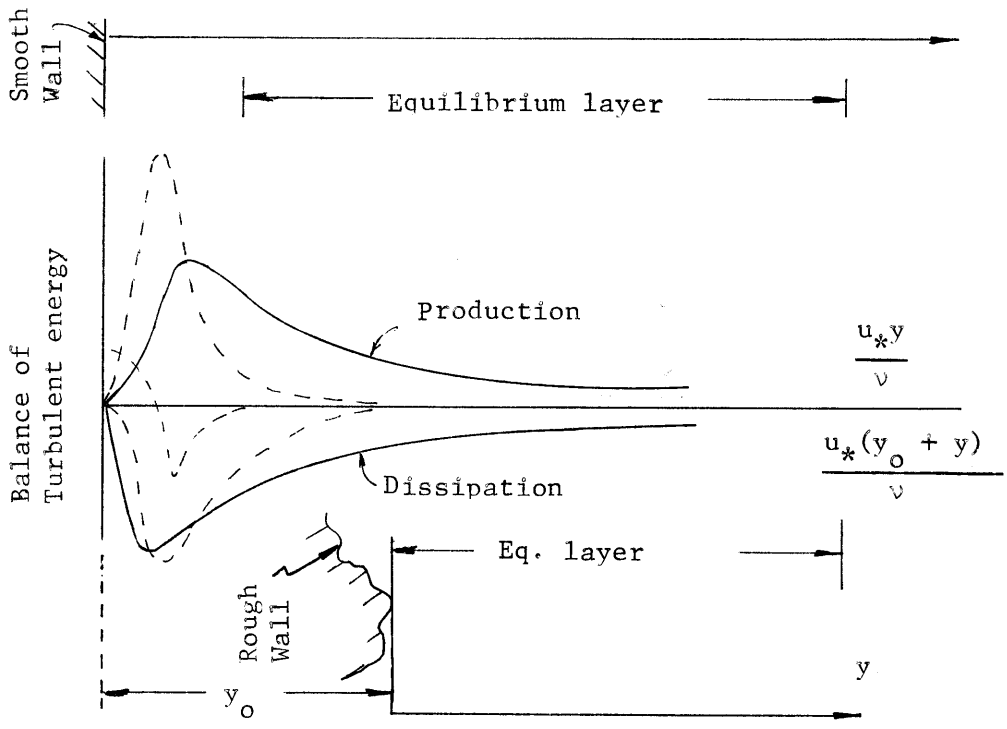

Fig. 2-2 Sketch of equilibrium layer concept in rough wall flow

$$U = \frac{u_*}{\kappa} \ln y_B + b$$

and

$$\frac{dU}{dy} = \frac{u_*}{\kappa y_B} = \frac{u_*}{\ell}$$

which agrees with (2-22).

A different approach to the analysis of the roughness effects was taken by Morris (1955, 1959), who attempted to classify the various regimes of flow that can be established according to the depth, spacing, etc. of the roughness pattern. His work was done mainly in terms of the pipe friction factor, which precludes a direct comparison with mean velocity distributions close to the wall. However, he was able to show that some configurations of roughness, such as corrugated metal, can produce what he called "hyperturbulent flow", characterized by much smaller velocity gradients close to the wall and friction factor increasing with Reynolds number (contrary to the commonly accepted Colebrook-White expression). Morris' explanation for these unusual occurrences assumes that individual roughness elements are not close enough to conform a semi-smooth boundary, but enough for each one to interfere with the wake produced by the previous one. Morris' approach is significant in the light of a recent survey of the field by Robertson, et al., (1965), who have shown that the behavior of the pipe friction factor is mapped very closely by the variations in velocity distribution.

Another approach is the concept of the equilibrium layer, proposed by Townsend (1961), on the basis of the well-known measurements of turbulent energy distribution by Laufer (1954) and others. These measurements, conducted in a smooth pipe, show that there is a layer with the property that the production of turbulent energy essentially balances the turbulent dissipation, and hence, there is negligible interchange of turbulent energy with other portions of the flow. From the experiments, the condition for the existence of such an equilibrium layer is seen to hold from the limit of the viscous sublayer to some fraction of the radius, where the production of turbulent energy becomes too small. In other words, it roughly coincides

with the region where the logarithmic law of the wall is valid for smooth walls. It is significant that the hypothesis of energy balance together with an assumption of similarity lead to an expression analogous to Prandtl's mixing length. Townsend does it in the following way. The term representing the production of turbulence in the energy equation is of the form $-\overline{uv}\,\frac{\partial U}{\partial y}$; thus, if e is the rate of turbulent energy dissipation, the equation for the equilibrium layer is:

$$-\overline{uv}\,\frac{\partial U}{\partial y} = e. \tag{2-23}$$

Now, the hypothesis of similarity indicates that there is a scale of velocity V and a scale of length L which specify the local motion. By dimensional considerations:

$$e = \frac{V^3}{L} \quad \text{and} \quad \left|-\overline{uv}\right| = a\,V^2$$

where a is a constant of proportionality. Introducing in (2-23),

$$(-\overline{uv})^{1/2} = a^{3/2}\,L\,\frac{\partial U}{\partial y}$$

which becomes identical with (2-12) if $a^{3/2}\,L = \ell$. Of course, it is still necessary to assume an expression for ℓ or L. Townsend has extended this reasoning to consider also the redistribution of turbulent energy within the equilibrium layer by lateral transport. This results, for the particular case of pipe flow, in a modified expression for the mixing length,

$$\ell = \kappa y\,\frac{1 - \frac{y}{R}}{1 - (G+1)\,\frac{y}{R}} \tag{2-24}$$

where G is a universal constant. For (y/R) small, again the logarithmic law is obtained. The relevance of the equilibrium layer approach lies in the fact that it provides a clear physical picture of the mechanism by which such a simplified concept as the mixing length can obtain. It

is seen that the procedure of adjusting the measurements to a straight line in the semi-logarithmic plot does not represent properly a way of finding the effective position of the wall, but it is rather a way of determining the actual length scale of turbulence. With reference to fig. 2-2, it can be seen that the limit of the equilibrium layer close to the wall is fairly sharply defined, but the outer limit (away from the wall) is not so clear. This fact corresponds to the gradual departure from the logarithmic law found towards the center of the pipe, which is one of the ambiguities in the determination of the slope $1/\kappa$. If it is postulated that the distribution of turbulent energy is universal in an equilibrium layer in terms of the coordinate $y_B = y_o + y$, then the following distinction can be made between flows with smooth and rough walls, as indicated in fig. 2-2. In a flow with smooth wall, energy is efficiently dissipated through the viscous term $\mu \frac{dU}{dy}$, allowing for high velocities, whereas in flows with rough walls, the same energy is converted to turbulence, giving negligible mean velocity. Except for this difference, which occurs right at the wall, the rest of the flow is essentially the same. A consequence of this concept of universal energy distribution is that, as y_o increases, the thickness of the equilibrium layer should decrease. For extremely high roughness, the layer could become so thin that it would not be detected by actual measurements. This is probably what Morris called the flattening of the velocity profile for hyperturbulent regime.

With regard to the universal Kármán constant κ, it seems reasonable to assume that the similarity within an equilibrium layer is universal in nature, and therefore, κ should be truly a constant. However, propositions to the contrary are numerous. Vanoni (1957, see also Committee on Sedimentation, 1963) has indicated that κ can change by as much as a factor of 2 depending on the amount of suspended material present in the flow; he explains the fact by a dampening of the turbulence by the work necessary to keep the sediment in suspension. Hinze (1962) has re-analyzed Nikuradse's results, avoiding the core region of the flow; he finds some indications of a systematic variation of κ with Reynolds number. Lettau (1961), in his global analysis of the flow, reaches the conclusion that κ should be a constant

only for fully rough flow, but not for smooth or transitional flow. It seems that much of the confusion comes from the lack of a good definition of what κ is supposed to be, as well as from the inherent ambiguity in its measurements. For instance, a semi-logarithmic straight line is often drawn through a complete velocity profile, sometimes neglecting the points very close to the wall. If it is true that κ represents the internal structure of an equilibrium layer, clearly the points towards the core region have nothing to do in its determination. Of course, there is no definite criterion to define the extent of the equilibrium layer.

The previous review can be summarized as follows. The mixing length approach is a valid model for the flow near a solid wall, provided the correct length scale is used, in the form of a modified coordinate $y_B = y + y_o$ defined by the roughness pattern. The region of validity is defined by a state of equilibrium between production and dissipation of turbulent energy. Under these conditions, κ should be a universal constant, but it is not clear whether the same constant should be determinant for the flow in the core region.

2.2 Turbulence in Pipe Flow

If there is disagreement between different investigators in relation to mean velocity distributions, they disagree much more when actual measurements of turbulence are involved, one of the reasons being the many difficulties in the operation of such complex instruments as the hot wire anemometer. Some of those factors will be discussed in Chapter 3.

The outstanding measurements in smooth wall continue to be those presented by Laufer (1954), which are reproduced in most books on the subject. In general, one should expect the same similarity structure found for the mean velocity distribution to hold for turbulence distributions. Laufer's measurements indicate good agreement for u'/u_* vs. $\frac{u_* y}{\nu}$ only for $\frac{u_* y}{\nu} < 20$, which is about the limit of the viscous sublayer. Beyond that point, noticeable changes with Reynolds number exist. These may be due to instrumental errors rather than implying a significant departure from the similarity law. In the core region, for $y/R > 0.4$, again good agreement exists in the plot

of $\frac{u'}{u_*}$ versus $\frac{y}{R}$ for different Reynolds numbers.

Sandborn (1955), by examining a number of published measurements, suggested some influence of the Reynolds number on the intensity at the centerline, of the form

$$\frac{u'}{U_{max}} = 0.144\,Re^{-0.146} \qquad (2\text{-}25)$$

Similar comparisons made by Robertson and Martin (1966; see also Robertson et al., 1965), suggest an exponent of -0.084 rather than -0.146. However, by considering a normalization in terms of u_* instead of U_{max}, they state that u'/u_* does not seem to vary with Reynolds number. It must be realized that these comparisons are highly speculative, since the scatter of the points is several times larger than the variation involved in expressions like (2-25).

There are very few measurements of intensity of tubulence for flows along rough walls. Logan and Jones (1963) have studied the flow development after a sudden change from smooth to rough wall. They used an 8" pipe and sand roughness, with an average grain size of 0.073". They were mostly concerned with the characteristics of the developing flow and their pipe was too short to obtain strictly uniform flow. However, their data indicate an essential agreement between the distribution of u'/u_* at the downstream end (12.75 diameters from the beginning of the roughness) and at the smooth portion of the pipe. The same general trend can be observed in similar measurements conducted by Carper, Heilhecker and Logan (1965) in a two-dimensional channel.

More extensive measurements in fully developed flow in rough pipes have been conducted by Robertson, Burkhart and Martin (1965). They used two different pipes, one 3" in diameter with sand roughness, the other 8" in diameter with natural roughness. Their results show appreciable scatter, but when the intensities u' and v' are normalized with respect to the shear velocity u_*, they tend to a substantial agreement with the values

for smooth walls. No systematic variation with Reynolds number is reported, although the experimental scatter would have masked any eventual dependence. To elaborate further the point, Robertson and Martin (1966) have compared all their data for u'/u_* at a fixed distance from the wall, equal to 10% of the radius. They include in the comparison all the available information from similar measurements in boundary layers along smooth and rough walls and they reach the conclusions, first, that there is no influence of the Reynolds number, and secondly, that the average value of u'/u_* is independent of the nature of the wall. Such a trend can be clearly seen if the data of Corrsin and Kistler (1954) for a boundary layer on a corrugated plate (reproduced in Hinze, 1959) are compared with classical studies on smooth walls.

Further evidence in the same sense is provided by the measurements of Arndt and Ippen (1967) conducted in water in a boundary layer along a surface roughened with triangular grooves. The interesting feature of these experiments is the use, as turbulence probe, of a stagnation tube coupled to a pressure transducer. The normalized axial intensity u'/u_* is again in essential agreement with past experiments on smooth walls. There are, however, indications of a systematic variation with the roughness height k, the maximum value of u'/u_* decreasing from 2.1 for k = 0.0125" to 1.5 for k = 0.100".

Another study of a turbulent boundary layer on a rough surface has been presented by Uram (1966) who tested several regular configurations of circular cylinders and some natural roughness. His basic conclusion regarding the turbulent intensity measurements is that the roughness effect is to markedly increase the anisotropy ratio v'/u'. This would contradict the expectation of a truly universal distribution. Unfortunately, Uram's data are not presented in a normalized form suitable for comparison with other data. However some recomputations indicate that his

claim of a large change in the anisotropy is not clearly substantiated by his own data.

From this review, a general conclusion may be inferred, in the sense that there are strong indications that the intensities of turbulence normalized with respect to the shear velocity follow a more or less universal behavior. This might appear surprising at first glance, but really it is not so. For, from the equations of motion, it can be inferred (see, for instance, Rotta, 1962) that the production of turbulent energy $-\overline{uv}\frac{\partial U}{\partial y}$, is converted entirely to the u- component of turbulence and is redistributed to the v- and w- components by the pressure fluctuations. It was stated in the previous section that a characteristic of the equilibrium layer is a definite pattern for the rate of production of turbulent energy, which must balance the rate of dissipation. As the significant reference velocity is u_*, it is therefore reasonable to expect u'/u_* to have a universal behavior in this layer, and the same must be true of the other components. In the core of the flow, the similarity of $\frac{u'}{u_*}$, $\frac{v'}{u_*}$, $\frac{w'}{u_*}$, still exists because the equilibrium layer acts as a buffer zone, isolating the core from a direct dependence on the nature of the wall, except as reflected by the value of u_*. It is significant in this respect that, according to the discussion in the preceding section, the mean velocity gradient is essentially independent of the nature of the wall throughout the pipe, the conditions at the wall manifesting themselves mostly as a change in the boundary condition for the velocity profile. As a result, substantial changes in such overall parameters as the friction factor do not necessarily imply a simultaneous change in the normalized turbulence distribution. All this only reinforces the view expressed above that an improvement in the understanding of turbulent pipe flow requires an integrated approach towards the behavior of both mean flow and turbulence.

2.3 The Case of a Porous Wall

As it was stated in the Introduction, the porous wall is conceived only as a modification in the boundary conditions, and not as a physical alteration of the geometry of the pipe. That is to say that no substantial

mean flow should occur within the porous material, the motion of the fluid being produced only by the turbulence in the pipe. Of course, these are ideal requirements, which cannot be fulfilled in practice, but which should be approximated in the best possible way.

At any rate, a theoretical analysis that would predict the effect of known characteristics of the porous wall on the pipe flow is not possible at the present, just as for the case of the rough wall, as it was explained in the previous sections. However, it is important to attempt some analytical description of the flow occurring in the porous wall, even if it cannot be directly coupled with the principal flow. Such a theory will be useful for the design of the proper experimental conditions, and it can further provide some guidelines for the evaluation of the results.

Before going into the analysis, it is interesting to derive some inferences from the discussion of the rough wall case. First, it was said that the roughness has been found to produce no change at all in the normalized intensities of turbulence. No doubt, a porous wall will be even less restrictive than a rough wall with respect to the turbulent fluctuations. But it seems reasonable to expect the same effect, that is, no change in the turbulence. Secondly, with regard to the mean velocity distribution, it was found that the roughness increases the length scale of turbulence in the close proximity of the wall (i.e., the mixing length) and, as a consequence, the velocity is reduced by a constant term, $\frac{\Delta U}{u_*}$. If the same model holds, the expectation is that the length scale of turbulence will increase much more than what would be expected from the surface roughness of the porous material; thus, the porosity of the wall will show itself mostly as an additional apparent roughness.

Turning now to an analysis of the flow within the porous material, two approaches can be considered. One is the so-called canopy flow model, important in micro-meteorology (see, for instance, Inoue, 1963). It consists of a uniform wind blowing over some thick vegetal cover. The drag force produced by the obstructing elements is balanced by a shear stress gradient in the fluid, since the pressure is essentially constant. If some reliable assumption can be made concerning the variation of the shear, then a

differential equation for U(y) results, either by assuming a totally viscous shear stress or by a turbulent mixing length expression. The equation is not necessarily easy to solve, always being nonlinear. This approach was not considered suitable to the present purpose, since it assumes that a substantial part of the flow takes place within the obstructed layer, which contradicts the ideal conditions proposed at the beginning of this section.

Therefore, another model was adopted for the analysis, consisting of a porous medium subject to a given pressure distribution at the surface (pipe wall). The known pressure distribution is assumed to be the same as would exist at the wall if the wall were solid and smooth. This assumption is rather arbitrary and can be accepted only within the context of a very preliminary approximate evaluation of the problem. It must be noted, however, that Sternberg (1962; see also Kistler, 1962), in his theory for the viscous sublayer, accepts a somewhat related principle, assuming that the pressure fluctuations associated with the flow in the outside region are imposed throughout the layer, originating the observed fluctuations.

A basic assumption implicit in the porous medium model is that the scale of the fluid motion is large enough to neglect the details of the flow in each elementary pore or channel and, therefore, that the usual macroscopic equations for the flow in porous media are valid. Since the motion under consideration is rapidly fluctuating and has an essentially local character, the assumption is not straightforward, and requires some elaboration. If the turbulence induced motion were comparable in size to an elementary pore, the resistance offered by the interconnecting channels would effectively block any transmission to the neighboring pores, the wall in this case acting merely as a surface roughness. In order to have a substantial change in the flow regime, it is necessary that large eddies, when impinging on the wall, may continue their motion as bulk flow through the porous medium and, hence, the macroscopic description is adequate.

The acceptance of the macroscopic approach poses as the next question the definition of the suitable governing equation, for a Darcy-type expression is known to be valid only for very low Reynolds numbers. Based on

dimensional considerations, Ward (1964) has proposed for steady, one-dimensional flow through porous media an equation of the form

$$\frac{1}{\rho}\frac{dp}{dx} = \frac{\nu q}{K} + 0.550\frac{q^2}{\sqrt{K}} \qquad (2\text{-}26)$$

where p is the pressure, K the permeability of the medium and q the specific discharge in the direction x (i.e., q is the discharge per unit cross-sectional gross area of the medium). In support of (2-26), Ward shows substantial experimental evidence. A similar expression was proposed by Rumer and Drinker (1966), who explain the quadratic term by the corresponding change in the drag coefficient of a sphere with increasing Reynolds number. A more general derivation has been presented by Bachmat (1965), based on the assumptions that the flow is laminar and the resistance forces are due only to viscous friction and are, therefore, proportional to the velocity. Bachmat describes the solid matrix by a number of parameters rather than by a single scalar permeability, and obtains

$$\alpha\rho\frac{\partial\vec{V}}{\partial t} + \mu\vec{V} + \beta\rho|\vec{V}|\vec{V} = -\frac{\bar{\bar{K}}}{n}\cdot\nabla p \qquad (2\text{-}27)$$

where α, β are scalar characteristics of the medium, $\bar{\bar{K}}$ a permeability tensor, n the porosity and $\vec{V}$ the actual average velocity of the fluid, $n\vec{V} = \vec{q}$. These various characteristics of the porous medium are unknown. Assuming the medium to be perfectly isotropic, and neglecting the second order term to make the equation tractable, (2-27) is transformed into the more usual form (see, for instance, Polubarinova-Kotchina, 1962)

$$\frac{\rho}{n}\frac{\partial\vec{q}}{\partial t} + \frac{\mu}{K}\vec{q} = -\nabla p. \qquad (2\text{-}28)$$

The linearization of (2-27) is acceptable only if the neglected term is much smaller than the others. An estimation of the relative orders of magnitude can be obtained from one-dimensional experiments similar to those described by Ward. The point will be discussed in Chapter 3.

The boundary condition consists of the specification of the pressure

at the surface of the porous medium, the implicit assumption being that equation (2-28) holds everywhere in the medium, up to the surface y = 0. Measurements by Willmarth and Wooldridge (1962) in a boundary layer and by Corcos (1964) in a pipe have shown that the turbulent pressure field on a smooth wall is convected with an essentially constant velocity, approximately 0.8 of the mean velocity. Therefore, as a simple first approximation, the wall pressure can be represented by a single sinusoidal wave. A more accurate method is to define the pressure as a random variable and use the available information in terms of the pressure spectrum to compute mean square values for the velocity in the porous medium.

Both methods of solution will be presented in the following sections. Assuming that the radius of curvature of the porous layer is large compared to its thickness, it is possible to treat the problem in Cartesian coordinates as an infinite horizontal layer. Furthermore, fluctuations in the lateral direction will not be considered, because there is little available information that could be used to specify the boundary condition. This is not considered to be a serious drawback, in comparison with other more radical simplifications, such as the linearization of (2-27) or the use of smooth wall pressure information as a boundary condition. It must also be recalled that this analysis will provide only an initial understanding of the mechanism of the flow in a porous boundary and is not, at this point, extended to give a complete prediction of the modifications in the pipe flow itself.

2.4 Single Wave Specification of the Boundary Pressure

With reference to fig. 2-3, the mathematical problem consists of solving equation (2-28) for a two-dimensional field (x,y) extending from y = 0 to y = - h, with p given at y = 0 and the normal velocity vanishing at y = - h. The fluid is assumed incompressible. With $\vec{q} = (q_x, q_y)$,

$$\left.\begin{aligned} \frac{\rho}{n}\frac{\partial q_x}{\partial t} + \frac{\mu}{K} q_x &= -\frac{\partial p}{\partial x} \\ \frac{\rho}{n}\frac{\partial q_y}{\partial t} + \frac{\mu}{K} q_y &= -\frac{\partial p}{\partial y} \\ \frac{\partial q_x}{\partial x} + \frac{\partial q_y}{\partial y} &= 0 \end{aligned}\right\} \qquad (2\text{-}29)$$

$$p = P \cos (kx - \omega t) \qquad \text{at } y = 0$$

$$\frac{\partial p}{\partial y} = 0 \qquad \text{at } y = -h$$

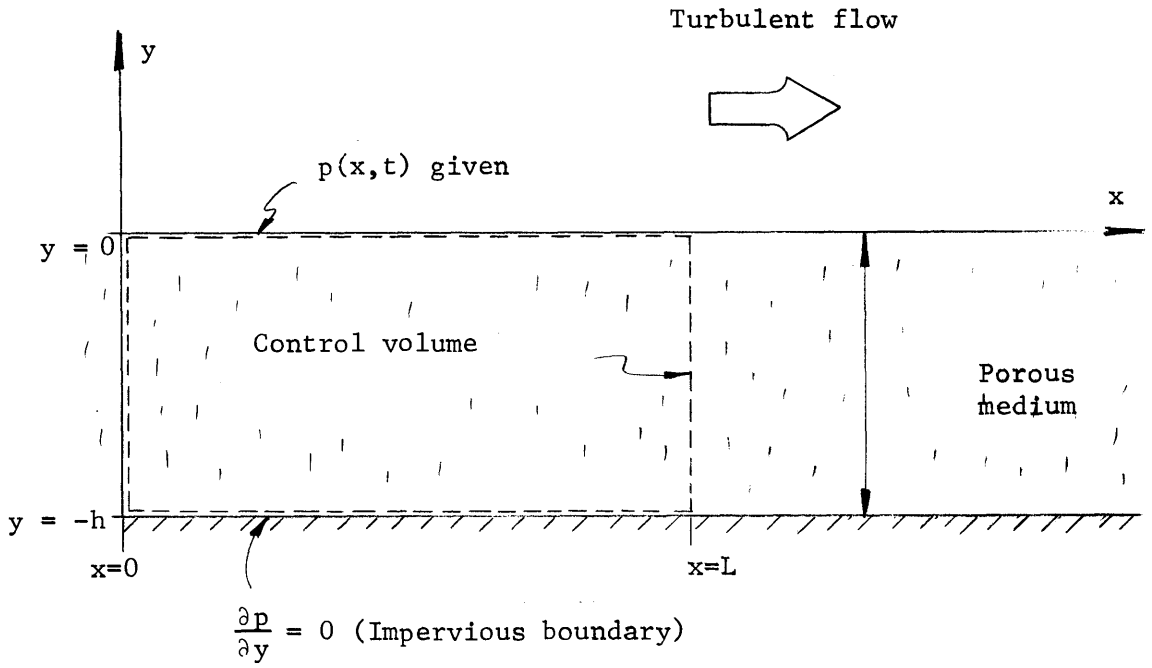

Fig. 2-3 Definition sketch for analysis of flow in porous medium.

In this formulation, $\vec{q}$ is not given by grad p. However, it is simple to show that the second boundary condition leads to the same result as the condition $q_y = 0$. In (2-29), p is the pressure fluctuation with respect to its average value; k is the wave number $2\pi/L$, ω is the frequency $2\pi/T$, with both k and ω being considered as constants and related to the convection velocity specified before by $U_c = \omega/k$. An estimation of the values of k and ω will be made in the next section, in comparison with the results of the statistical approach. P is a constant defined by the empirical result,

presented by Corcos (1964), that, at the wall,

$$\frac{P}{\sqrt{2}} = \sqrt{\overline{p^2}} = a\ \tau_o \qquad (2\text{-}30)$$

with "a" approximately equal to 3. Taking the divergence of (2-28), continuity gives

$$\nabla^2 p = 0$$

and therefore,

$$p(x,y,t) = P\ \frac{\cosh k(y + h)}{\cosh kh}\ \cos (kx - \omega t) \qquad (2\text{-}31)$$

From (2-31), with $p' = \sqrt{\overline{p^2}}$

$$\frac{p'(y)}{p'(0)} = \frac{\cosh k(y + h)}{\cosh kh} \qquad (2\text{-}32)$$

and, at y = - h, i.e., at the outer solid wall surrounding the porous layer,

$$\frac{p'(-h)}{p'(0)} = \frac{1}{\cosh kh}\ . \qquad (2\text{-}33)$$

It is of interest to compare (2-32) with the distribution obtained from the assumption of infinite depth h. If $p'_\infty (y)$ denotes the value of p' at y under the assumption that $h \to \infty$, then

$$\frac{p'_\infty(y)}{p'(0)} = e^{ky} \qquad (2\text{-}34)$$

In fig. 2-4, the ratio $(p'(y)/p'(0))^2$ is plotted in function of y/L for various values of h/L, in accordance with equations (2-32) and (2-34). With a relative thickness of 0.3, the exact solution is in essential agreement with the approximation which assumes an infinite porous layer.

When (2-31) is introduced into (2-29), first order differential

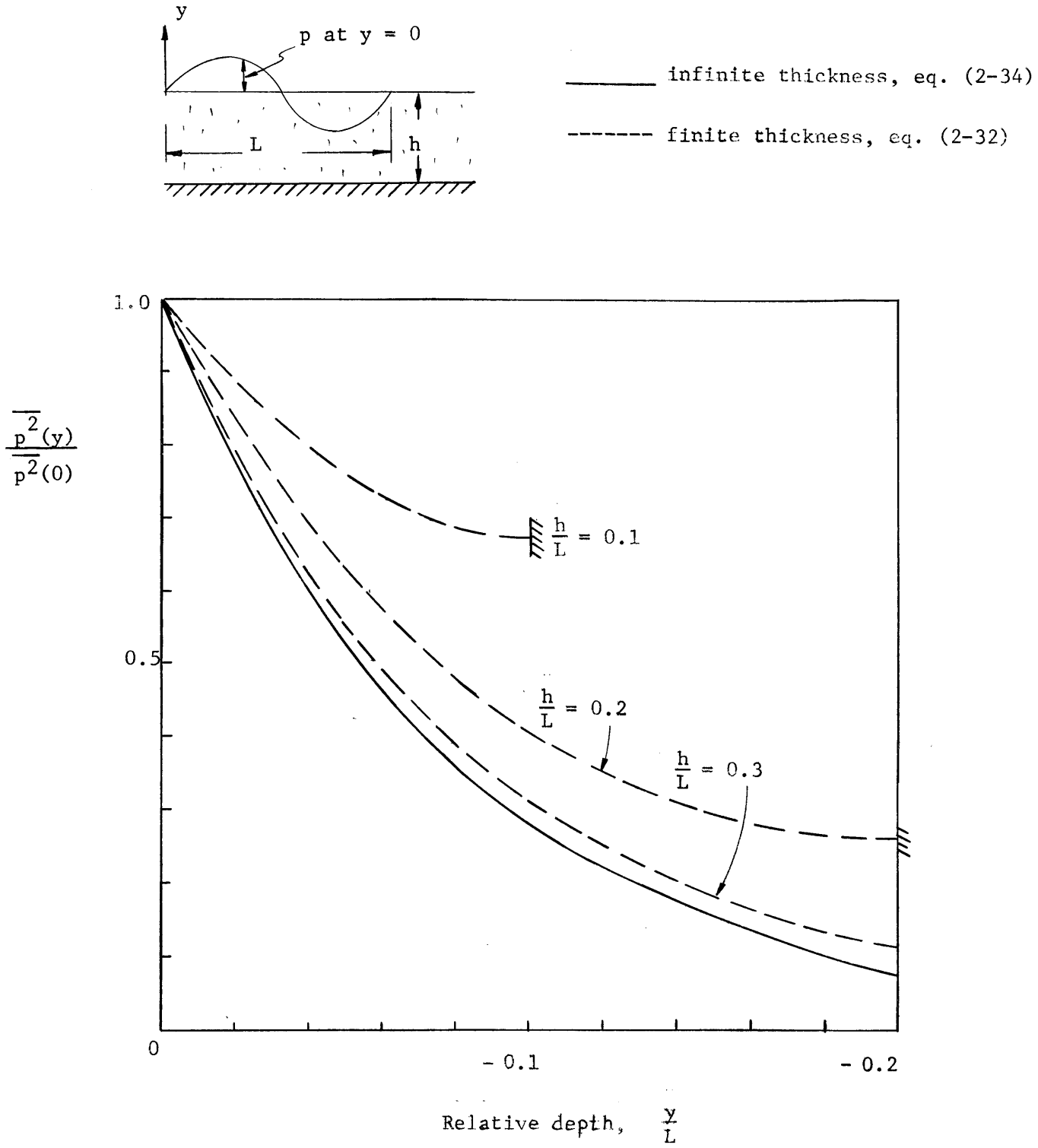

Fig. 2-4 Mean square pressure fluctuation in porous medium as a function of depth and thickness of the porous layer.

equations in t are obtained for q_x and q_y. The solutions are

$$\left.\begin{aligned} q_x\,(x,y,t) &= \frac{kKP}{\mu}\;\frac{\cosh k(y+h)}{\cosh kh}\;\frac{\sin(kx-\omega t+\delta)}{\sqrt{1+\left(\frac{K\omega}{n\nu}\right)^2}} \\ q_y\,(x,y,t) &= -\frac{kKP}{\mu}\;\frac{\sinh k(y+h)}{\cosh kh}\;\frac{\cos(kx-\omega t+\delta)}{\sqrt{1+\left(\frac{K\omega}{n\nu}\right)^2}} \end{aligned}\right\} \quad (2\text{-}35)$$

where δ is a constant defined by

$$\sin\delta = \frac{\frac{K\omega}{n\nu}}{\sqrt{1+\left(\frac{K\omega}{n\nu}\right)^2}} \quad \text{and} \quad \cos\delta = \frac{1}{\sqrt{1+\left(\frac{K\omega}{n\nu}\right)^2}} \qquad (2\text{-}36)$$

The maximum amplitudes for q_x and q_y occur at $y = 0$. The mean values are zero. Continuity at $y = 0$ between the flows in the porous media and in the pipe requires

$$q_x = (u)_{pipe} \quad \text{and} \quad q_y = (v)_{pipe}$$

since $\vec{q} = (q_x, q_y)$ is the specific discharge. From (2-36), the intensities can be computed as

$$q_x' = \sqrt{\overline{q_x^2}} \quad \text{and} \quad q_y' = \sqrt{\overline{q_y^2}}$$

which, after introduction of the value of P, can be written as

$$\left.\begin{aligned} \frac{q_x'}{u_*} &= a\,\frac{u_*}{U_c}\;\frac{\frac{K\omega}{\nu}}{\sqrt{1+\left(\frac{K\omega}{n\nu}\right)^2}}\;\frac{\cosh k(y+h)}{\cosh kh} \\ \frac{q_y'}{u_*} &= a\,\frac{u_*}{U_c}\;\frac{\frac{K\omega}{\nu}}{\sqrt{1+\left(\frac{K\omega}{n\nu}\right)^2}}\;\frac{\sinh k(y+h)}{\cosh kh} \end{aligned}\right\} \quad (2\text{-}37)$$

and hence, $q'_y = q'_x \tanh k(y + h)$. In the limit, as h tends to infinity, the flow becomes isotropic. The mean product $\overline{q_x q_y}$, from (2-35), is zero everywhere. This seems to be a shortcoming of the theory, arising from the linearization of the differential equations, since one might expect that some turbulent transfer of momentum to the deeper layer of the porous wall should occur. For large $K\omega/n\nu$ (2-37) becomes independent of the permeability K and of the viscosity,

$$\left.\begin{aligned} \frac{q'_x}{u_*} &= an \frac{u_*}{U_c} \frac{\cosh k(y + h)}{\cosh kh} \\ \frac{q'_y}{u_*} &= an \frac{u_*}{U_c} \frac{\sinh k(y + h)}{\sinh kh} \end{aligned}\right\} \quad \frac{K\omega}{n\nu} >> 1 \qquad (2\text{-}38)$$

This is the same result that would be obtained from (2-29) by neglecting the resistance term $\frac{\mu}{K} \vec{q}$. The fluid motion then represents a balance of inertial and pressure forces.

It is of interest to determine what average velocity Q_x will be produced in the porous medium by the overall pressure gradient in the pipe. As the equation of motion has been linearized, superposition is valid. By introducing in (2-28) the pipe pressure gradient $dp/dx = 4\tau_o/D$, where D denotes the interior diameter of the pipe,

$$Q_x = \frac{4 K \tau_o}{\mu D}$$

from which

$$\frac{Q_x}{u_*} = \frac{4 K u_*}{\nu D} \qquad (2\text{-}39)$$

and, at y = 0,

$$\frac{q'_x}{Q_x} = \frac{akD}{4\sqrt{1 + \left(\frac{K\omega}{n\nu}\right)^2}} \qquad (2\text{-}40)$$

This expression allows an estimation of the relative importance of Q_x in regard to the linearization of (2-27).

An indication of the importance of the porous medium flow relative to the overall pipe motion can be obtained by comparing the energy dissipation in each case. The rate of dissipation e_L in the porous medium can be computed in relation to a control volume $\forall$ of surface S,

$$e_L = -\int_{S_p} \left(p + \frac{1}{2}\rho V^2\right) \vec{V}\cdot d\vec{S}_p + \frac{\partial}{\partial t}\int_{\forall_p} \frac{1}{2}\rho V^2 \, d\forall_p \qquad (2\text{-}41)$$

where $d\vec{S}_p$ points towards the interior of the control volume, $\vec{V}$ is the actual velocity $\vec{q}/n$, $\forall_p$ is the open volume, S_p is the open cross section and the gravity term has been neglected. The control volume is chosen of one wave length, unit width and the thickness of the porous layer (fig. 2-3). By introducing the porosity in (2-41) in the form $V = q/n$, $\forall = \forall_p/n$, $S = S_p/n$,

$$e_L = -\int_S \left(p + \frac{1}{2}\rho \frac{q^2}{n^2}\right) \vec{q}\cdot d\vec{S} + \frac{\partial}{\partial t} \int_{\forall} \frac{1}{2}\rho \frac{q^2}{n} \, d\forall$$

With reference to fig. 2-3, the contribution to the surface integral from the two boundaries x = 0, L cancels out, and obviously $\vec{q}\cdot d\vec{S}$ vanishes at y = - h. Furthermore, the volume integral of q^2 over one wave length does not depend on time, so the last term also vanishes. Thus, all the energy dissipated corresponds to the energy being transmitted from the turbulent pipe flow to the porous medium, as should be expected, and

$$e_L = \int_{\substack{x=0 \\ (\text{at } y=0)}}^{x=L} \left(p + \frac{1}{2}\rho \frac{q^2}{n^2}\right) q_y \, dx$$

Introducing (2-31) and (2-35), it is easily shown that the contribution from $q^2 q_y$ cancels out, so, per unit area of interface,

$$e = \frac{e_L}{L} = \frac{1}{L}\int_{(\text{interface})} pq_y \, dS = \frac{a^2 \tau_o^2}{\rho U_c} \frac{K\omega}{\nu} \frac{\tanh kh}{1 + \left(\frac{K\omega}{n\nu}\right)^2} \, . \qquad (2\text{-}42)$$

An alternative method of finding e is to take the scalar product of q and the equation of motion (2-28) to obtain an energy equation. This shows that the viscous dissipation term is of the form $\frac{\mu}{K} q^2$, which, after a volume integration, gives the same result as (2-42). It is interesting to note that, by differentiating (2-42) with respect to the permeability K, the dissipation e is seen to reach a maximum when $\frac{K\omega}{n\nu} = 1$.

If (2-41) is now applied to a control volume including the complete open section of the pipe, the dissipation E is seen to be, per unit area of wall interface,

$$E = \frac{dp}{dx} \frac{\bar{U}D}{4} = \tau_o \bar{U} \tag{2-43}$$

and, therefore, the ratio between the energy transmitted to the porous medium, and the energy dissipated in the main flow is

$$\frac{e}{E} = a^2 \frac{u_*}{\bar{U}} \frac{u_*}{U_c} \frac{K\omega}{\nu} \frac{\tanh kh}{1 + \left(\frac{K\omega}{n\nu}\right)^2} = \frac{a}{\sqrt{1 + \left(\frac{K\omega}{n\nu}\right)^2}} \frac{v'}{\bar{U}} \tag{2-44}$$

where v' represents q'_y at y = 0. It must be noted that the ratio computed in (2-44) does not represent the additional energy dissipated in the pipe because of the presence of a porous wall. That additional dissipation is already included in the factor u_*, whose value cannot be predicted from the present analysis. However, in a general way, it is reasonable to assume that the porosity of the wall will noticeably affect the pipe flow only when a significant portion of the total energy has to be transported to the porous medium and, therefore, e/E is a measure of the influence of the porous wall.

2.5 Statistical Specification of the Boundary Pressure

The problem formulated in (2-29) can be solved in much the same way if the pressure at y = 0 is given as a known random function of position and time. A fairly similar problem, the irrotational motion at the boundary of a free jet, has been treated by Phillips (1955) and Stewart (1956).

The first boundary condition for (2-29) is written as a Fourier-Stieltjes integral

$$p = \int_{-\infty}^{\infty} e^{i(kx + \omega t)} \, dB(k,\omega) \quad \text{at } y = 0 \tag{2-45}$$

where $dB(k,\omega)$ is a random point function and the integral is taken over all values of k and ω. Readers not familiar with the notation of (2-45) are referred to any book on the theory of random functions; a good introduction is presented by Lee (1960). In a similar way to the single wave analysis, the solution to (2-29) with (2-45) is found to be

$$\left.\begin{aligned} p(x,y,t) &= \int_{-\infty}^{\infty} e^{i(kx + \omega t)} \frac{\cosh k(h + y)}{\cosh kh} \, dB(k,\omega) \\ q_x(x,y,t) &= -i \int_{-\infty}^{\infty} e^{i(kx + \omega t)} \frac{Kk/\mu}{1 + i \frac{K\omega}{n\nu}} \frac{\cosh k(h + y)}{\cosh kh} \, dB(k,\omega) \\ q_y(x,y,t) &= - \int_{-\infty}^{\infty} e^{i(kx + \omega t)} \frac{kK/\mu}{1 + i \frac{K\omega}{n\nu}} \frac{\sinh k(h + y)}{\cosh kh} \, dB(k,\omega) \end{aligned}\right\} \tag{2-46}$$

Explicit expressions for p, q_x or q_y do not exist. It is possible, however, to find the mean square values in the following way. The correlation function for the pressure at y = 0 at two points separated by a displacement ξ and a time interval τ, is

$$R(\xi,\tau) = \overline{p^*(x,0,t) \, p(x + \xi, 0, t + \tau)}$$

where * denotes the complex conjugate. Introducing p from (2-46), it can be shown (see, for instance, Batchelor, 1960, Chapter 2) that

$$R(\xi,\tau) = \iint_{-\infty}^{\infty} e^{i(k\xi + \omega\tau)} \overline{dB^* dB} \, . \tag{2-47}$$

Defining the total Fourier transform of R by

$$E(k,\omega) = \frac{1}{4\pi^2} \iint_{-\infty}^{\infty} R(\xi,\tau) e^{-i(k\xi + \omega\tau)} \, d\xi d\tau \tag{2-48}$$

it follows that

$$\overline{dB^* dB} = E(k,\omega) \, dk d\omega. \tag{2-49}$$

From (2-46), mean square values can be found by multiplying each variable by its complex conjugate at the same position and time. As p, q_x, q_y are real,

$$\left.\begin{aligned}
\overline{p^* p} &= \overline{p^2} = \iint_{-\infty}^{\infty} \frac{\cosh^2 k(h+y)}{\cosh^2 kh} \; \overline{dB^* dB} \\
\overline{q_x^* q_x} &= \overline{q_x^2} = \iint_{-\infty}^{\infty} \frac{(Kk/\mu)^2}{1 + \left(\frac{K\omega}{n\nu}\right)^2} \frac{\cosh^2 k(h+y)}{\cosh^2 kh} \; \overline{dB^* dB} \\
\overline{q_y^* q_y} &= \overline{q_y^2} = \iint_{-\infty}^{\infty} \frac{(Kk/\mu)^2}{1 + \left(\frac{K\omega}{n\nu}\right)^2} \frac{\sinh^2 k(h+y)}{\cosh^2 kh} \; \overline{dB^* dB} \\
\overline{q_x^* q_y} &= \overline{q_x q_y} = -i \iint_{-\infty}^{\infty} \frac{(Kk/\mu)^2}{1 + \left(\frac{K\omega}{n\nu}\right)^2} \frac{\sinh 2k(h+y)}{2\cosh^2 kh} \; \overline{dB^* dB}
\end{aligned}\right\} \tag{2-50}$$

Therefore, if $E(k,\omega)$ is known, (2-50) can be integrated to obtain explicit expressions for the intensities of pressure and velocity. From measurements of the wall pressure fluctuations in a smooth pipe, Corcos (1964) has shown that $E(k,\omega)$ can be expressed in terms of a partial transform $\Gamma(\xi,\omega)$ defined by

$$R(\xi,\tau) = \int_{-\infty}^{\infty} e^{i\omega\tau} \Gamma(\xi,\omega) d\omega$$

Thus,

$$E(k,\omega) = \frac{1}{2\pi}\int_{-\infty}^{\infty} e^{-ik\xi}\ \Gamma(\xi,\omega)d\xi \tag{2-51}$$

A frequency spectrum is defined by

$$\Phi(\omega) = \frac{1}{2\pi}\int_{-\infty}^{\infty} R(0,\tau)\ \cos\ \omega\tau\ d\tau \tag{2-52}$$

Corcos has measured the cross-spectral function Γ in the form

$$\Gamma(\xi,\omega) = |\Gamma|\ e^{-i\eta} = A(\xi,\omega)\ \Phi(\omega)e^{-i\eta}$$

and he found that $A = |\Gamma|/\Phi$ is a function only of η. Writing η as a similarity variable $\eta = \frac{\omega\xi}{U_c}$, a convection velocity U_c is defined, which is found to be only a weak function of frequency, and can be taken to be a constant, equal to 0.8 times the average velocity in the pipe. Therefore,

$$\Gamma(\xi,\omega) = \Phi(\omega)\quad A\left(\frac{\omega\xi}{U_c}\right) e^{-i\ \frac{\omega\xi}{U_c}} \tag{2-53}$$

Introducing (2-53) in (2-51), and by a suitable transformation,

$$E(k,\omega) = \overline{\frac{dB^{*}dB}{dk\ d\omega}} = \frac{U_c\Phi(\omega)}{|\omega|}\quad E_o\left(1 + \frac{U_c k}{\omega}\right) \tag{2-54}$$

where E_o is the transform of A, defined by

$$E_o(\delta) = \frac{1}{2\pi}\int_{-\infty}^{\infty} A(\eta)\ e^{-i\delta\eta}\ d\eta \tag{2-55}$$

Corcos gives A only as a plot of experimental points. Gardner (1965), by a theoretical analysis of the pressure equations in the wall layer, has shown that $A(\eta)$ can be approximated by

$$A(\eta) = \frac{1}{1 + (m\eta)^2} \tag{2-56}$$

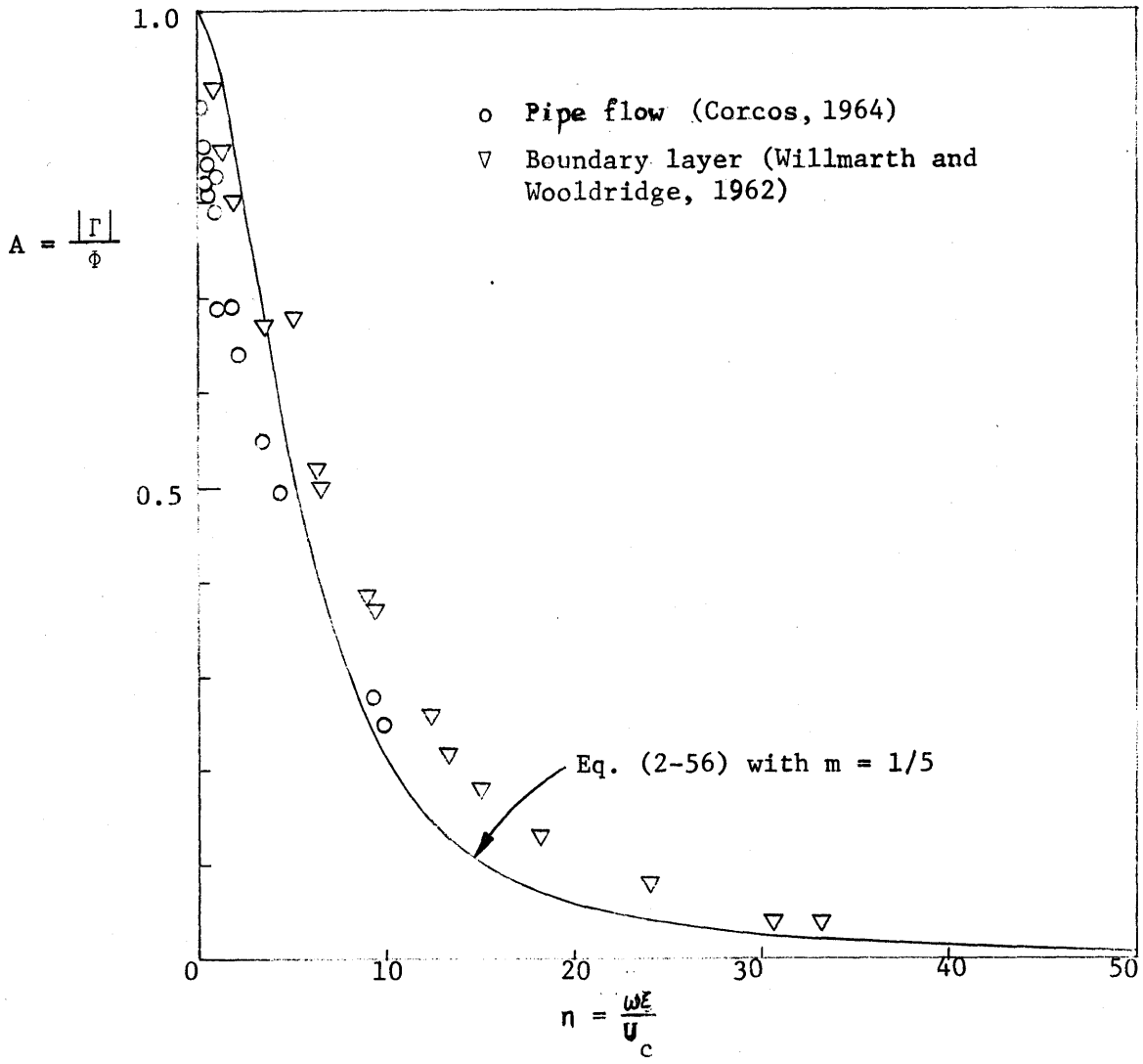

Fig. 2-5 Representation of the cross-spectral function of the wall pressure, A(η).

where m is the exponent in a power law representing the velocity distribution close to the wall. The agreement of (2-56) with observations is not very good (fig. 2-5), but can be accepted for the present purpose. In fig. 2-5, m has been taken as 1/5. From (2-55) and (2-56),

$$E_o\left(1 + \frac{U_c k}{\omega}\right) = \frac{1}{2m} \exp\left(-\frac{1}{m}\left|1 + \frac{U_c k}{\omega}\right|\right) \tag{2-57}$$

To completely specify (2-54), it is still necessary to have an explicit expression for $\Phi(\omega)$, the power spectrum of the wall pressure. Corcos (1962) indicates that a universal behavior results from the use of the dimensionless variables

$$\Phi' = \frac{\Phi \bar{U}}{\tau_o^2 D} \; ; \; f' = \frac{D\omega}{2\pi\bar{U}} \tag{2-58}$$

where $\bar{U}$ is the mean velocity and D the diameter of the pipe, and that the data are well represented by

$$\Phi' = 0.418 \; \frac{\exp(-0.0224 f')}{f'} \tag{2-59}$$

However, (2-59) cannot be used for the present purpose, because it does not integrate to the correct value of p'. It seems appropriate to use instead an expression similar to that commonly used for the velocity spectrum, such as

$$\frac{\Phi}{\overline{p^2} T_s} = \frac{1}{1 + \left(\pi T_s \omega\right)^2} \tag{2-60}$$

where T_s is the time integral scale defined by

$$T_s = \frac{1}{2\pi} \int_{-\infty}^{\infty} \frac{R(0,\tau)}{\overline{p^2}} \, d\tau \tag{2-61}$$

Comparison with (2-52) shows that

$$T_s = \frac{\Phi(0)}{\overline{p^2}} \tag{2-62}$$

With (2-60), it is possible to fit Corcos' data in the low frequency range, which is the most significant since it contains the largest portion of the energy. Rather large departures occur at the high frequencies (fig. 2-6). With (2-54), (2-57) and (2-60), equations (2-50) are completely determined. An immediate result comes from the fact that $\overline{dB^*dB}$ is an even function with respect to the vector (k,ω). Therefore, $\overline{q_x q_y} = 0$, as was the case for the single wave analysis. More similarities between the two solutions will be pointed out as the equations are developed. The integration of (2-50) is rather cumbersome and, for the purposes of this investigation, it is convenient to restrict the analysis to the case of an infinite thickness h. The implications of this assumption for the application of the theory will be discussed later. If the power spectrum of $\overline{p^2}$ at a depth y ($y < 0$) in the porous medium is defined by

$$\overline{p^2}\,(y) = \int_{-\infty}^{\infty} \Phi(\omega,y)\,d\omega \tag{2-63}$$

then integration of the pressure equation in (2-50) with respect to k leads to

$$\frac{\Phi(\omega,y)}{\Phi(\omega,0)} = \frac{e^{2Y|\Omega|} + 2me^{-\frac{1}{m}Y|\Omega|}}{1 - (2mY\Omega)^2} \tag{2-64}$$

where Y is a dimensionless depth defined by

$$Y = \frac{y}{U_c T_s} \tag{2-65}$$

and Ω is a dimensionless frequency defined by

$$\Omega = T_s\omega. \tag{2-66}$$

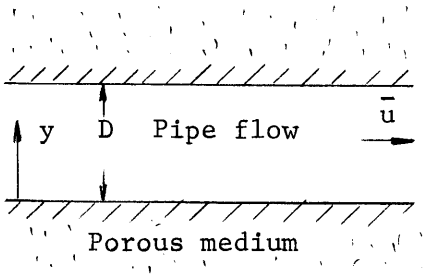

$$Y = \frac{\bar{u}}{U_c} \frac{y}{D} \approx \frac{y}{D}$$

○ Wall pressure measurements by Corcos (1964)

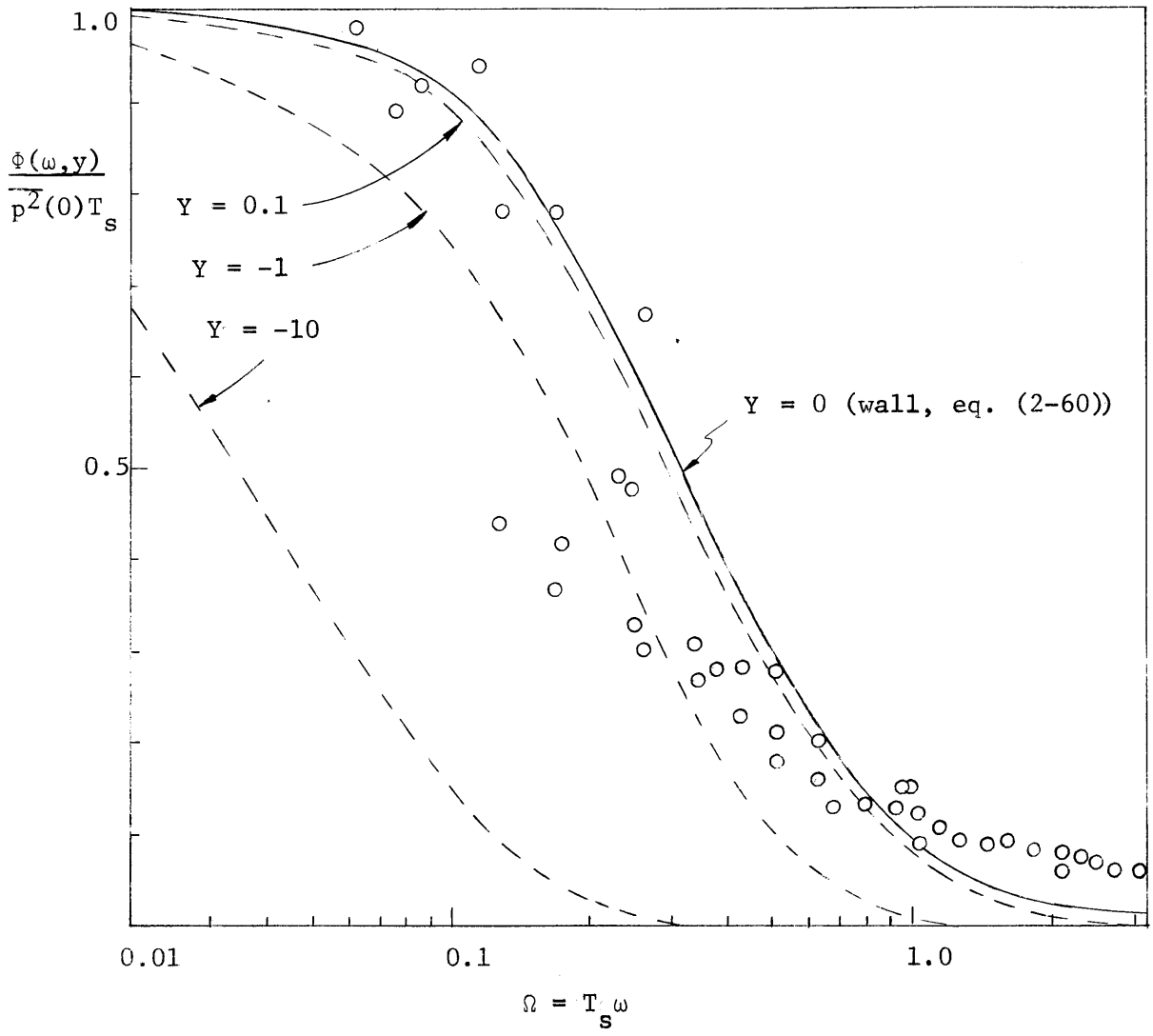

Fig. 2-6 Normalized pressure spectrum in the porous medium, eq. (2-64)

It must be noted that Y is always negative, and, by a suitable rearrangement of (2-64), it can be seen that $\Phi(\omega,y)$ remains finite when $2mY|\Omega| = -1$. In fig. 2-6, the pressure spectrum at the interface y = 0 has been plotted as given by (2-60), together with the spectrum at various depths in accordance with (2-64). In the same figure, a comparison is made with Corcos' measurements of the wall pressure in a pipe, which he presented in terms of the similarity variables (2-58). The implicit equivalence is $T_s = D/\overline{U}$. The data for Φ have been reduced by a factor of 2, to take account of the negative frequencies, which do not have a physical reality. To interpret fig. 2-6 for the case where the porous layer constitutes the wall of a pipe, T_s can be expressed as $D/\overline{U}$ and, recalling that $U_c \approx 0.8\ \overline{U}$, Y becomes approximately equal to the ratio between the depth y and the diameter of the pipe. As depth increases, the high frequencies are severely attenuated. Some evaluation of the validity of the assumption of infinite thickness of the layer can be made from the plot. At Y = -0.1, the significant low frequencies are passed almost unimpeded and even at Y = -1 the attenuation is rather small. Therefore, for the layer to be considered of infinite depth, the relative thickness $\frac{h}{U_c T_s}$ has to be much larger than 1.

Further integration of (2-63) gives for the pressure intensity

$$\frac{\overline{p^2(y)}}{\overline{p^2(0)}} = \frac{2}{\pi} \frac{Ci\left(-\frac{2Y}{\pi}\right)\sin\left(-\frac{2Y}{\pi}\right) - si\left(-\frac{2Y}{\pi}\right)\cos\left(-\frac{2Y}{\pi}\right) - \frac{2}{\pi}MY}{1 + \left(\frac{2mY}{\pi}\right)^2} \qquad (2\text{-}67)$$

where M is a numerical constant defined by

$$M = \frac{1}{2}m\left[e^{-\frac{1}{m}}Ei\left(\frac{1}{m}\right) + e^{\frac{1}{m}}E_1\left(\frac{1}{m}\right)\right] = 0.044$$

with m = 1/5, and Ci, si, Ei and E_1 are exponential integral functions. It is of interest to examine the behavior of (2-67) for small values of Y. The following approximations are valid for small values of the argument:

$$Ci(x) \approx 0.577 + \ln x$$

$$si(x) \approx x - \frac{\pi}{2}$$

$$\sin(x) \approx x$$

$$\cos(x) \approx 1.$$

Then, (2-67) becomes

$$\frac{\overline{p^2(y)}}{\overline{p^2(0)}} \approx 1 + \frac{2}{\pi}\left(-\frac{2Y}{\pi}\right)\ln\left(-\frac{2Y}{\pi}\right) \qquad \text{for Y small.} \qquad (2\text{-}68)$$

Both (2-67) and (2-68) have been plotted in fig. 2-7. This result can now be compared with the single wave analysis for the same assumption of infinite h, that is, equation (2-34). In that analysis, nothing was said concerning the actual values of the wave parameters L and T. Approximating Y by y/D, equation (2-34) has been plotted for various values of L/D in the same fig. 2-7, and it can be seen that, in general, the decay in the turbulent pressure intensity is much faster for the single wave analysis than for the statistical analysis, and furthermore, that L/D has to be at least of order 10 to have some degree of equivalence between the two solutions. This is rather surprising, since one might expect the significant wave length to be of the order of the pipe diameter D. The explanation may be found in the pressure spectrum represented in fig. 2-6, where the significant frequencies Ω are less than 0.5. As $\Omega = T_s\omega$ is approximately equal to Dk, this corresponds to ratios D/L smaller than about 0.1. Of course, these inferences are dependent upon the accuracy of the low frequency spectrum measurements as well as of their analytical representation (2-60).

Turning now to the integration of the velocity equations in (2-50), the assumption of infinite depth produces $q'_x = q'_y$. Integration is readily done only for the special case of y = 0, which gives

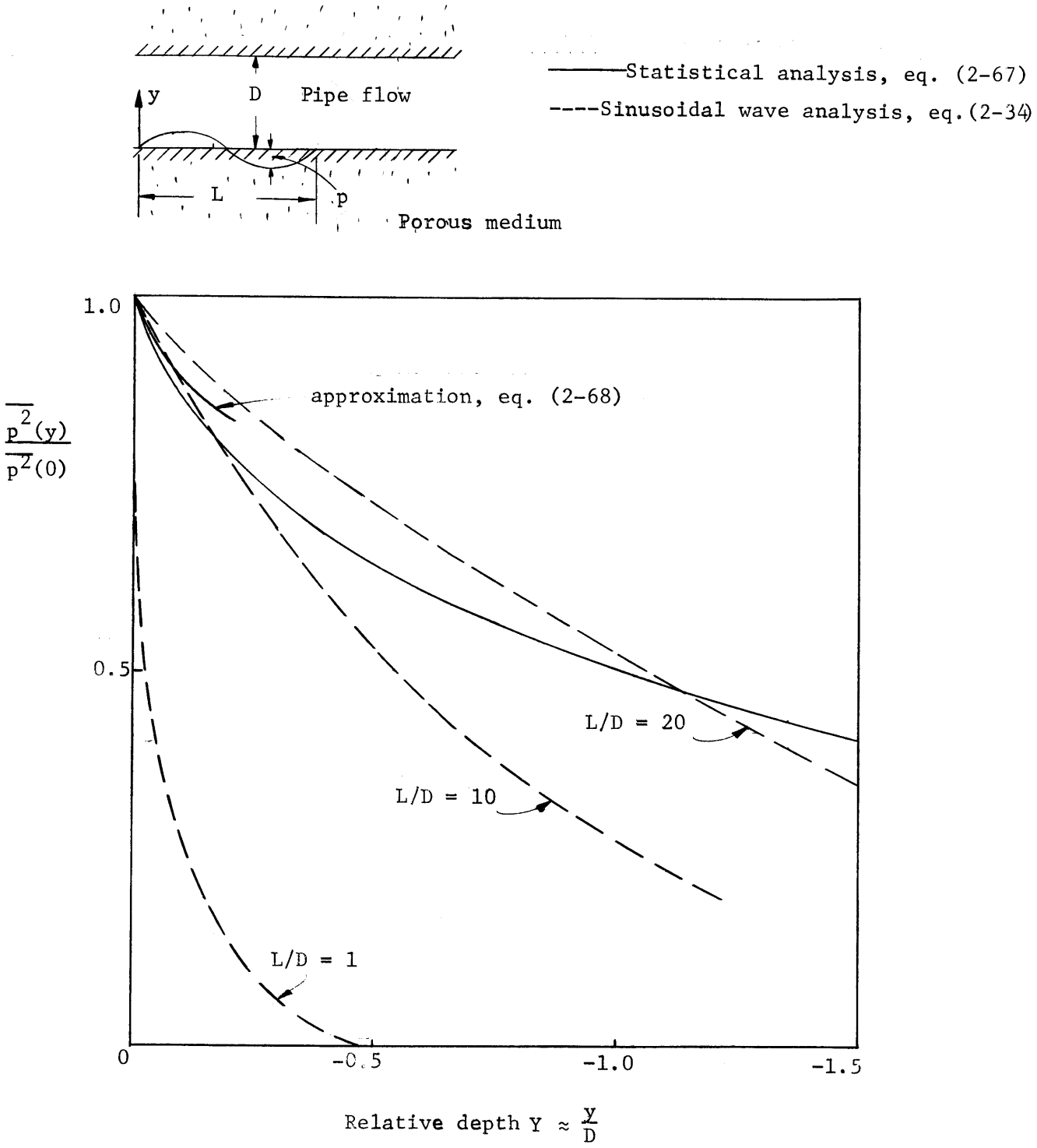

Fig. 2-7 Sinusoidal wave analysis compared with statistical analysis in terms of mean square pressure distribution (infinite thickness of porous layer).

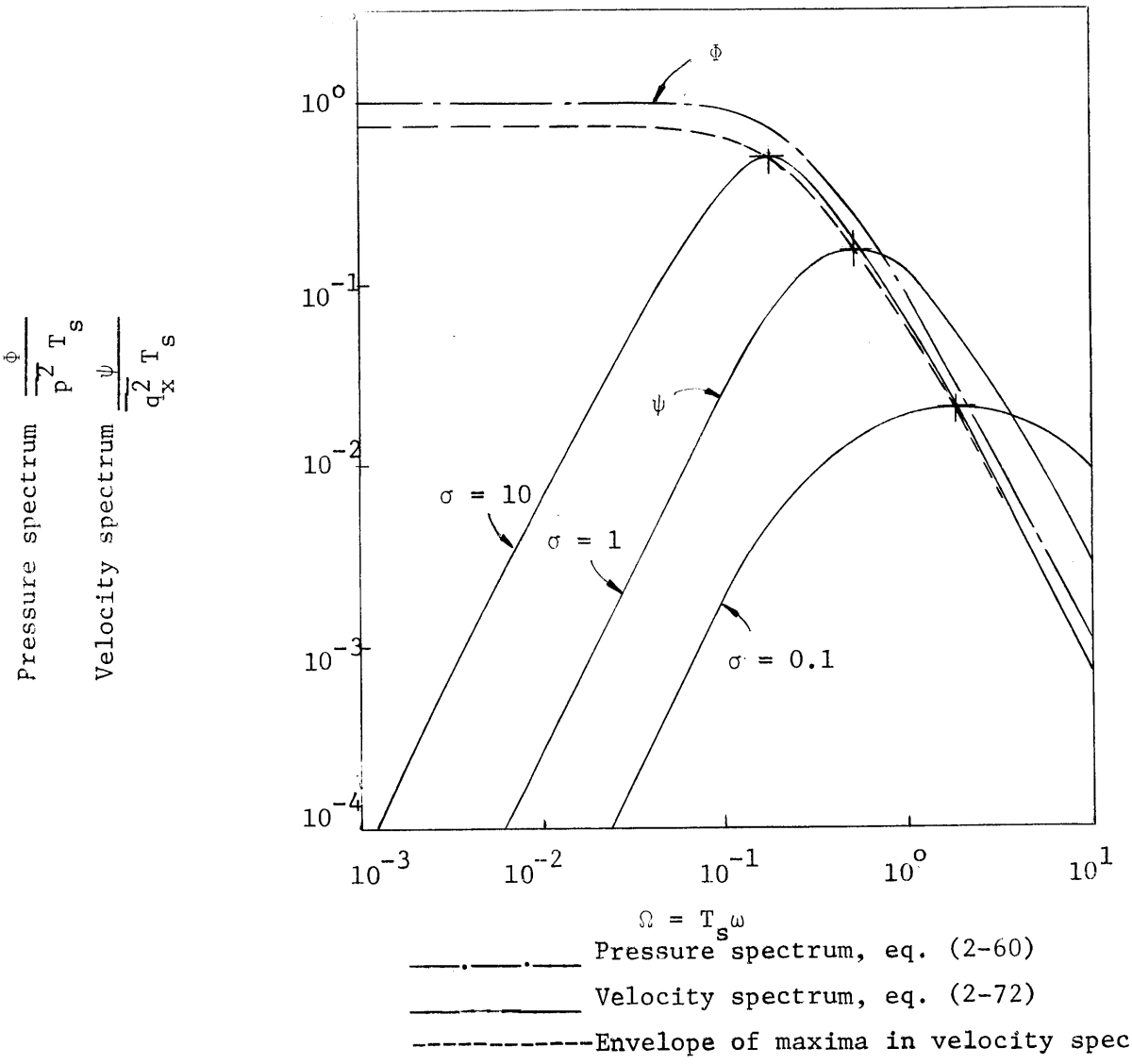

Fig. 2-8 Normalized velocity spectrum at y = 0 computed from eq. (2-71) (Porosity n = 0.70)

$$\overline{q_x^2} = \overline{q_y^2} = \int_{-\infty}^{\infty} (2m^2 + 1) \left(\frac{K}{\mu U_c}\right)^2 \frac{\Phi(\omega)\ \omega^2}{1 + \left(\frac{K\omega}{n\nu}\right)^2}\ d\omega \quad \text{at } y = 0 \tag{2-68}$$

and, after introduction of $\Phi(\omega)$ from (2-60),

$$\frac{\overline{q_x^2}}{u_*^2} = \frac{\overline{q_y^2}}{u_*^2} = (2m^2 + 1)\ a^2 \left(\frac{u_*}{U_c}\right)^2 \frac{\frac{n\sigma}{\pi}}{1 + \frac{\sigma}{\pi}} \quad \text{at } y = 0 \tag{2-69}$$

where σ is a dimensionless characteristic frequency defined by

$$\sigma = \frac{K}{n\nu}\ \frac{1}{T_s} \tag{2-70}$$

From its definition, for a given boundary material, σ is inversely proportional to the time scale of the imposed turbulent field. If the velocity spectrum $\psi(\omega)$ is defined by

$$\overline{q_{x,y}^2} = \int_{-\infty}^{\infty} \psi(\omega) d\omega \quad \text{at } y = 0$$

then the combination of the above equations gives

$$\psi' = \frac{\psi(\omega)}{\overline{q_{x,y}^2}\ T_s} = n\left(1 + \frac{\pi}{\sigma}\right) \frac{\sigma^2\Omega^2}{\left(1 + \pi^2\Omega^2\right)\left(1 + \sigma^2\Omega^2\right)} \tag{2-71}$$

which is plotted in fig. 2-8 for various values of σ. Differentiation of (2-71) shows that ψ' has a maximum at $\pi\sigma\Omega^2 = 1$, and the value of ψ'_{max} is

$$\psi'_{max} = \frac{n}{1 + \frac{\pi}{\sigma}} \tag{2-72}$$

As $\sigma \to \infty$, ψ'_{max} approaches n. In fig. 2-8 , the porosity n has been taken as 0.7. Changes in n will produce only slight displacements of the computed curves. Inspection of fig. 2-8 shows that the resonance peak in

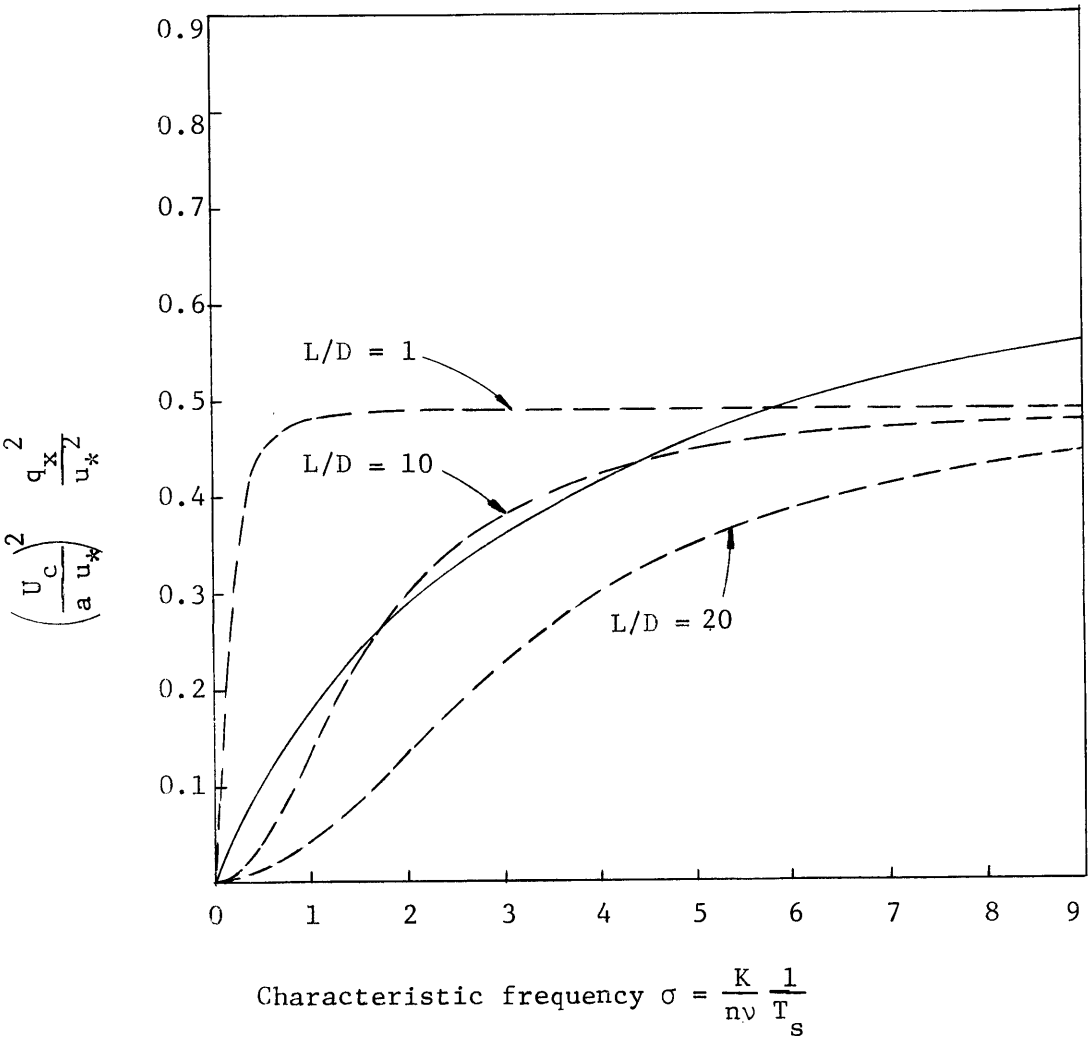

Fig. 2-9 Sinusoidal wave analysis compared with statistical analysis in terms of mean square velocity fluctuation at y = 0 (porosity n = 0.70).

the velocity spectrum is rather sharp. Only a narrow band of frequencies in the pressure fluctuations contribute to produce motion of the fluid. Thus, the magnitude of the velocity fluctuations is roughly proportional to the value of the pressure spectrum at the resonance frequency. As the spectrum tends to a constant for low frequencies, the velocity intensities also tend to a constant, which is independent of viscosity and permeability, as shown by equation (2-69). To compare with the single wave solution, equation (2-37) can be transformed by

$$\frac{K\omega}{n\nu} = \frac{2\pi K}{n\nu T} = 2\pi\sigma \frac{T_s}{T}$$

Expressing T_s by $D/\overline{U}$ and T by L/U_c,

$$\frac{K\omega}{n\nu} \approx 2\pi\sigma \frac{D}{L} . \qquad (2\text{-}73)$$

Thus, for $y = 0$ and $h \to \infty$, (2-37) becomes

$$\frac{\overline{q_{x,y}^2}}{u_*^2} = a^2 n^2 \left(\frac{u_*}{U_c}\right)^2 \frac{\left(2\pi\sigma \frac{D}{L}\right)^2}{1 + \left(2\pi\sigma \frac{D}{L}\right)^2} . \qquad (2\text{-}74)$$

Equations (2-69) and (2-74) have been plotted in fig. 2-9 for various values of L/D, again showing that qualitative agreement requires L/D to be of order 10.

2.6 Summary of the Porous Layer Flow Analysis

From the previous analysis, the single wave and statistical approaches must be regarded as mutually complementary. The first provides wider results, whereas the second is a guide for their evaluation. The main features of the solution are the vanishing of the momentum transfer term $\overline{q_x q_y}$ everywhere and the presence of a rather sharp resonance peak in the response of the flow to the fluctuating boundary pressure. The porous medium acts as a

filter with respect to the velocity fluctuations, depending on the dimensionless number σ which combines the permeability and porosity of the medium, the viscosity of the fluid and the time integral scale of the imposed pressure distribution. It should be expected, however, that both features could be substantially affected if the complete nonlinear equation (2-27) were used to describe the flow.

Concerning the application of this theory to the case of a porous wall pipe, some conclusions may be drawn. First, the thickness of the layer must be, from fig. 2-4, at least 0.3 L to be considered as infinite. But L has been shown to be of the order of 10 D. Therefore, the relative thickness h/D should be at least 3, which basically agrees with the conclusion drawn from fig. 2-6, but, on the other side, such a thickness would greatly contradict the assumption of a horizontal layer. There is no need, however, of assuming an infinite depth for the single wave analysis and, therefore, it is possible to approach the problem by estimating the significant parameters of a representative pressure wave from the statistical analysis, and then, using the single wave analysis to examine the flow.

As stated before, it is not possible to derive from this analysis the changes produced in the turbulent pipe flow by the presence of a porous wall. In general, in the equations for the porous medium flow, u_* is treated as an externally determined input, but in fact there is a feedback process, in which the pipe flow induces the motion in the porous medium and is in turn distorted by it. The balance of forces represented by u_* must be, therefore, a function of the porous medium flow. Accepting this fundamental limitation of the analysis, the equations developed in the previous sections provide reasonable criteria to judge the influence exerted by a porous wall on pipe flow.

CHAPTER 3

EXPERIMENTAL EQUIPMENT AND METHODS

3.1 Experimental Objectives

In accordance with the analysis presented in the previous chapter, an experimental program was designed, aimed at the comparison of the effects produced by two different types of wall on the major characteristics of turbulent pipe flow. The program included the following points:

(a) Construction of two pipelines, one with a conventional type of artificial roughness and the other with a thick layer of porous material lining the wall, both long enough to insure the development of uniform flow.

(b) Measurement of mean velocity distributions and pressure gradient for fully developed turbulent flow conditions, using standard pitot tubes.

(c) Measurement of intensity of turbulence in the axial and radial directions and of the corresponding Reynolds stress, using hot wire anemometry with single wire and x-array arrangements.

(d) Measurement of the turbulent energy spectrum.

In the next sections, a general description of the experimental equipment is given first, followed by the design considerations in selecting a suitable porous material and a discussion of the various experimental techniques.

3.2 General Description of the Equipment

The open-circuit air flow system is shown in figs. 3-1 and 3-2, and includes:

(a) an inlet box, approximately cubic in shape, with sides 4 ft. long, containing four M-S-A Dustfoe M-1000 air filters, rated at 1,000 cfm each, to protect the hot wires from dust deposit;

(b) the test pipe, approximately 40 ft. long and 10" diameter;

(c) a flexible hose connection to the blower, to reduce vibrations in the pipe;

(d) an American-Standard AH-13 blower at the downstream end, driven by a 10 h.p. squirrel cage induction motor.

Flow regulation was established through a Wood MSC-10-W variable speed belt drive which allowed for continuous blower speed control between 1,000

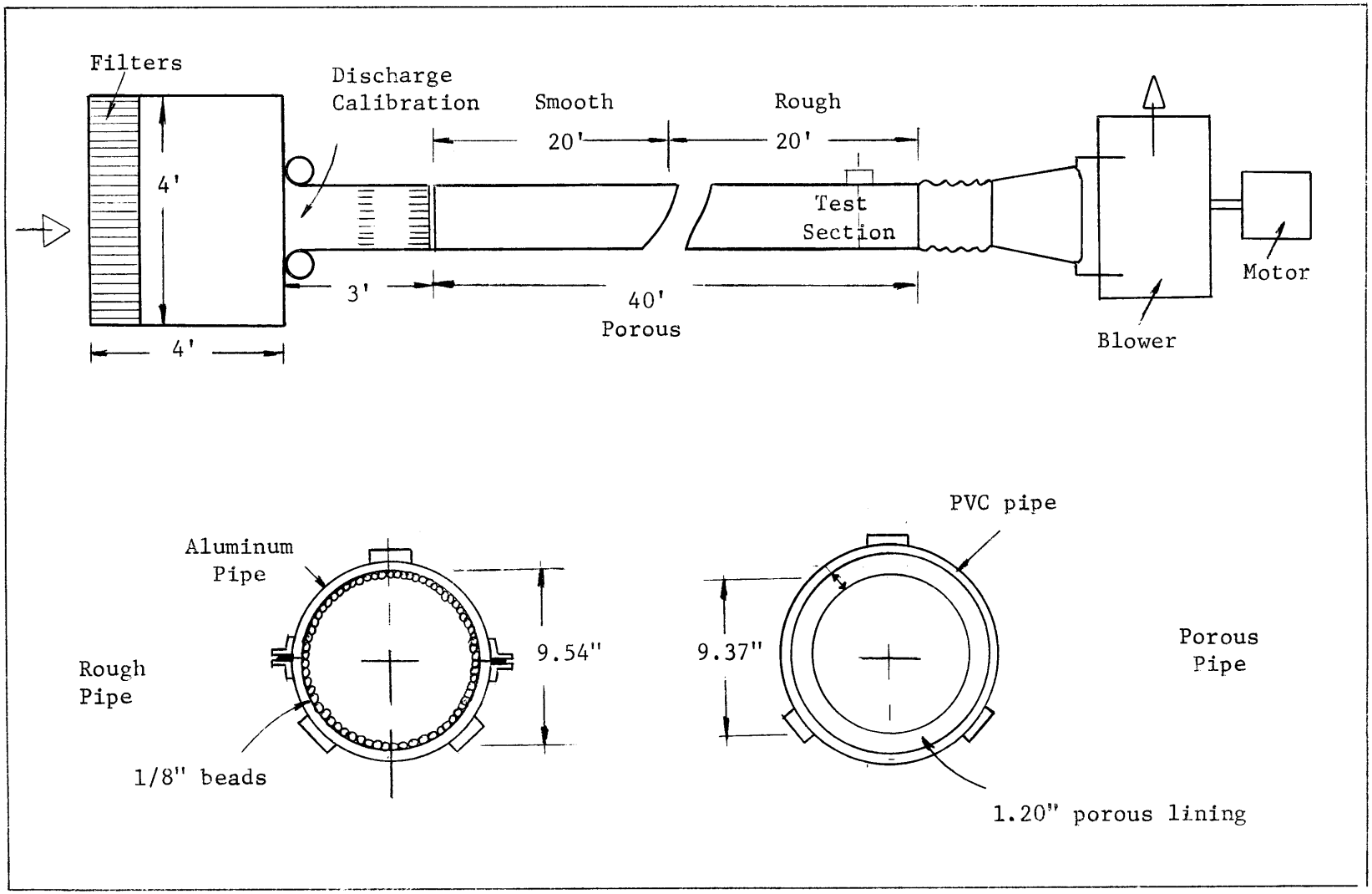

Fig. 3-1 Schematic description of the experimental equipment

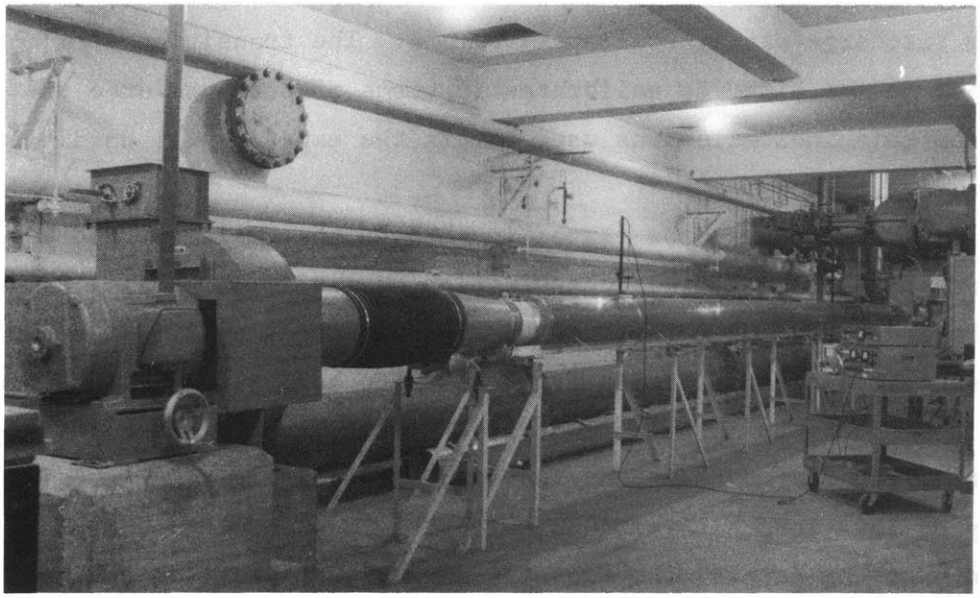

Fig. 3-2 General view of the equipment

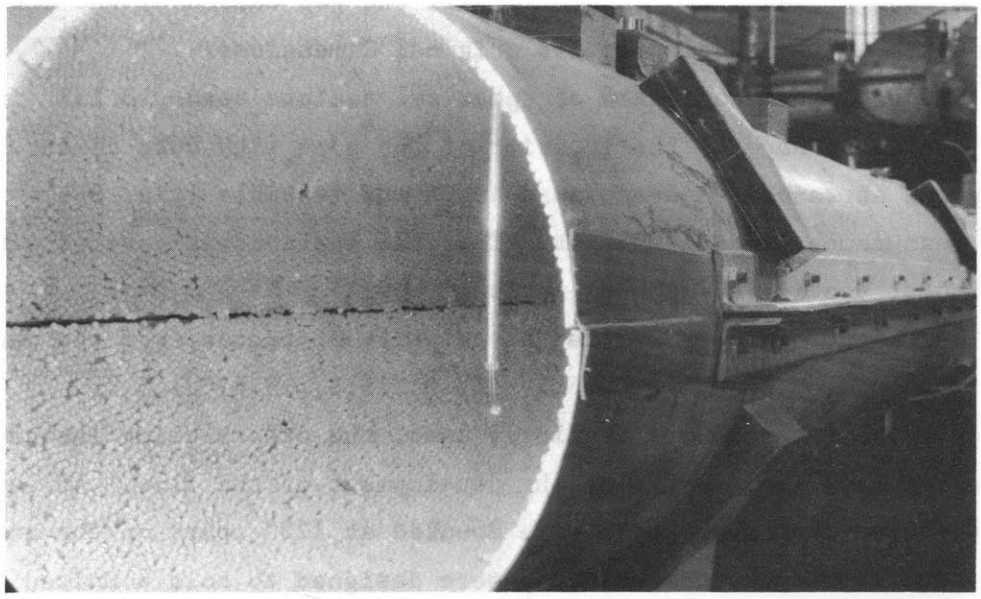

Fig. 3-3 Test section of rough pipe

and 1,750 rpm, and through an adjustable damper. As installed, the maximum discharge was approximately 50 cfs. The transition from the inlet box to the pipe was calibrated in terms of pressure drop vs. flow rate, and this indication was used to fix the experimental conditions for each run.

The first pipe to be tested (called in the following the "rough" pipe) was made from aluminum construction tubing, with nominal dimensions 10" O.D. and 0.094" wall thickness. A first length of 3 ft. contained the calibrated, rounded transition from the inlet box, plus three sections of Hexcel honeycomb, to insure symmetrical flow. The pipe itself was 40 ft. long, the last 20 ft. being covered with artificial roughness. The suitability of this length to produce uniform flow will be discussed in the next section. At the joints, the two ends were brought to flat contact and covered with duct tape to provide an air-tight seal. A steel coupling, 6" long, was tightened around the joint, forcing the two aluminum tubes to adjust to approximately the same shape.

The length of pipe to be roughened was split longitudinally and 1"-aluminum angles were mounted throughout the length for re-assembly (fig. 3-3). A rubber gasket was chosen to fill the gap caused by the cut and, therefore, keep the section to its original dimensions.

The roughness consisted of spherical acetate beads, 0.137" in diameter, bonded by hand to the interior of the pipe with Duco cement. The packing was at random, and as dense as it was feasible (fig. 3-4). A sample measurement indicated that 72% of the surface was covered with beads (the closest packing of spheres would give 91%).

Test sections were located at relative distances from the beginning of the roughness of x/D = 2.0, 6.25, 11.0, 15.8, 19.4, 21.5 and 23.0; in fact, only the last one was regularly used, the others being intended only for preliminary measurements of the development of the flow. At each test section, three aluminum blocks were mounted at 120° apart on the exterior of the pipe with epoxy cement; they were designed to hold a United Sensor manual traverse unit with vernier readings of 0.01", suitable to support every instrument used in this investigation (fig. 3-6).

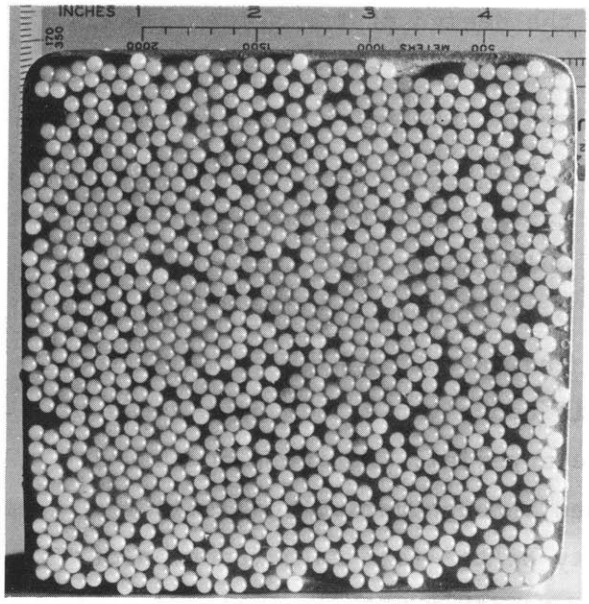

Fig. 3-4 Roughness Pattern (0.137" beads)

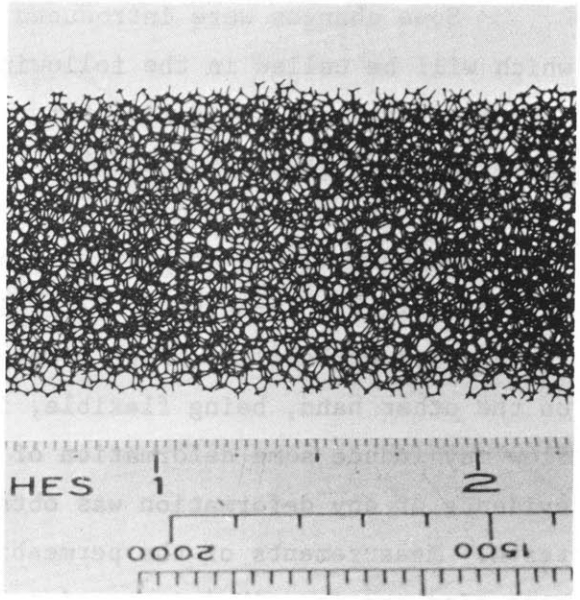

Fig. 3-5 Porous foam (sample shown is 1/8" thick)

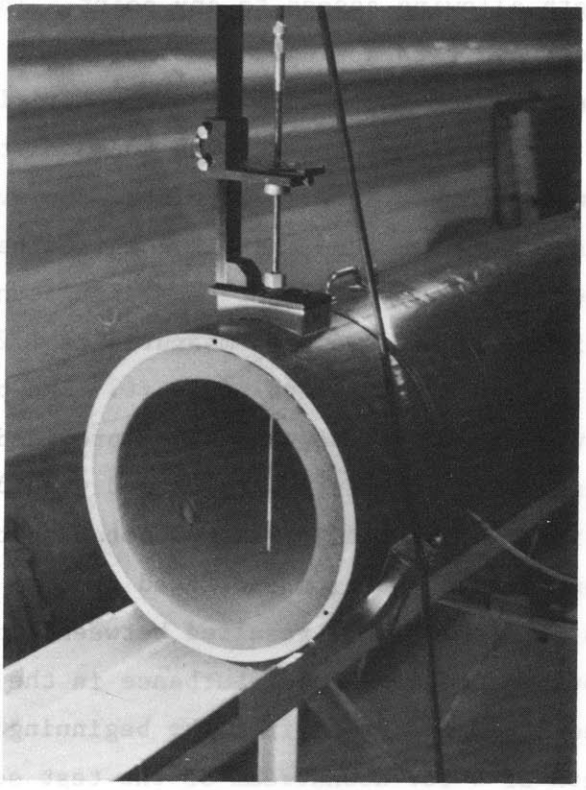

Fig. 3-6 Test section of porous pipe, showing traverse mechanism

Some changes were introduced in the design of the second pipe, which will be called in the following the "porous" pipe. In order to have approximately the same interior diameter as in the first case, polyvinyl chloride (PVC) pipe of 12.75" O.D. and 0.406" wall thickness was used. For the porous lining, a commercially available polyurethane material was chosen, Scott Industrial Foam, which has a very open skeletal structure with a porosity of 97% (fig. 3-5). Advantages of this material are its workability, high strength and extremely high permeability; on the other hand, being flexible, it is conceivable that high rates of flow may induce some deformation of the material. However, no visual evidence of any deformation was obtained through various preliminary tests. Measurements of the permeability of the foam as a function of pore size are described in section 3.4, together with an evaluation of its behavior based on the analysis presented in Chapter 2. A texture of 30 pores/inch was chosen, with a permeability of 1.3×10^{-6} ft^2.

To mount the interior lining, the PVC pipe was cut into 4 ft. long sections, this length allowing access to any point. The interior wall of every section was covered with a single sheet of foam. The longitudinal joint could be made very smooth because of the elasticity of the lining material. No bond was necessary between the foam and the pipe, friction and elasticity being enough to keep it in place. However, to prevent deformation during assembly, the ends and the longitudinal joint were bonded with silicone rubber cement. Details of the lining can be seen in figs. 3-5 and 3-6. The in situ thickness was measured as 1.20 inches. The same lining was applied to the total length of 40 ft. The pipe was continuously supported by a 4" wide aluminum channel, which provided at the same time the necessary alignment. The joints were sealed with duct tape. Close inspection of the interior of the joints was not possible, but what could be seen from the end of each section indicated that no protrusions existed; rather gaps, of no more than 1/8", resulted between consecutive sections but this should not produce a major disturbance in the flow. The test section was located at 43 diameters from the beginning of the porous lining. An additional length of 4 ft. downstream of the test section was intended

to protect it from any disturbance originating at the sudden end of the porous lining.

The instrumentation included pitot tubes for mean velocity measurements and a two-channel system of constant temperature hot wire anemometers, Flow Corporation model CTA3 (figs. 3-17 to 3-19). A Technical Products wave analyzer was available for energy spectral analysis. Details of the characteristics and operation of these instruments are given in the corresponding sections.

3.3 Development of Uniform Flow

There is little available information concerning the necessary length of a pipe to assure fully developed flow after a substantial change in wall roughness. On the basis of the classical studies of Nikuradse and others, it is usually recommended to have an inlet length of at least 40 diameters. However, a recent study by Barbin and Jones (1963) indicates that the length should be even higher. Barbin and Jones have measured not only mean velocity distribution and pressure gradient, but also the distribution of the three intensities of turbulence and of the principal Reynolds stress, in a smooth pipe with a total length of 43 diameters. Their conclusion is that neither of these characteristics has reached a uniform distribution after such a length, and that both turbulent intensities and Reynolds stress attain in the process of development values that are higher than those corresponding to fully developed conditions. More relevant to the present discussion are the measurements reported by Logan and Jones (1963) on flow development in a pipe after an abrupt increase in roughness, and by Carper, Heilhecker and Logan (1965) for a similar case in a two dimensional channel. In the first case, fully developed flow was approached but not attained in a length of 15 diameters of rough pipe, whereas in the second, a fully developed mean velocity profile was established within 20 widths of channel, but the turbulence pattern did not seem to have attained the uniform condition. In both cases, values of the Reynolds stress higher than the fully developed condition were obtained during the transition. From these results, it could be inferred that in many reported experimental studies, including the present one, the length was too short to yield reliable data on fully

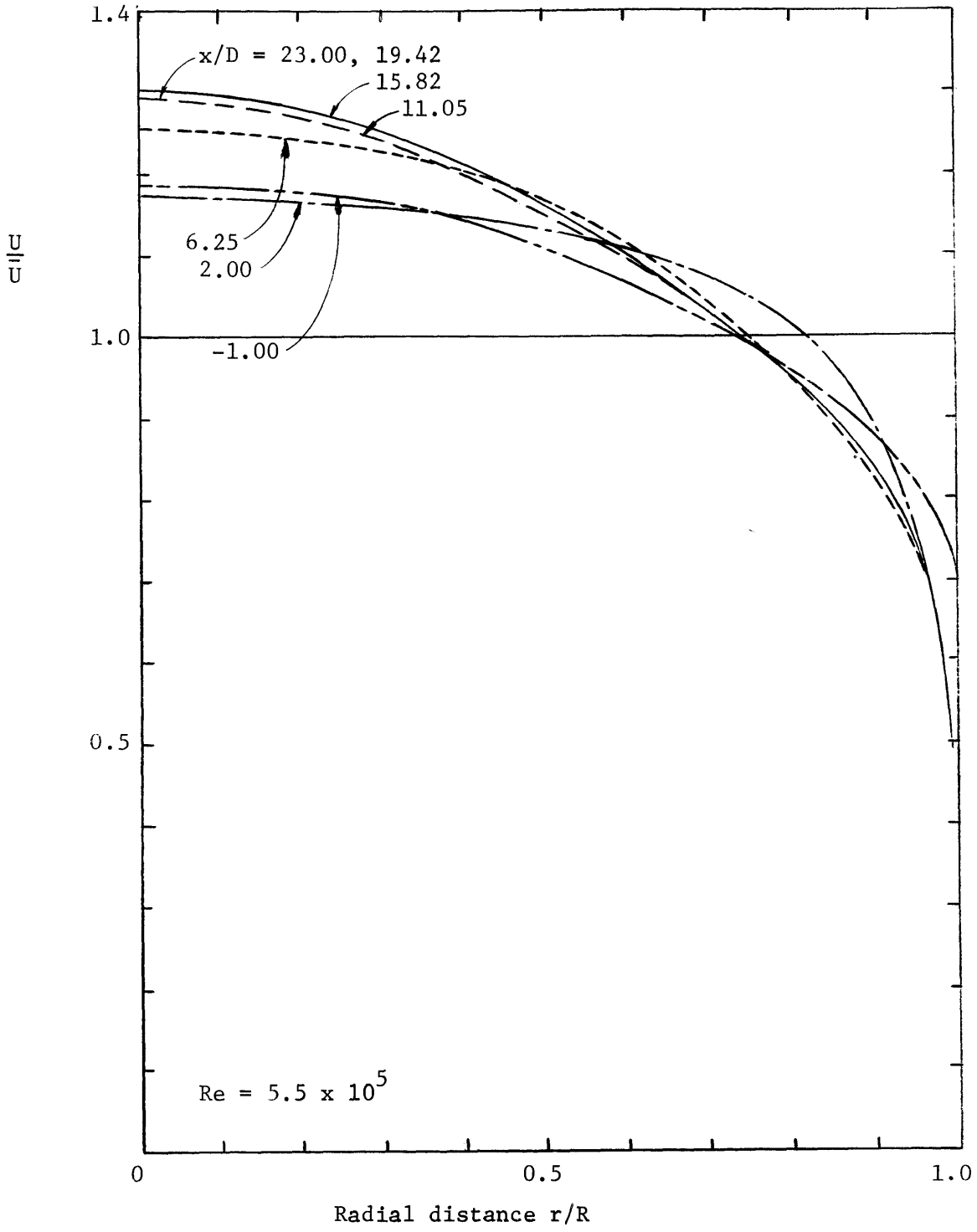

Fig. 3-7 Development of mean velocity profile in rough pipe (Moran, 1967)

developed flow. However, the same results show that, in the region close to the wall, the final distribution of turbulent intensities is approached within only 5 to 10 diameters, and that after this distance, most of the variations occur in the center portion of the flow. Therefore, a length of 23 diameters of rough pipe, as used in the present investigation, should give distributions of mean and turbulent velocities very close to the fully developed condition, especially in the wall region, which is the most significant.

A confirmation of the above results was provided by the preliminary measurements conducted in the rough pipe by Moran (1967). Figs. 3-7 and 3-8 are reproduced from this study, showing the mean velocity and axial turbulent intensity distributions at various sections. It is reasonable to expect that the fully developed condition, if not attained, will not be substantially different from the results at the last test section. To gain further evidence, the last 3 ft. of smooth pipe were lined with brass wire mesh, made of 0.054" wire with an opening of 0.279". The ratio of these dimensions was selected to produce an equivalent roughness several times higher than the pipe roughness, according to experiments by Stevenson as reported by Robertson, et al., (1965). The relative intensity of turbulence was measured at the test section before and after the installation of the wire mesh. The results, shown in fig. 3-9, indicate no trace of influence of the upstream change, giving further credit to the conclusion that the rough pipe was long enough to produce satisfactory results. It was not considered necessary to make similar measurements of flow development in the porous pipe, as its length, 43 diameters, was almost twice that of the rough pipe.

3.4 Design of the Porous Material

As explained in the previous section, the diameter of the pipe, the thickness of the porous layer and the type of material to be used were selected mostly on the basis of practical considerations. In order to determine the most adequate permeability, the equations developed in Chapter 2 were used. The various requirements to be satisfied were high intensity of

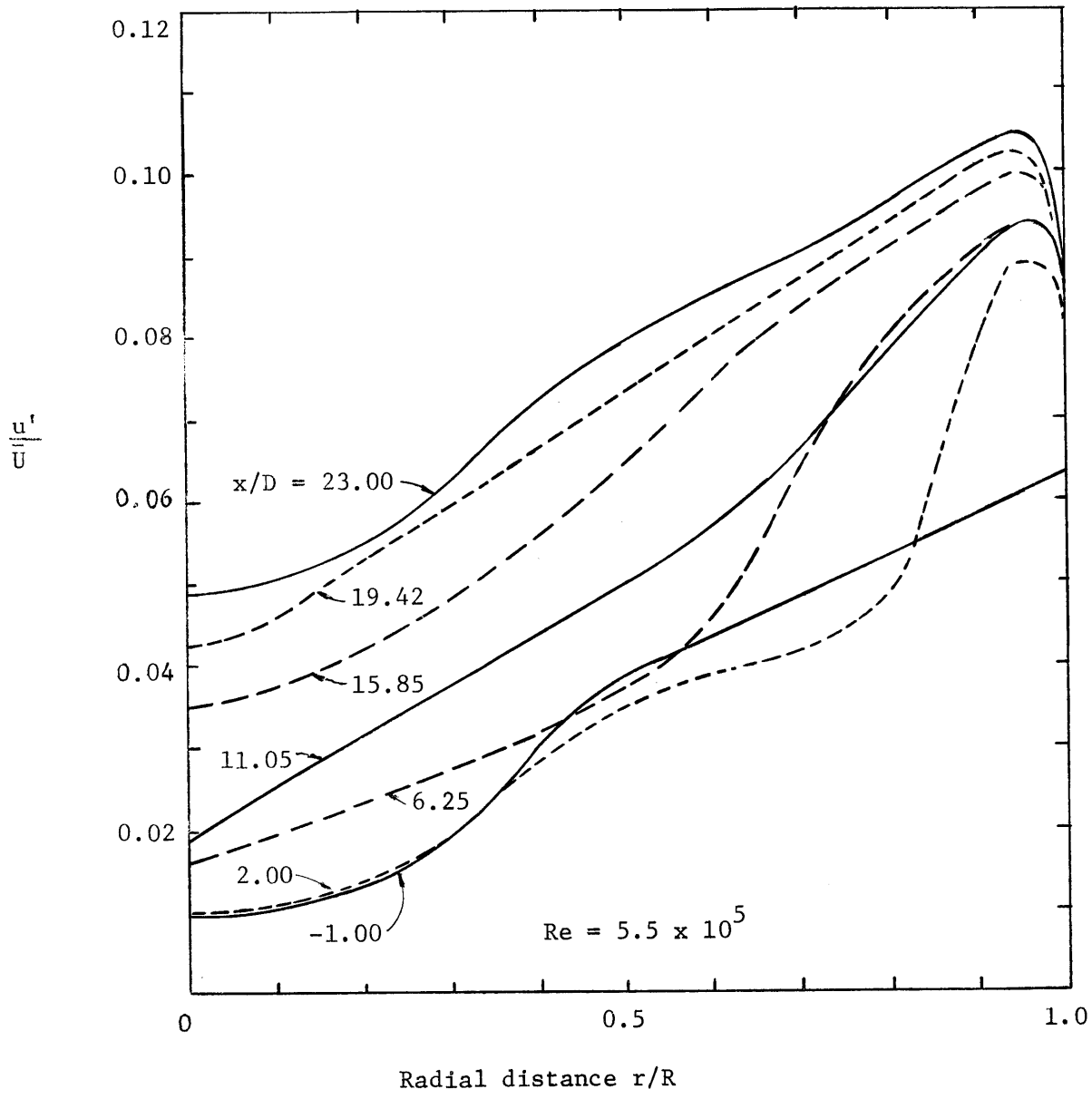

Fig. 3-8 Development of turbulent intensity distribution in rough pipe (Moran, 1967)

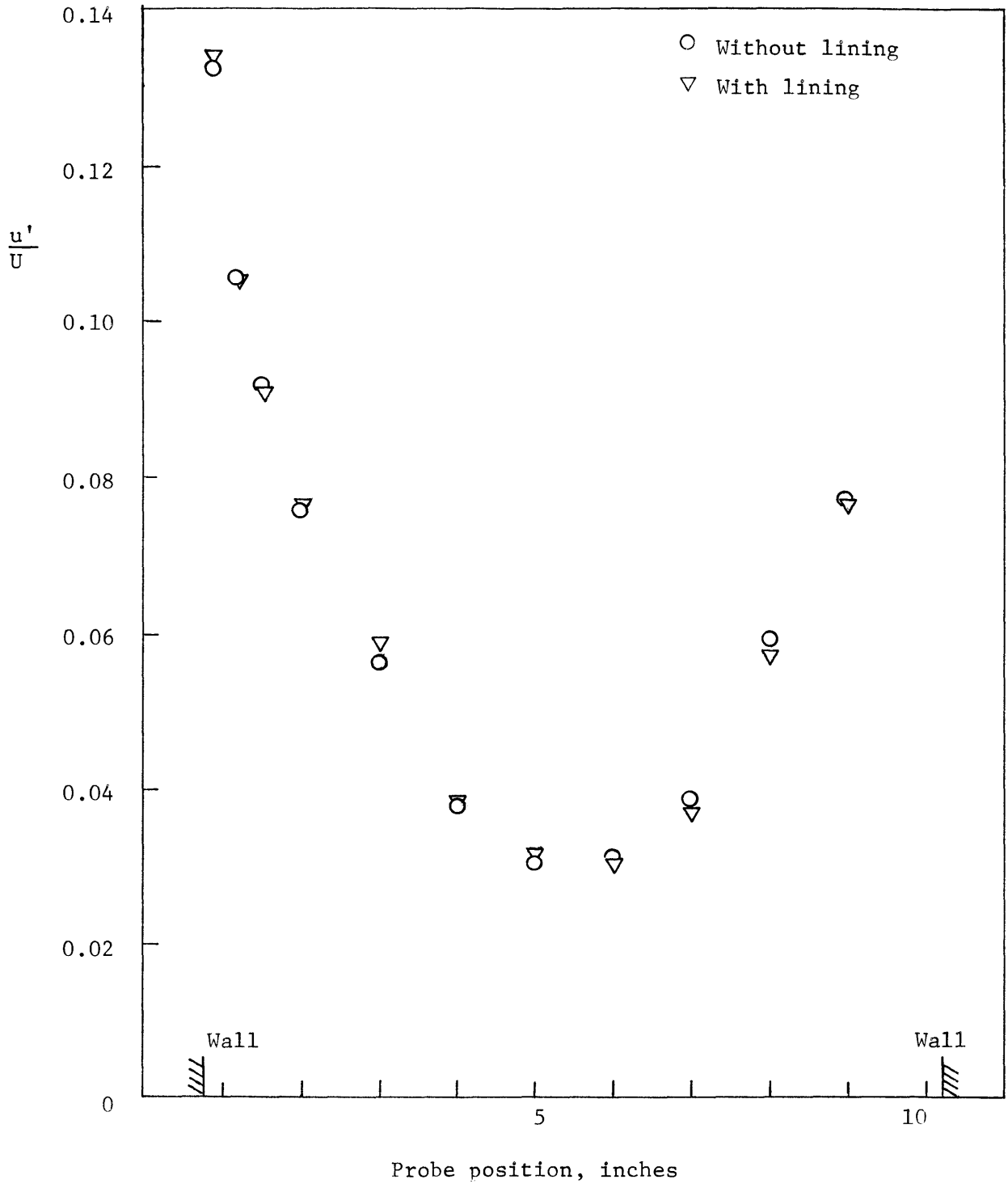

Fig. 3-9 Effect of wire cloth lining upstream of rough pipe on turbulence distribution in test section.

turbulence and high energy dissipation to assure substantial effects on the pipe flow, and, at the same time, low mean velocity through the porous medium and low permeability, in order that the linearized analysis of Sections 2.4 and 2.5 may be applicable. It was shown there that the single wave analysis yields results roughly comparable to the more accurate statistical analysis if a wave length of 10 D is used. Thus, the single wave equations will be used here.

For the purposes of a numerical comparison, it is convenient to simplify the equations by the introduction of suitable approximations. The porosity n = 0.97 of the material is taken as 1. The ratio $u_*/\overline{U}$ is approximated to 0.1 (the later results indicated that this value is quite accurate). With $U_c = 0.8\ \overline{U}$ and L = 10 D, the frequency becomes

$$\omega = k\, U_c \cong 0.5\, \frac{\overline{U}}{D}\ .$$

With the further introduction of a = 3 from (2-30) and $T_s = D/\overline{U}$,

$$\frac{K\omega}{n\nu} = 0.5\ \frac{K\overline{U}}{n\nu D} = 0.5\sigma$$

and the various results of the single wave analysis are transformed as follows:

(2-37) →

$$\begin{cases} \dfrac{q_x'}{u_*} = \dfrac{0.19\sigma}{\sqrt{1+\left(\dfrac{\sigma}{2}\right)^2}} \\ \dfrac{q_y'}{u_*} = \dfrac{q_x'}{u_*}\ \tanh kh \end{cases} \qquad (3\text{-}1)$$

(2-39) →

$$\frac{Q_x}{u_*} = 0.4\sigma \qquad (3\text{-}2)$$

(2-42) →

$$\frac{e}{E} = \frac{0.055\sigma}{1+\left(\dfrac{\sigma}{2}\right)^2}\ \tanh kh \qquad (3\text{-}3)$$

It is necessary next to evaluate the limitations of the linearization introduced in the equation of motion (2-27). For this purpose, a series of permeability measurements was conducted with samples of Scott Industrial Foam of 3 different textures, namely, 20, 45 and 80 pores/inch. Cylindrical samples of various lengths between 3 and 6" were placed in a 2" I.D. plexiglass air tunnel, in the same arrangement which was later used for velocity calibrations (fig. 3-23). The specific discharge was measured with nozzles of 1", 1/2" and 1/4" in diameter connected to a micromanometer reading to 0.001" of water. As the permeability of the material is very high, this equipment was not suited to measure the pressure drop for velocities low enough to be in the range of validity of Darcy's law. Therefore, K had to be computed from the complete equation (2-26). Preliminary computations indicated that the measurements could not be fitted to (2-26) with a coefficient 0.550 as proposed by Ward (1964). By trial-and-error, the constant was estimated as 0.13, this value giving a good universal behavior, as shown in fig. 3-10. Equation (2-26) has been transformed to

$$f_K = \frac{1}{Re_K} + C \qquad (3\text{-}4)$$

where

$$f_K = \frac{\sqrt{K}}{\rho q^2} \cdot \frac{dp}{dx} \quad , \quad Re_K = \frac{q\sqrt{K}}{\nu}$$

and C is a constant, 0.550 according to Ward and 0.13 according to these measurements. Most likely, C must be dependent upon the structure of the porous matrix, which for this foam is quite different from the granular materials tested by Ward. From (2-26) or (3-4), the ratio r between the linear and the quadratic terms is given as

$$r = \frac{\frac{\nu q}{K}}{0.13 \frac{q^2}{\sqrt{K}}} = \frac{7.7}{Re_K} \quad . \qquad (3\text{-}5)$$

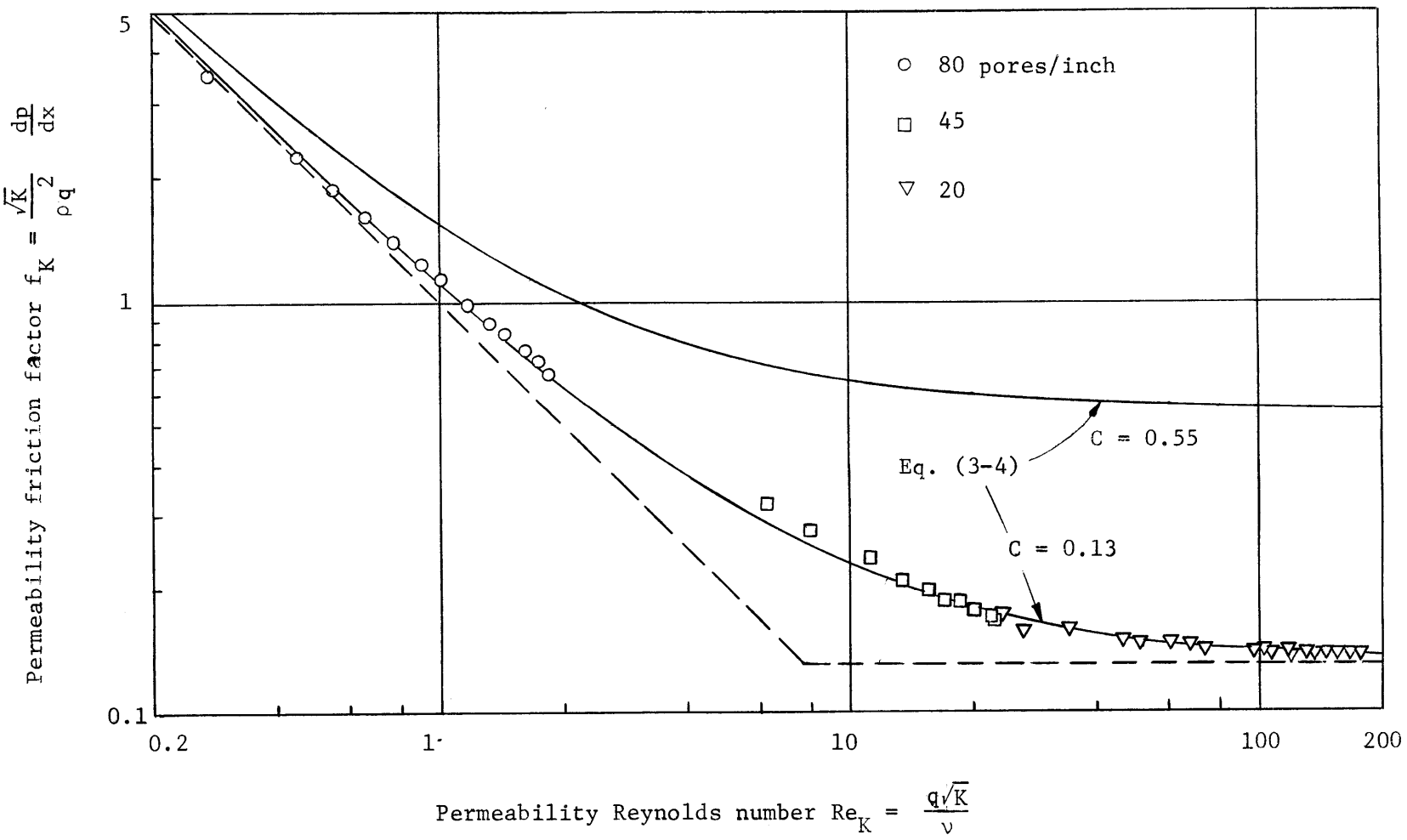

Fig. 3-10 Permeability tests with porous foam

Equation (3-5) can be used to estimate the limitations of the linear analysis, using as a representative velocity

$$q = Q_x + q'_x$$

and introducing the approximate numerical values of D = 0.8 ft. and $\nu = 1.6 \times 10^{-4}$ ft^2/sec. Linearization is valid for r >> 1, gradually deteriorates as r approaches 1 and is grossly in error for r << 1.

Equations (3-1), (3-2), (3-3) and (3-5) have been plotted in fig. 3-11, with $\frac{K}{\nu D}$ as abscissa, for values of $\overline{U}$ of 10, 50 and 100 fps (the actual velocities in the experiments were 20, 42 and 85 fps). In (3-3), h/D has been taken as 0.1, giving kh = 0.02π and tanh kh = 0.06. For reference, the intensity q'_x from the statistical analysis has also been plotted, in accordance with (2-69), which, after the same simplifications, becomes

$$\left(\frac{q'_x}{u_*}\right)_{\text{statistical}} = 0.38 \sqrt{\frac{\frac{\sigma}{\pi}}{1 + \frac{\sigma}{\pi}}} \qquad (3\text{-}6)$$

The variation produced in the ratio r by the use of (3-6) instead of (3-1) is also shown in the graph.

Fig. 3-11 serves to illustrate some of the limitations of the analysis presented in Chapter 2. For instance, the maximum in the energy dissipation occurs at a point where the threshold of linearization, r ≈ 1, has been greatly exceeded. The same is true of the point where the turbulence intensity becomes independent of permeability.

From Fig. 3-11, a design point of $\frac{K}{\nu D} = 10^{-2}$ was chosen as a compromise solution, satisfying more or less the requirements stated at the beginning. In fig. 3-12, the permeabilities measured in the tests previously described are plotted as a function of the pore size. A texture of 30 pores/inch was selected, with a permeability $K = 1.3 \times 10^{-6}$ ft^2,

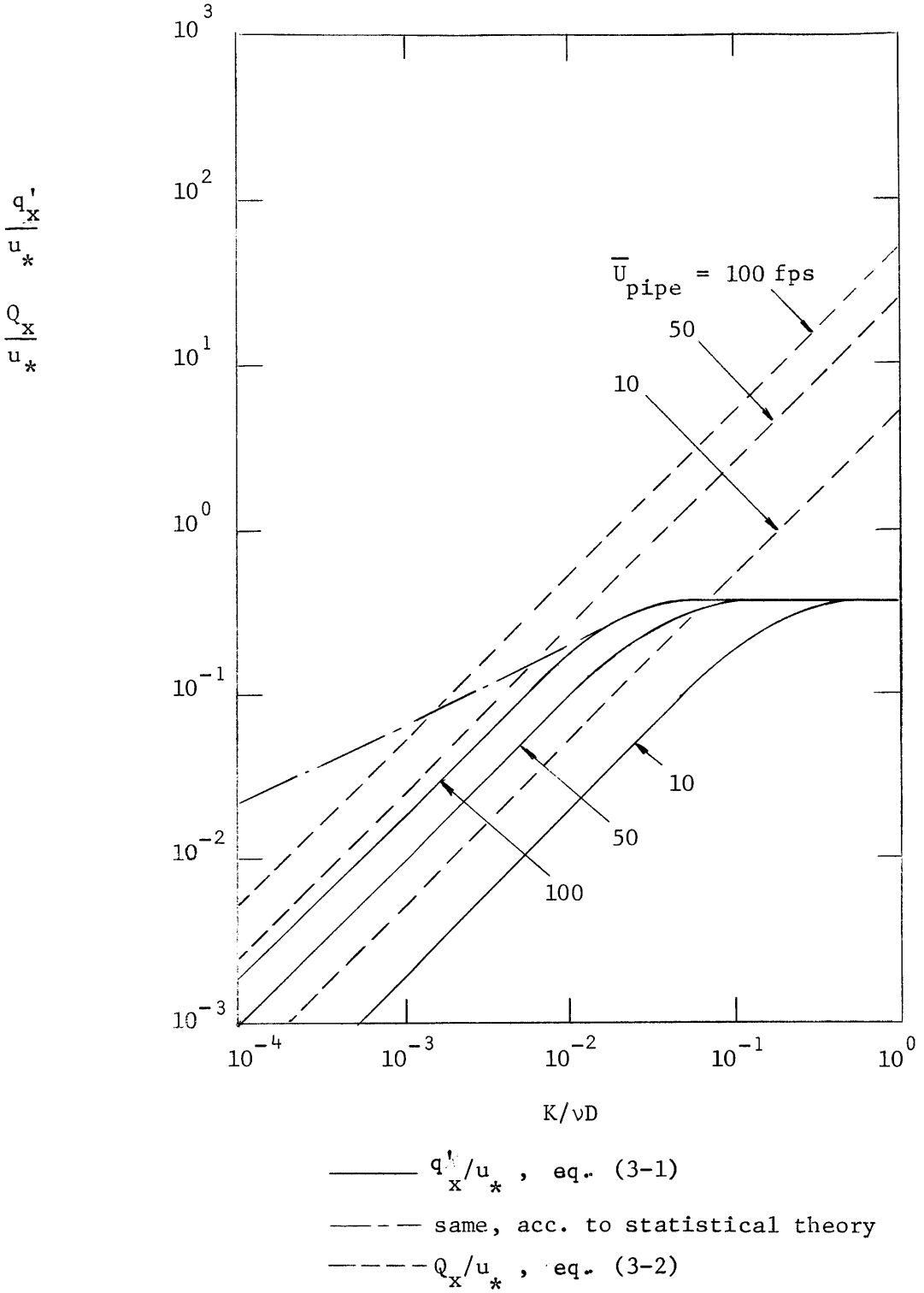

Fig. 3-11 (a) Representation of flow in the porous layer according to linearized theory with sinusoidal pressure at surface.

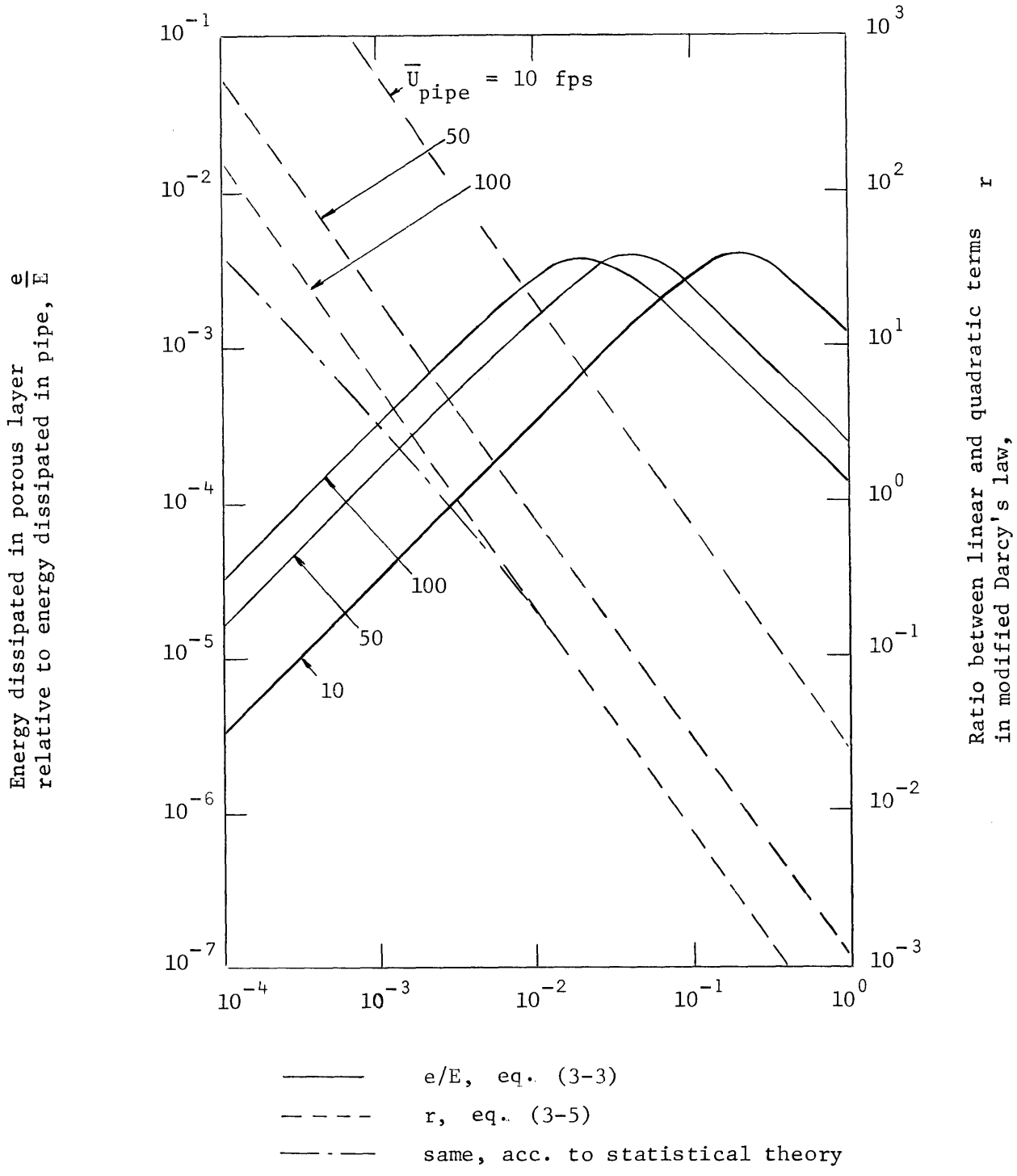

Fig. 3-11 (b) Representation of flow in the porous layer according to linearized theory with sinusoidal pressure at surface.

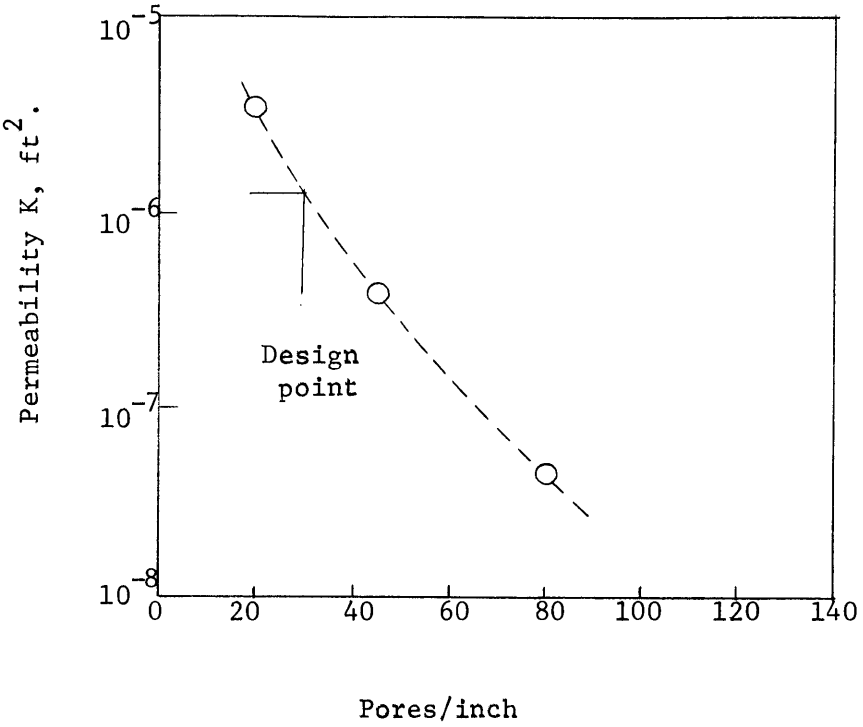

Fig. 3-12 Measured permeability of porous foam.

which, with D = 0.8 ft., gives $\frac{K}{\nu D} = 10^{-2}$ as required.

3.5 Measurement of Position in the Pipe

As it was discussed in Chapter 2, it is not possible to define on a geometrical basis the exact position of the wall for a substantially rough condition. Nonetheless, it is necessary to establish a reference origin to compare measurements taken with different probes and to define a diameter for normalization and for computations of discharge or mean velocity.

In the rough pipe, the method chosen was to express the position of the probe as the distance from the smooth aluminum pipe, which was measured as follows: after removing some roughness beads from the spot, a blunt rod was brought to contact with the wall; a topographic level was set up and the rod brought up to the optical axis; the difference between the two readings gives the distance from the optical axis to the wall. Then, the beads were replaced and the probe positioned on the optical axis. The method was reproducible within 0.01", which was the accuracy of the traversing mechanism. The diameters measured at three traverses, 120° apart, in the test section were 9.75, 9.68 and 9.83", with an average of 9.75". An effective distance y_B to the wall was defined by introducing a constant displacement in the origin for all traverses. Its determination will be presented together with the experimental results. The value chosen was 0.105", which, when subtracted from the average radius, gives an effective pipe diameter of 9.54". This value will be used to compute the mean velocity. For purposes of normalization, an effective radius R_B was defined as the effective distance y_B to the centerline, which in turn was found, not as the geometrical midpoint of the traverse, but rather as the axis of symmetry of the mean velocity profile. Differences between the axis of symmetry and the geometrical midpoint were of the order of 1/4" (fig. 3-13). In this way, the normalizing radii were different for the two sides of each traverse.

Essentially the same procedure was followed with the porous pipe. However, because the foam lining could not be removed at will, an arbitrary reference level was fixed during construction by bolting a metallic scale, graduated to 0.01", to the end of the pipe. The zero of the scale was referred to the wall of the PVC pipe. The mounting of the scale was tight enough to obtain reproducible positions; in this way, each probe could be referred to the scale by the use of a topographic level. The thickness of the lining was measured in place as 1.20 inches. This value was used to compute y, the distance to the wall. Because of the method of construction, this pipe was more regular than the previous one. Diameters (of the PVC pipe) measured at the test section at 120° apart were

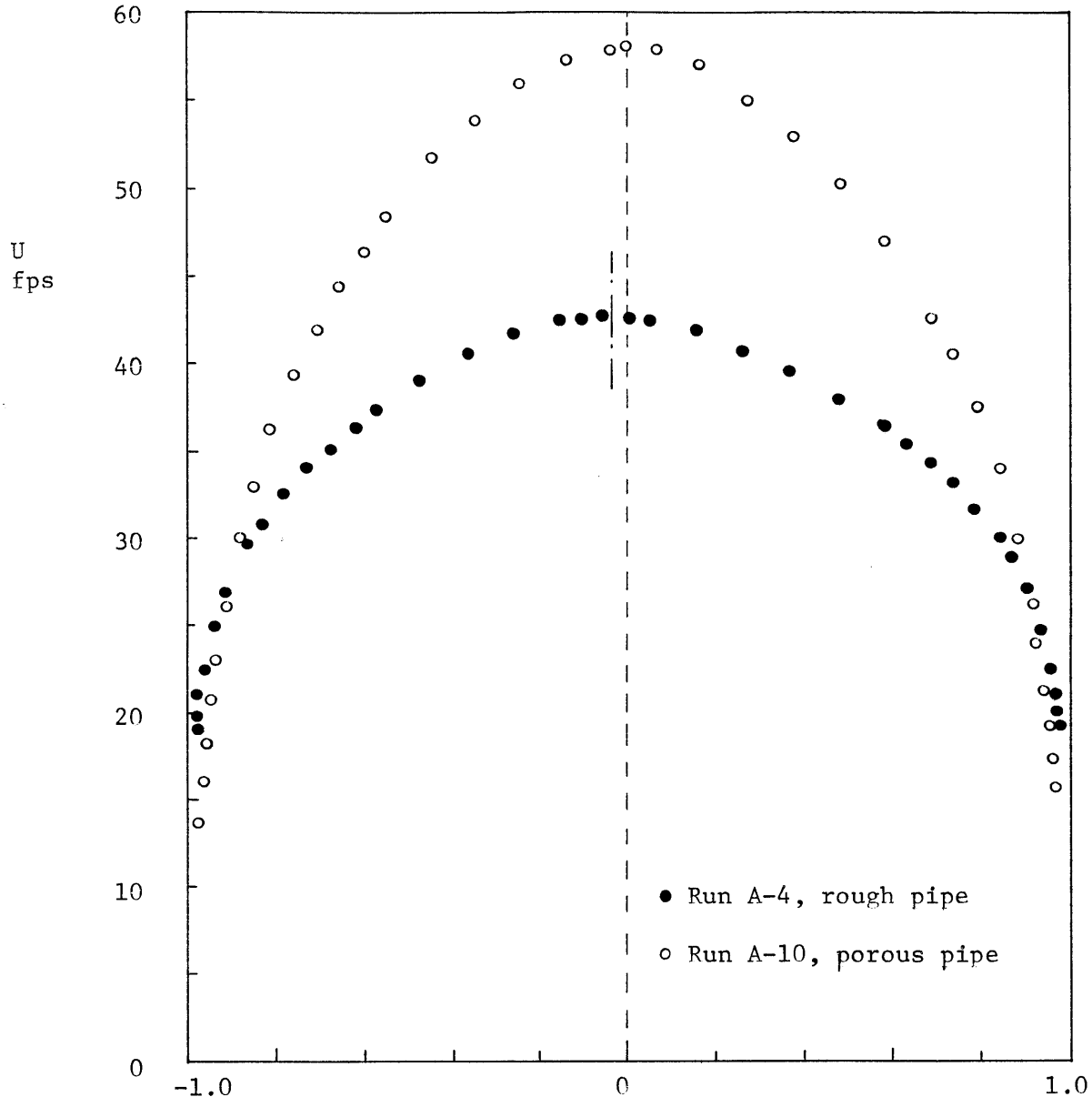

Fig. 3-13 Typical mean velocity distribution, showing slight asymmetry in rough pipe profile.

11.825, 11.80 and 11.84". The average pipe diameter, up to the interior surface of the porous material, was 9.42". The flow was very symmetrical, with the maximum velocity occurring within 0.03" of the geometric midpoint (fig. 3-13). Therefore, R_B was taken as one half of the geometric diameter.

3.6 Measurements of Static Pressure

Static pressure measurements are necessary to determine the pressure gradient and, hence, the friction factor and the shear velocity, and to compute the mean velocity from total head tube readings. In the first case, systematic errors are not important, because they will not change the overall gradient, but they may become important in the second case. There is little available information concerning the behavior of wall pressure holes in the presence of roughness. Polzin (1939) compared the pressure at a wall roughened with sandpaper with the static pressure read by a pitot tube in the center of the duct, for air velocities up to 50 ft/sec. The roughness height ranged from 0.005 to 0.02 inches and the hole diameter from 0.02 to 0.35 inches. In all cases the measured wall pressure was lower than the indication of the pitot tube, the difference in general tending to increase with velocity, but without a clear functional relationship. Polzin stresses the fact that the pressure difference is very sensitive to the roughness configuration around the hole. The largest differences were 2% of the velocity head at the centerline. This kind of experiment is difficult to evaluate, because of the uncertainty about the behavior of the pitot tube itself. Shaw (1960) has studied the effect of hole size on the pressure reading on a smooth wall. He found a fairly universal relationship between the pressure deviation ($\Delta p/\tau_o$) and the Reynolds number (du_*/ν), where Δp is referred to the extrapolated pressure as the diameter d of the hole approaches zero. The largest error Δp is + 2.8 τ_o. He also studied the effect of burrs produced by imperfect drilling. For the largest burr (0.03 d in height), the error Δp increased by a factor of 7. At any rate, these variations are very small; for a hole diameter as large as 10% of the pipe diameter, the error is of the order of 1% of the mean velocity

head. Chao and Sandborn (1965) have measured the pressure distribution around the spherical elements of the boundary roughness for a radial wall jet. They found some pressure variation in the upper surface of the spheres, but the pressure around the bottom half was essentially constant.

It can be concluded, therefore, that for pressure gradient measurements the roughness should not be a major source of error. In fact, the systematic error can be minimized by producing similar roughness configurations around each hole, and, of course, the importance of accidental variations is reduced by the averaging involved in the process. Accordingly, pressure holes were installed in the rough pipe as follows: at each test section, six holes, 1/16" in diameter, were drilled 60° apart; around each hole, four beads were glued to the wall in a square pattern. The surrounding roughness pattern was random, but closely packed. Such test sections were located at distances from the beginning of the roughness of $x/D = 3.80$, 8.60, 13.40 and 18.20. All six pressure holes at each section were individually tested. In general, the variation between each two holes was less than 1% of the mean velocity head, the largest ones being smaller than 2%; holes deviating noticeably from the average were discarded. Pressure differences were measured with a Dwyer No. 1420 water micromanometer, with an accuracy of 0.001" (of water) (see fig. 3-23).

For the porous pipe, little flow was expected to occur near the solid wall. Therefore, the design of the holes was not thought to be critical. Three holes, 1/16" in diameter, were drilled at 120° apart, every 2 ft. throughout the length of the pipe. As every piece of pipe was 4 ft. long, pressure test sections were located at 1 ft. from each end. As expected, deviations between individual pressure holes were smaller than in the rough pipe. The largest were of 0.5% of the average velocity head, in general being of the order of 0.2%, which is approximately the limit of accuracy of the micromanometer.

A more difficult problem is the determination of the local static pressure, to be used in connection with total head tube readings to find the mean velocity. Hinze (1959), while discouraging the use of static

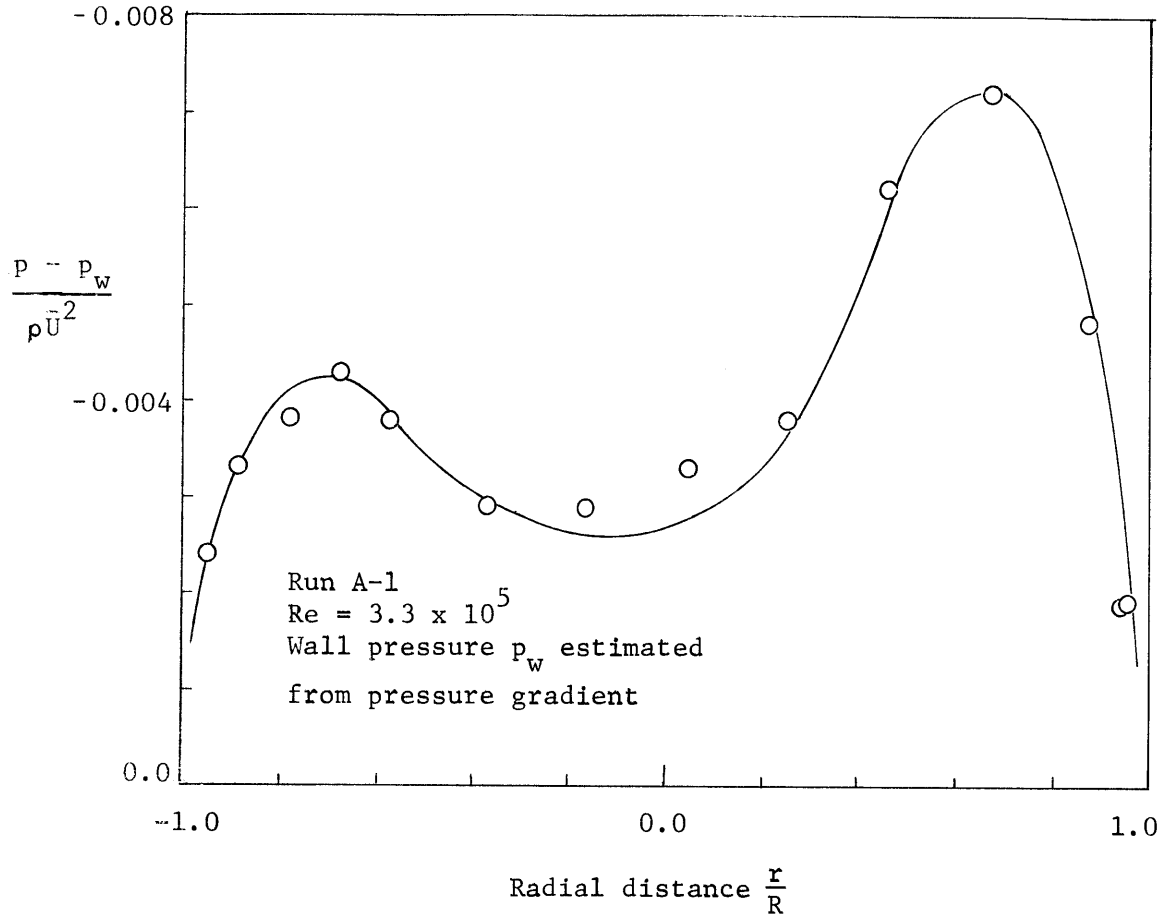

Fig. 3-14 Static pressure distribution in rough pipe, measured with static pressure tube

pressure tubes because of turbulence induced errors, points out the lack of any more reliable alternative. Sandborn (1955) has evaluated the pressure distribution from turbulence measurements in a smooth pipe. His results show a maximum deviation referred to the wall pressure of 0.3% in terms of the centerline velocity head. This figure is in agree-

ment with an earlier, similar estimate by Fage (1936). Fage also indicates that the static pressure tube itself shows only from one half to one fourth of the pressure deviation, depending on the local turbulence levels. Some static pressure tube traverses were made during the preliminary stages of this investigation in the rough pipe, using a 1/8" tube, with two 1/32" holes located 3/4" from the upstream end. Some results are shown in fig. 3-14, the maximum deviations being of the order of 1% of the average velocity head. The trend is similar to the curves shown by Fage and Sandborn, but the absolute deviations are larger, which is consistent, because the relative levels of turbulence are higher in a rough pipe. In view of the uncertainty covering the subject, the procedure was simplified by using a constant static pressure throughout the cross section, equal to the wall pressure as determined from interpolation in the pressure gradient profile at the location of the tip of the total head tube. In the region close to the centerline, such method does not introduce errors larger than 0.5% in the computed velocity. However, close to the wall, where the velocities are much lower and the pressure deviations the highest, errors of up to 2% are to be expected.

3.7 Measurements of Mean Velocity

Although mean velocities can be obtained from hot wire readings simultaneously with turbulence values, the reliability of the method is low. Therefore, independent measurements were taken with a cylindrical total head tube, 0.125" outside diameter (figs. 3-15 and 3-21). The pressure coefficient for the tube was assumed to be 1.0. Hurd, Chesky and Shapiro (1953) have shown that this assumption is true for $Re > 2{,}000$, with the Reynolds number Re defined in terms of local velocity and interior diameter of the tube. The minimum measured velocity was of 8 ft/sec, which gives $Re \approx 500$. For this value, a pressure coefficient of 0.99 is to be expected; however, since very few measurements fell in this range, no correction was applied.

Other factors that are usually corrected for are turbulence, velocity

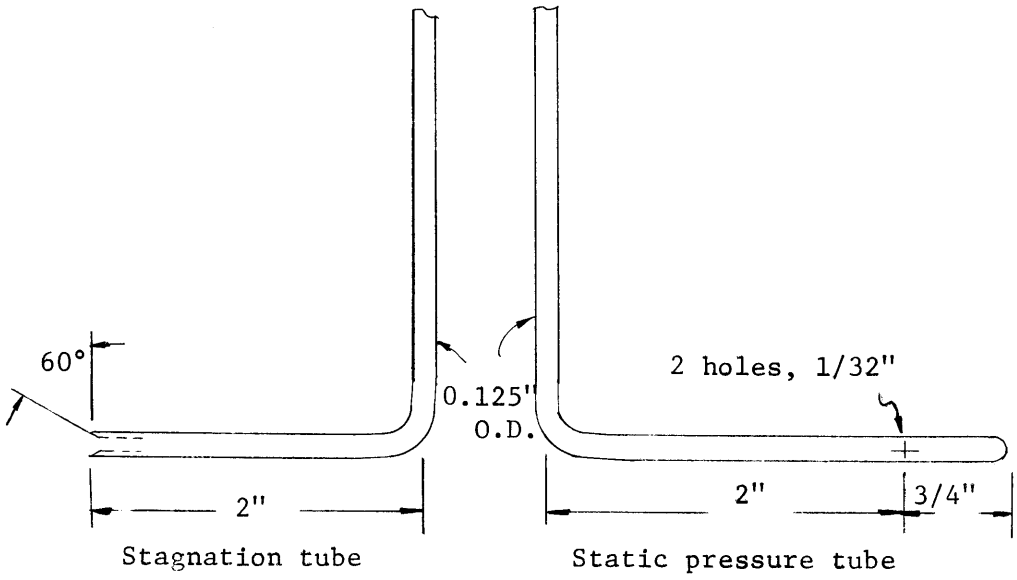

Fig. 3-15 Pitot-tube sketch.

gradient and wall proximity. Goldstein (1936) proposes a turbulence correction based on the total intensity of turbulence, $q^2 = u'^2 + v'^2 + w'^2$:

$$p_{total} - p_{static} = \frac{1}{2} \rho U^2 + \frac{1}{2} \rho q^2$$

Hinze (1959) finds more proper to use only u'^2 in the correction, but he also mentions some experiments where turbulence actually decreased the pressure difference. For the present purpose, the correction is important only close to the wall, where the turbulence is highly anisotropic. Therefore, q^2 is not very different from u'^2, allowing the use of

$$p_{total} - p_{static} = \frac{1}{2} \rho U^2 \left[1 + \left(\frac{u'}{U} \right)^2 \right] \qquad (3\text{-}7)$$

Other corrections were applied using the following results of MacMillan (1957). Because of the velocity gradient, there is a displacement of the effective position of the tube given by 0.15 d, where d is the outside diameter. On the other hand, because of the wall proximity, the true velocity is larger than the measured velocity by an amount ΔU, which MacMillan gives in a graph of $\frac{\Delta U}{U}$ versus y/d. Data reduction was made with the IBM 360 computer at the M.I.T. Computation Center. For this purpose, the above corrections had to be expressed in an analytic format. First, the measured velocity U_m was computed from:

$$U_m = \sqrt{2g\ \Delta h_w\ \frac{\rho_w}{\rho_a}} \tag{3-8}$$

where Δh_w is the reading of the micromanometer referred to the wall pressure, in height of water, and ρ_w, ρ_a are the densities of water and air. ρ_w was assumed constant, and equal to 997 g/ℓ. ρ_a was corrected for temperature and atmospheric pressure by

$$\rho_a = 1.2929\ \ \frac{273.13}{T}\ \ \frac{P}{760}\ \ g/\ell \tag{3-9}$$

where T is the absolute temperature in degrees centigrades and P is the atmospheric pressure in mm Hg. T was measured to 0.1°C with a standard mercury thermometer, located in the pipe downstream from the test section.

The turbulence correction was formulated in terms of smooth wall turbulence measurements, normalized to shear velocity. It was assumed, as a starting point, that a similar distribution for u'/u_* would obtain in the rough and porous pipe. This expectation was substantiated by the later measurements (see Chapter 4), and the form of the correction was left unchanged. In fig. 3-16, Laufer's measurements for u'/u_* are plotted in a semilogarithmic graph versus y/R. A good fit is given by:

$$\frac{u'}{u_*} = \exp\ (0.805 - 1.15\ \frac{y}{R}) \tag{3-10}$$

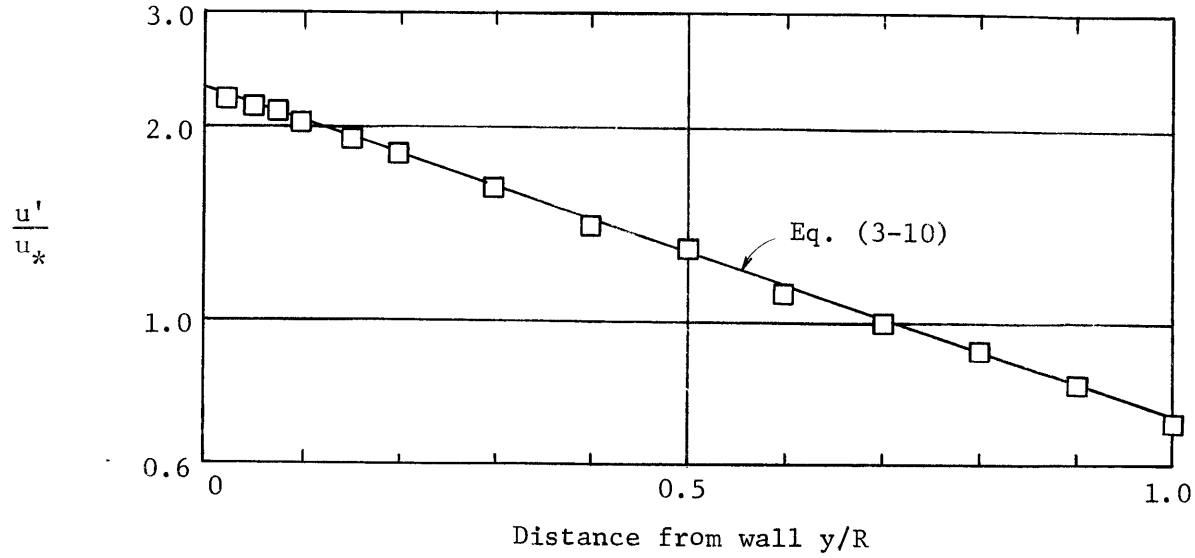

Fig. 3-16 Pitot-tube correction for turbulence. Data by Laufer (1954).

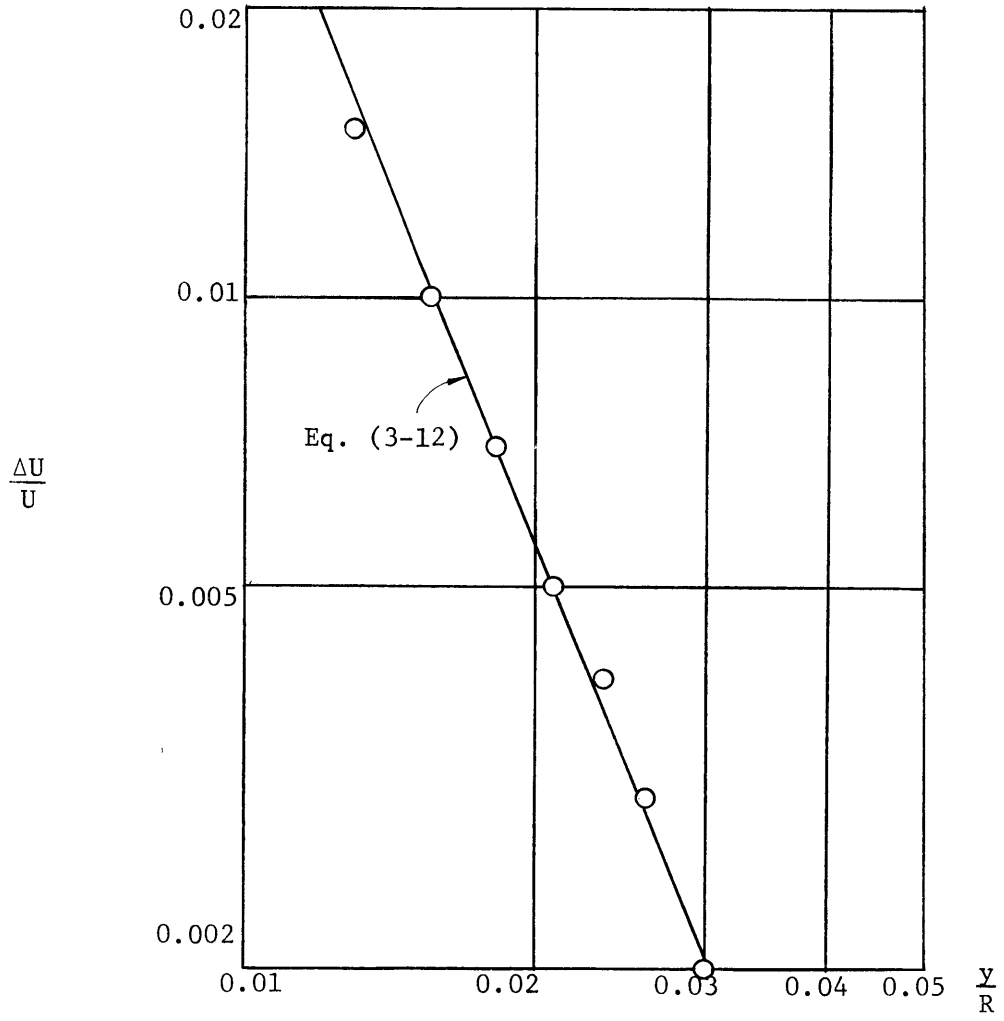

Fig. 3-17 Pitot-tube correcton for wall proximity according to MacMillan (1957), for tube diameter 0.125", pipe diameter 9.54".

Obviously, such an expression is not valid close to the wall, but the total head tube could not be placed closer to the wall than the limit of validity of (3-10). For y and R, y_B and R_B as defined in section 3.4 were used.

The correction for velocity gradient amounted to a constant shift in y, since only one tube was used. Thus:

$$y_c = y + 0.15\ d = y + 0.019 \text{ inches} \tag{3-11}$$

where y_c is the corrected distance to the wall. Finally, MacMillan's correction for wall proximity was fitted to the expression

$$\frac{\Delta U}{U} = 3.65 \times 10^{-7} \left(\frac{y}{R}\right)^{-2.46} \tag{3-12}$$

which is plotted in fig. 3-17. The true velocity is computed then as

$$U = U_m \sqrt{1 - \left(\frac{u'}{u_*}\right)^2 \left(\frac{u_*}{U_m}\right)^2} \left(1 + \frac{\Delta U}{U_m}\right) \tag{3-13}$$

It must be noted that there is considerable uncertainty as to the validity of applying these corrections, found on smooth walls, to a rough pipe and more so to a porous boundary. An indication of the magnitude of the correction is given in fig. 3-18, which shows some typical comparisons between corrected and uncorrected velocity distributions for both pipes.

The pressure drop between the inlet chamber and a section of the pipe 1 ft. downstream was calibrated in terms of discharge by two total head tube traverses in the smooth aluminum pipe 1 ft. before the beginning of the roughness. The calibration curve is shown in fig. 3-19, together with the discharge integration performed from the mean velocity distributions in the test section of both the rough and porous pipes. No velocity corrections were applied in the discharge computations.

3.8 Hot Wire Anemometry

The turbulence measurements were made with a two-channel system

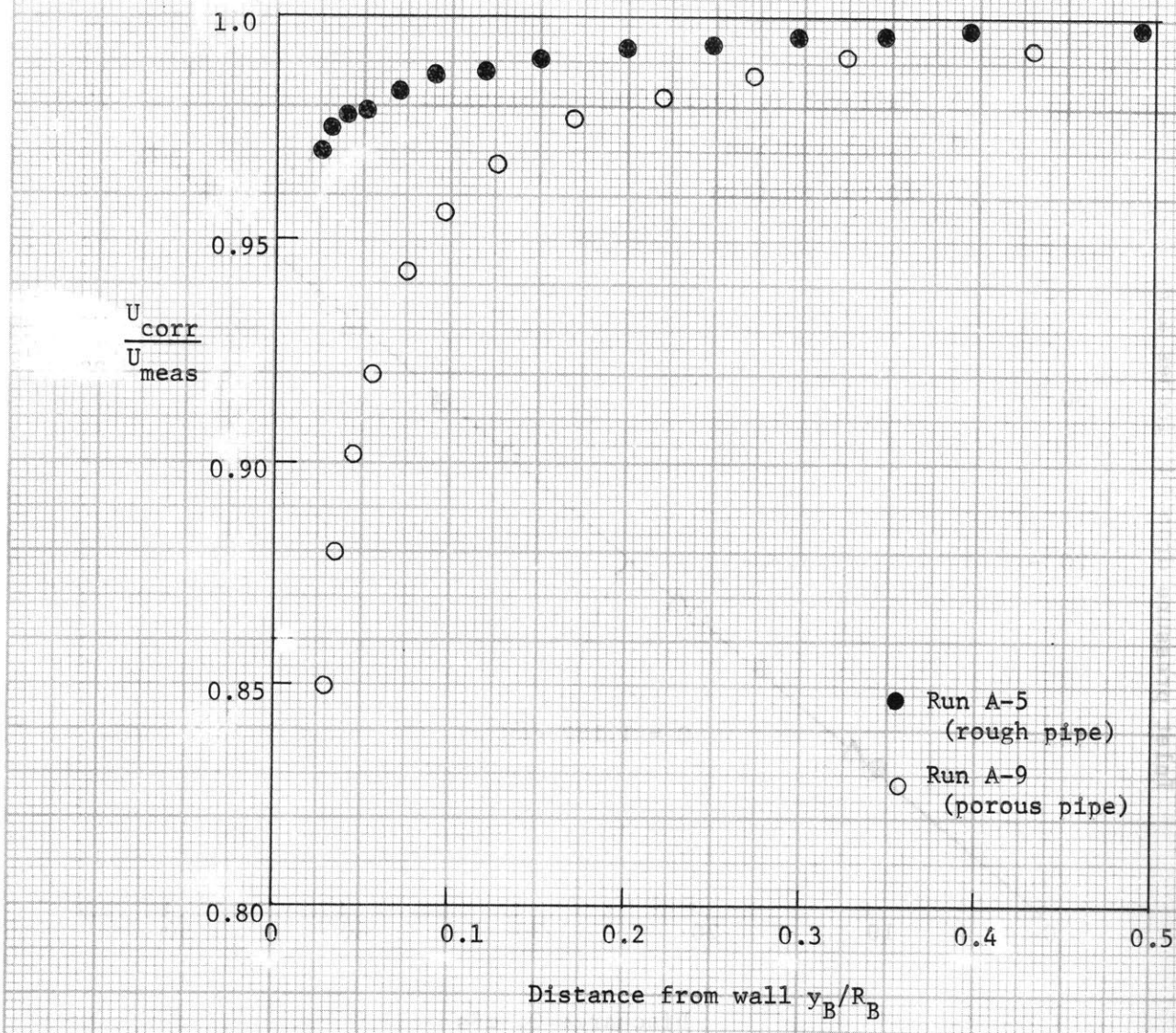

Fig. 3-18 Ratio of corrected velocity to velocity measured by pitot tube.

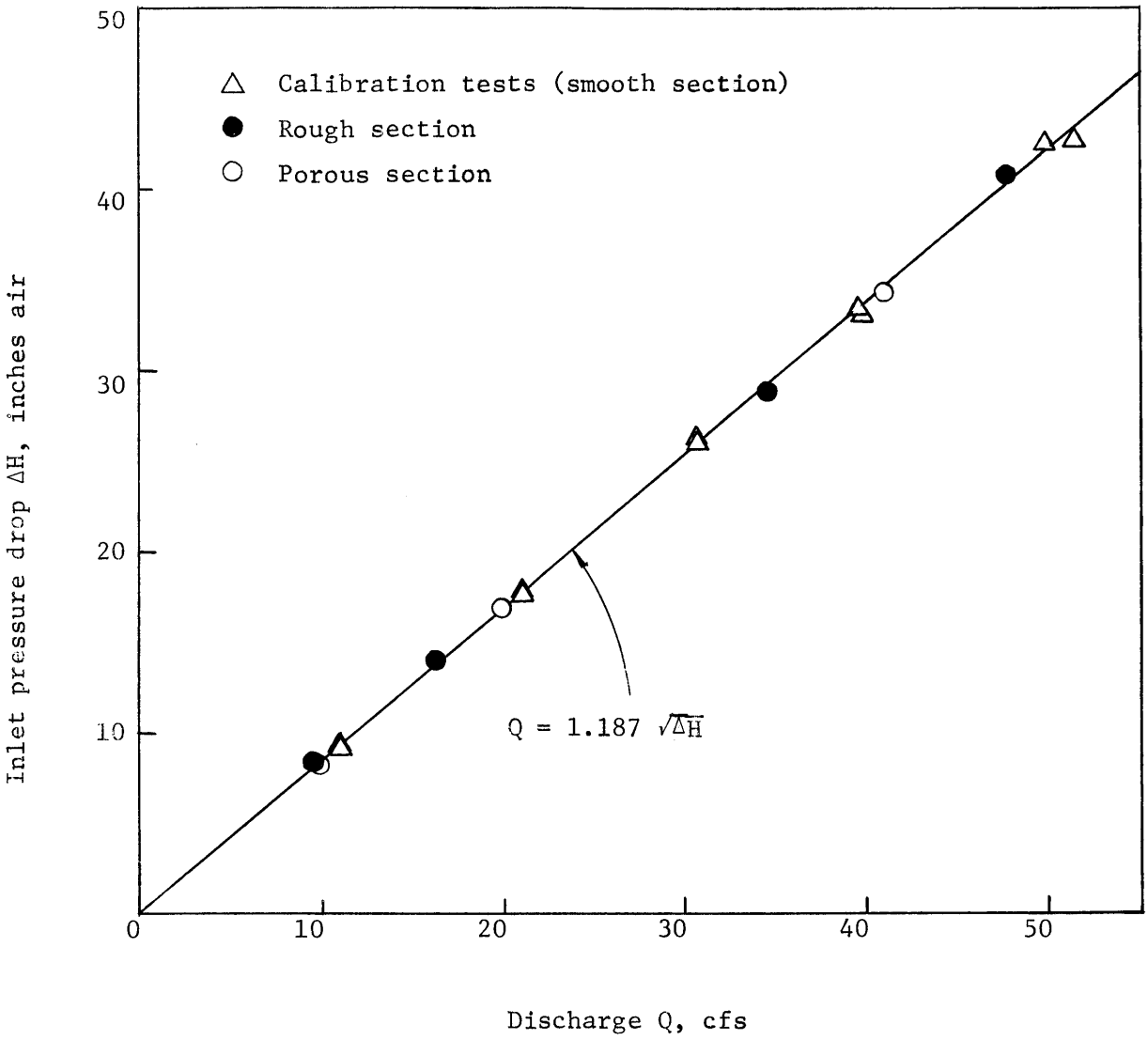

Fig. 3-19 Discharge measurements.

of constant temperature anemometers, manufactured by Flow Corporation, model CTA3 (fig. 3-20). Occasionally, a linearizer, model 4835C of Flow Corporation, was used. Mean voltages were measured with two DC voltmeters, Digitec model 201. For RMS voltages, Flow Corporation model 900-5 was used. This is a slightly modified version of Hewlett-Packard model 3400A true RMS meter, which extends the frequency range to 2 cps and provides an averaging time of 20 sec. A Technical Products wave analyzer system, consisting of analyzer model TP-627, oscillator model TP-626 and integrator model TP-645, was available for energy spectrum measurements.

Two probes were used (figs. 3-21 and 3-22). One was a straight, single-wire probe, 1/4" diameter, with the last 1-1/4" reduced to a diameter of 1/8". The other was an x-array probe, with the two wires mounted at the end of long, curved prongs to minimize the influence of the support. The tip was of the plug-in type, since such an arrangement did not permit to introduce the probe through the wall of the pipe. In all cases, tungsten wire, 0.00015" in diameter, was used with the two ends copper-plated to be soldered to the prongs. The nominal length of the sensitive portion of the wire was 0.044", with probable variations of 10 to 20% for individual wires.

The theory of operation of the hot wire anemometer is well covered in many publications, such as Kovasznay (1954) or Hinze (1959). The procedure, however, is rather involved and leaves room for many sources of error, as is testified by large disagreements among different published data. In order to clearly explain the method followed in the present investigation, some repetition of well-known equations is inevitable.

Essentially, the method consists of the cooling of an electrically heated thin wire by the fluid flow. A feedback system regulates the electric current in the wire to keep its resistance, i.e., its temperature, constant. Therefore, the basic equation of operation equates the power supplied to the wire with the heat transfer from the wire to the fluid. If I is the electric current in a wire of resistance R at an absolute temperature T_w, V is the velocity normal to the wire and T_a is the fluid temperature, then the empirical heat transfer relationship for a wire of

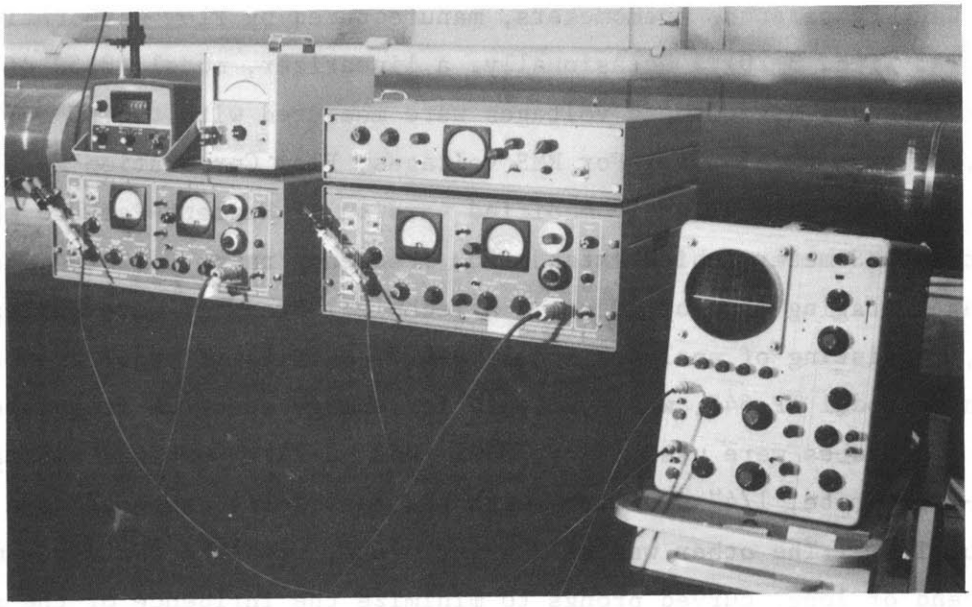

Fig. 3-20 Hot wire anemometry system

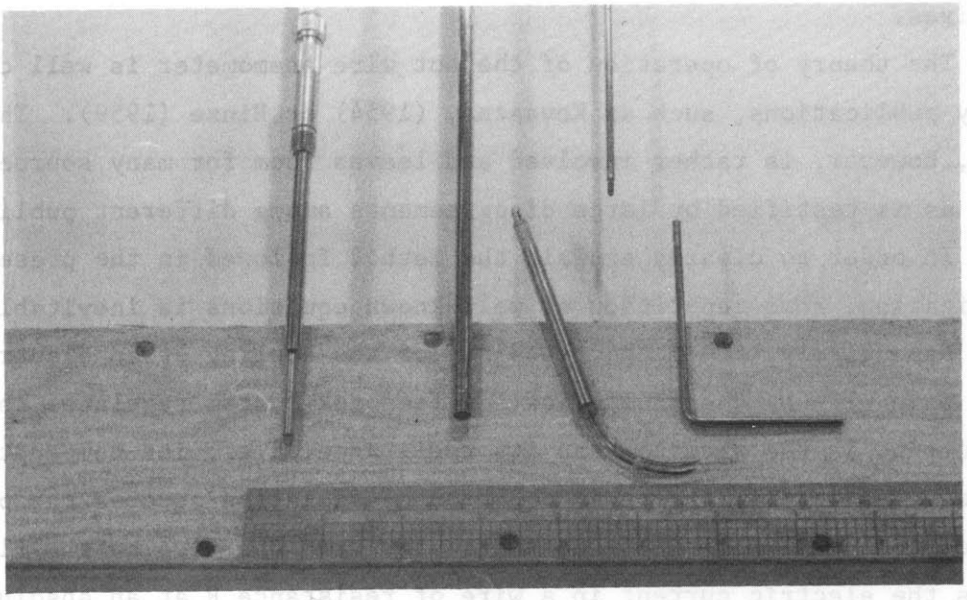

Fig. 3-21 Instruments: single wire probe, x-array probe with plug-in tip, stagnation tube

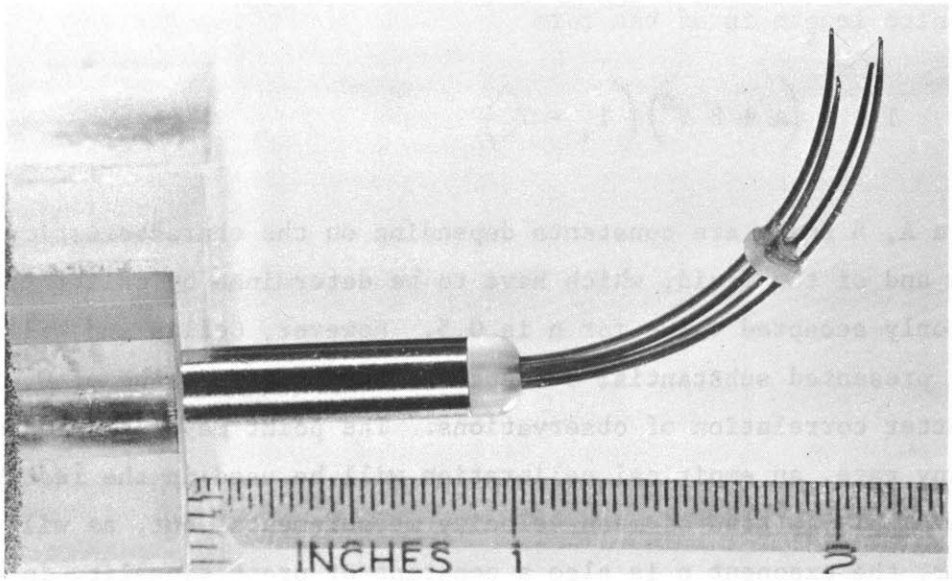

Fig. 3-22 Close-up view of x-array probe

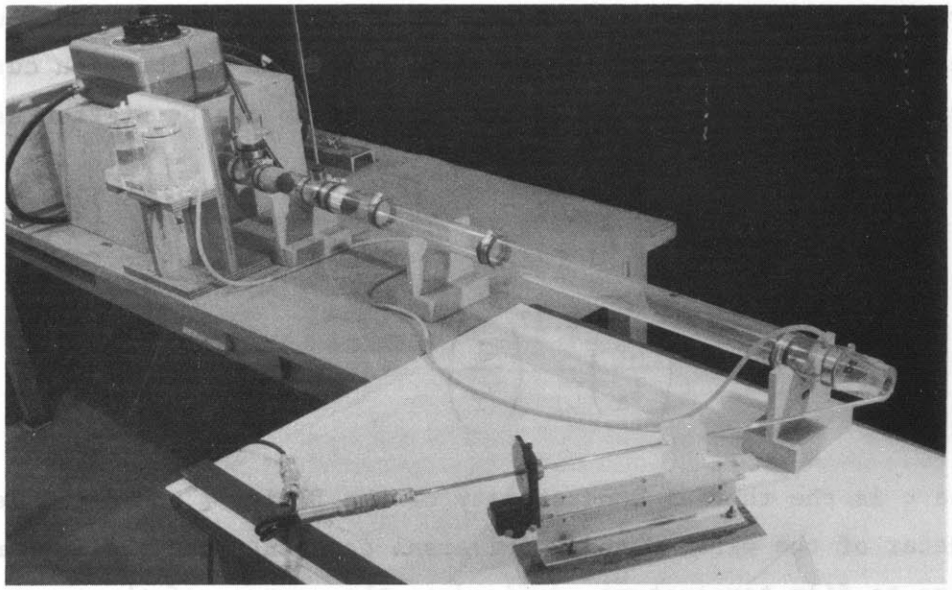

Fig. 3-23 Calibration unit

infinite length is of the form

$$I^2R = \left(A + B\,V^n\right)\left(T_w - T_a\right) \tag{3-14}$$

where A, B and n are constants depending on the characteristics of the wire and of the fluid, which have to be determined by calibration. The commonly accepted value for n is 0.5. However, Collis and Williams (1959) have presented substantial evidence to show that a value of 0.45 produces a better correlation of observations. The point may seem academic, since, at any rate, an empirical calibration will be used in the reduction of data. This is true of mean velocity measurements, but, as will be shown later, the exponent n is also a constant of proportionality in the expression for the intensity of turbulence (see eq. 3-25) and in this case the difference becomes significant. Both values for n were tested during this investigation. Fig. 3-24 shows some typical calibration curves, the use of the exponent 0.45 giving a clearly better fit to a straight line than 0.50. Therefore, the value 0.45 was definitely adopted.

Collis and Williams also give expressions for the constants A and B, which are useful not to predict their exact value, better found from experiments, but to establish corrections to the calibration curve for varying ambient conditions. Their expressions can be written as

$$\left.\begin{aligned} A &= C\,\pi\,l\,\kappa_f\left(\frac{T_f}{T_a}\right)^{0.17} \\ B &= D\,\pi\,l\,\kappa_f\left(\frac{T_f}{T_a}\right)^{0.17}\left(\frac{d}{\nu_f}\right)^n \end{aligned}\right\} \tag{3-15}$$

where κ is the thermal conductivity of the fluid, l and d the length and diameter of the wire, C and D universal constants and the subscript f refers to film temperature, defined as the average of the temperatures of the wire and of the fluid. From (3-15), an approximate temperature correction can be derived, noting that, for the range of temperatures

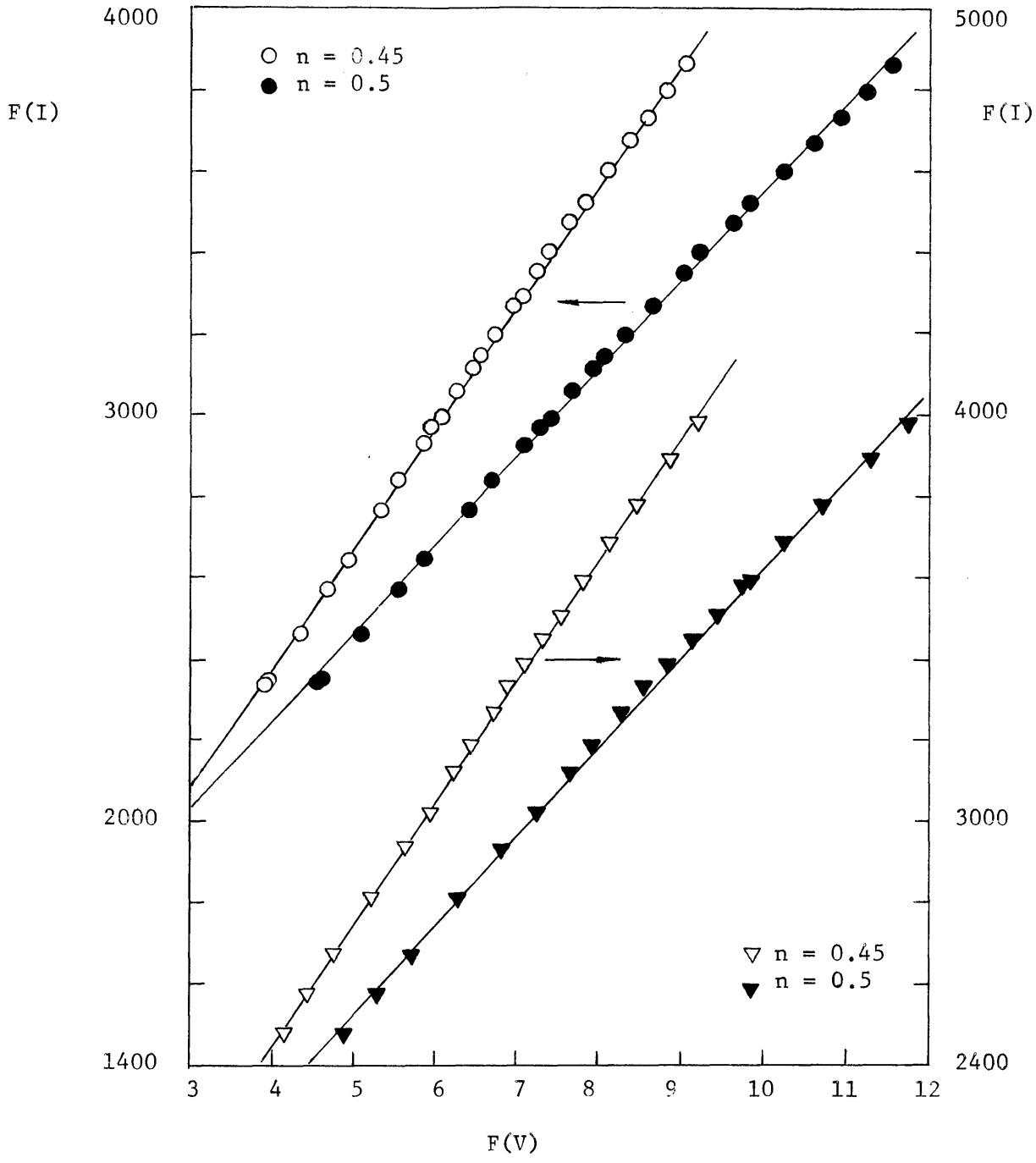

Fig. 3-24 Typical hot wire calibrations, computed with exponents n = 0.45 and n = 0.5.

occurring in these measurements, air properties can be closely represented by

$$\frac{\mu}{\mu_R} = \left(\frac{T}{T_R}\right)^{0.73} \quad ; \quad \frac{\kappa}{\kappa_R} = \left(\frac{T}{T_R}\right)^{0.85} \tag{3-16}$$

where the subscript R indicates any reference value. Both μ and κ can be taken as independent of pressure. Changes in ρ are represented by

$$\frac{\rho}{\rho_R} = \frac{T_R}{T}\,\frac{P}{P_R} \tag{3-17}$$

where P is the atmospheric pressure. Now (3-14) can be written for the condition of zero velocity with the subscript o, giving

$$I_o^{\,2} R = A_o \left(T_w - T_{ao}\right) \tag{3-18}$$

under the assumption that R and T_w are kept at a constant level during the whole operation. From (3-14) and (3-18),

$$\frac{I^2 \left(T_w - T_{ao}\right)}{I_o^{\,2} \left(T_w - T_a\right)} = \frac{A}{A_o}\left(1 + \frac{B}{A}\, V^n\right)$$

Introducing (3-15), (3-16) and (3-17),

$$\frac{I^2 \left(T_w - T_{ao}\right)}{I_o^{\,2} \left(T_w - T_a\right)} = \left(\frac{T_f}{T_{fo}}\right)^{1.02} \left(\frac{T_a}{T_{ao}}\right)^{-0.17} \left[1 + \frac{D}{C}\,\frac{d^n}{\nu_R{}^n} \left(\frac{T_R}{T_f}\right)^{1.73n} \left(\frac{P}{P_R}\right)^n V^n\right] \tag{3-19}$$

Restricting the case to small variations in temperature, if r is the ratio T_{fo}/T_{ao}, which is known,

$$\frac{T_f}{T_{fo}} = 1 + \frac{\Delta T_f}{T_{fo}} = \left(1 + \frac{\frac{1}{2}\,\Delta\, T_a}{r\, T_{ao}}\right) \approx \left(1 + \frac{\Delta T_a}{T_{ao}}\right)^{1/2r} = \left(\frac{T_a}{T_{ao}}\right)^{1/2r} \tag{3-20}$$

Introducing (3-20) in (3-19) and rearranging terms, the final equation is obtained,

$$I^2 \frac{T_w - T_{ao}}{T_w - T_a}\left(\frac{T_{ao}}{T_a}\right)^{\frac{1.02}{2r}} - 0.17 - I_o^2 = \frac{I_o^2}{a_1}\left(\frac{PV}{T_f^{1.73}}\right)^n \qquad (3\text{-}21)$$

where

$$a_1 = \frac{C}{D}\frac{\nu_R P_R^n}{d\, T_R^{1.73}}$$

is a constant for each wire. For convenience, the computer program was written in terms of

$$F(I) = I^2 \frac{T_w - T_{ao}}{T_w - T_a}\left(\frac{T_{ao}}{T_a}\right)^{\frac{1.02}{2r}} - 0.17$$

and

$$F(V) = \left[\frac{P}{760}\left(\frac{435}{T_f}\right)^{1.73} V\right]^n$$

with P in mm Hg and T_f in °C; in this way, $F(V) \approx V^n$. Equation (3-21) becomes

$$F(I) - I_o^2 = \frac{I_o^2}{a} F(V) \qquad (3\text{-}22)$$

In general, the overheat ratio was 1.5, thus r = 1.25. From (3-21), it can be seen that, for a variation in temperature of the order of 1°C, the correction is very small and can be neglected altogether. Therefore, if it is possible to calibrate and operate the wire within such a range of temperature, no correction is necessary. In the present case, however, because of the shape of the x-array probe, it was necessary to calibrate the wires at an open-end nozzle, the blower thus being located upstream from the probe. The heat generated by the blower produced changes of up to 8°C from the ambient temperature, making necessary the use of the complete equation (3-21). Table 3-1 shows the percentage change in the

velocity computed with (3-21) with respect to a computation neglecting the change in temperature, for various typical values of ΔT and I/I_o. An overheat ratio $T_w/T_{ao} = 1.5$ is assumed.

Table 3-1

Temperature Correction in Percentage of Velocity, According to (3-21)

ΔT_a \ I/I_o	1.3	1.6	2.0
2°C	6.5%	4%	3%
4°C	10.5%	8%	7%
6°C	18%	12.5%	10%

The magnitude of the correction is significant, especially if the calibration is performed at a temperature different from the operation conditions. With regard to I_o, by its definition (3-18), it could be measured by placing the wire in a closed container with still air. This is not, however, an accurate procedure because the heat dissipated by the wire produces convection currents that change the heat transfer relationship. From Collis and Williams' experiments, such free convection effects become noticeable at air velocities below 0.5 fps. Therefore, no attempt was made to measure I_o directly. It was determined instead as the zero intercept of a straight line fitted to the values of F(I) and F(V) by the least squares method, in accordance with (3-22). In every case, the resulting constant I_o was smaller than the current reading at zero velocity.

The calibration apparatus is shown in fig. 3-23. From left to right, it included an air filter, blower, by-pass valve, flow straighteners,

a 40" length of 2" I.D. plexiglass tubing and a nozzle contracting to 1". The temperature was measured at the beginning of the straight reach of pipe. The velocity at the nozzle was computed from

$$V = C_n \sqrt{\frac{2g\left(\rho_w/\rho_a\right)\ \Delta h_w}{1 - \left(D_n/D_p\right)^4}} \qquad (3\text{-}23)$$

where Δh_w is the pressure before the contraction with respect to the atmospheric pressure, measured in height of water; ρ_w, ρ_a are given as in (3-2) and (3-3); D_n, D_p are the diameters of the nozzle and of the tube, and C_n is the nozzle coefficient, measured with the total head tube giving 1.013. It is to be noted that, in fact, the use of this coefficient implies that the hot wire anemometer is calibrated with reference to the total head tube, the nozzle acting only as an intermediary.

The procedure adopted was to calibrate the wire before each run, and whenever it was possible, after the run too. An inspection of (3-21) shows that the response of the electronic system is highly dependent on the operating temperature T_w of the wire. Now, the controls of the instrument are not sensitive enough to insure that, each time that the bridge is balanced, exactly the same overheat ratio is achieved. Eq. (3-21) is adequate to compensate for minor changes in ambient temperature during operations, but it has been assumed in its derivation that T_w is accurately known. Therefore, changes in T_w are reflected in the constants of (3-22). Another source of variation in the constants comes from dust collecting in the wire, which, without air filtering, would render meaningless any attempt to calibrate. The filters installed in the test pipe were fairly effective for low rates of flow ($R_e \leqslant 2\times10^5$), the calibrations before and after the run being practically identical. Some variation was noticed for larger flow rates. In the calibration unit, however, a 500 cfm filter was installed, the maximum flow rate being of less than 100 cfm. In this case, remarkable stability of operation was achieved. Several tests of up to 12 hours of continuous operation showed no variation at all in the anemometer response. Fig. 3-25 illustrates these various effects by showing a number of successive calibrations on the same wire.

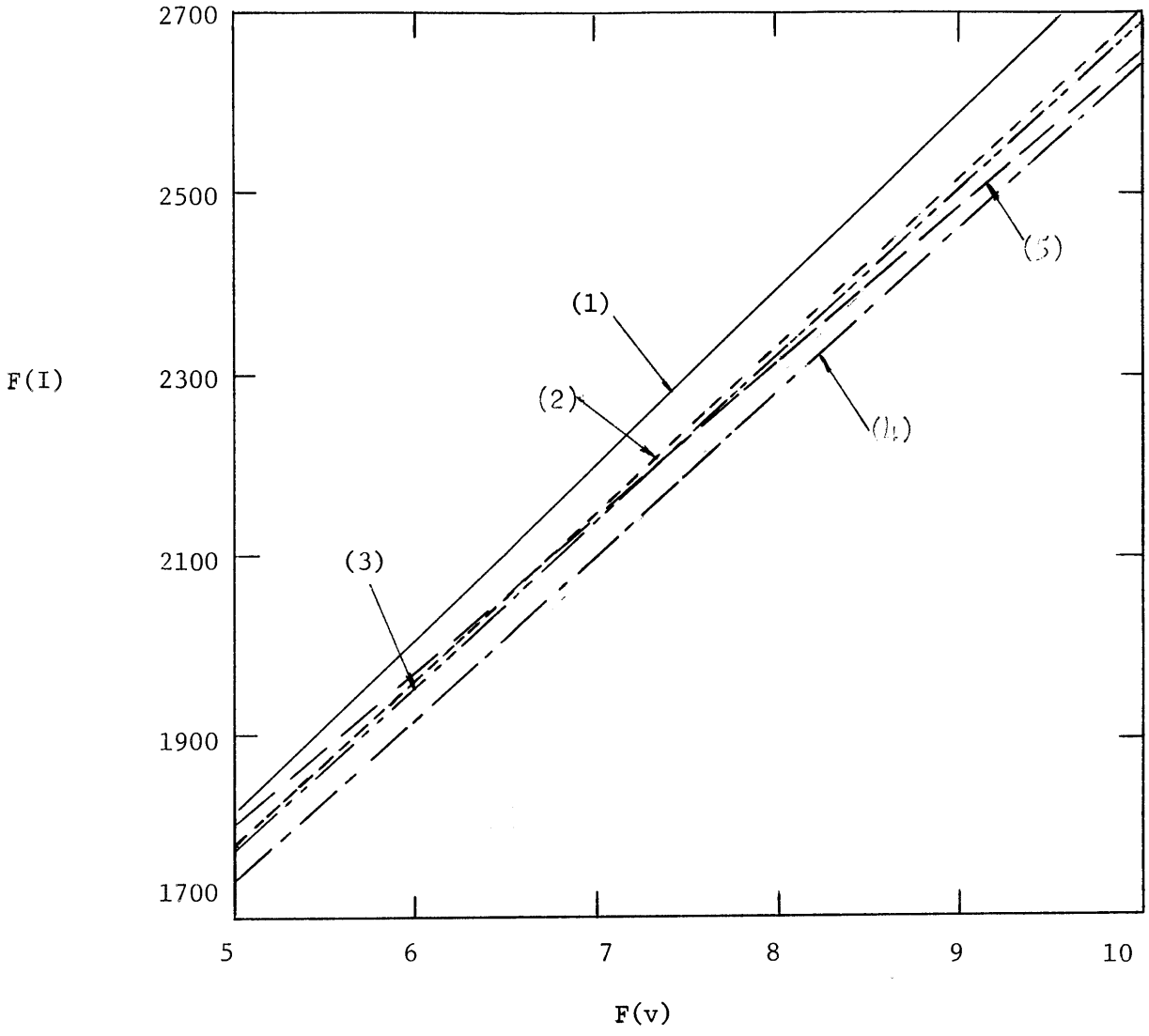

chronological order:

——— (1)
Run C-1, Re = 3.3×10^5
– – – (2)
Run C-2, Re = 1.0×10^5
Run C-3, Re = 1.6×10^5
—··— (3)
—·— (4)
Run C-4, Re = 4.8×10^5
——— (5)

Fig. 3-25 Successive calibrations of the same hot wire

The above considerations relate to the operation of the wire on a steady velocity field. There is no experimental information regarding the heat transfer relationship for rapidly fluctuating flow. It is assumed, therefore, that (3-14) is valid for the instantaneous velocity V. Let U be the average velocity, assumed normal to the wire, and u, v the instantaneous fluctuations in the normal and parallel directions. Thus,

$$V = \sqrt{(U + u)^2 + v^2}$$

and assuming that the fluctuations u, v are much smaller than U, the equation can be simplified to

$$V = U\left(1 + \frac{u}{U}\right)$$

$$V^n = U^n \left(1 + \frac{nu}{U}\right)$$

Introducing this expression into (3-14), together with $I = \bar{I} + i$, where $\bar{I}$ is the average current and i the instantaneous fluctuation, and repeating the same temperature correction analysis, the following expression is obtained for the relative velocity fluctuation:

$$\frac{u}{U} = \frac{\frac{2}{n}}{1 - b\left(\frac{I_o}{\bar{I}}\right)^2} \frac{i}{\bar{I}} \qquad (3\text{-}24)$$

where

$$b = \frac{T_w - T_a}{T_w - T_{ao}} \left(\frac{T_a}{T_{ao}}\right)^{\frac{1.02}{2r} - 0.17}$$

By taking root mean square,

$$\frac{u'}{U} = \frac{\sqrt{\overline{u^2}}}{U} = \frac{\frac{2}{n}}{1 - b\left(\frac{I_o}{\bar{I}}\right)^2} \frac{\sqrt{\overline{i^2}}}{\bar{I}} \qquad (3\text{-}25)$$

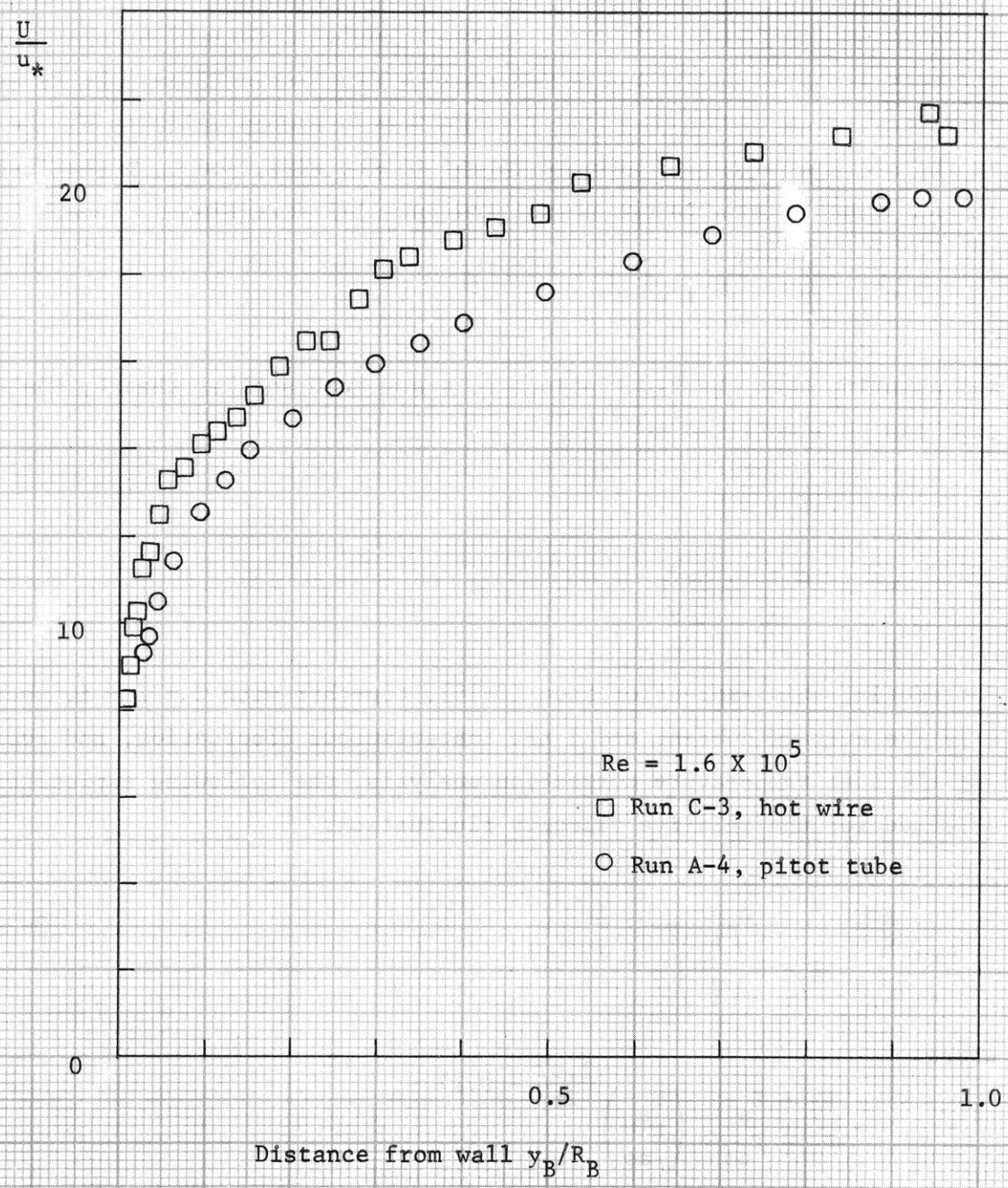

Fig. 3-26 Mean velocity measured with the hot wire and with the pitot tube.

It is interesting to note that (3-25) does not depend on the second constant B of (3-14), and depends only weakly on I_o. Thus, the measurement of relative intensities of turbulence is little affected by changes in the wire calibration. On the other hand, u'/U is seen to be inversely proportional to the exponent n in (3-14), whose choice becomes crucial to the interpretation of turbulence measurements. From (3-25), u' is obtained merely by multiplying by the mean velocity U. According to the derivation of the equation, it seems logical to use the mean velocity as measured by the wire itself. However, in spite of all the care exercised in the operation of the system, there was substantial disagreement between the hot wire results and those obtained with the pitot tube, even in cases where no variation occurred in the calibration curve of the wire during the run. A typical example of the deviations is shown in fig. 3-26. It was decided, therefore, to compute u'/U from the hot wire data, and then to obtain u' by using the interpolated mean velocity value from pitot tube traverses.

The linearization introduced in (3-24) restricts the use of (3-25) to small intensities of turbulence. Hinze (1959) presents an analysis according to which the error will be less than 3% for relative intensities below 20%. In the present case, this limit was widely exceeded, as will be shown in Chapter 4. There is some question, therefore, as to the accuracy of the measured relative intensities. Hinze indicates that considerable improvement results from the use of an electronic linearizing circuit. For constant resistance linearized operation, the theoretically expected deviation of the measured intensity is reduced by a factor of 3 with respect to the non-linearized measurement. Still, Hinze emphasizes that the correct measurement of high relative intensities is an impossibility. In order to estimate the reliability of the present measurements, one comparison test was made in each pipe using the linearizing circuit described at the beginning of this section. It is a less accurate instrument than the anemometer itself, since it is not possible in practice to compensate for local temperature variations, and it also exhibits a larger drift. For these reasons, it was used only to check the correct order of magnitude of the turbulence measurements. Fig. 3-27 shows the linearized average output as a function

of the local mean velocity as measured with the hot wire, and fig. 3-28 compares the distribution of axial relative intensity of turbulence u'/U as computed from (3-25) for the direct output of the hot wire, and from

$$\frac{u'}{U} = \frac{i'}{I} \tag{3-26}$$

for the linearizer output. There is some deviation in fig. 3-27 from a strictly linear response, and therefore, equation (3-26) may not be accurate. But, besides the details, the comparison shows an essential agreement between the linearized and the non-linearized responses, which lends confidence to the overall picture presented by these measurements.

One more remark has to be made relative to the actual measurements of turbulence. In the early runs, a conventional AC voltmeter was used, instead of a true RMS meter. The basic difference between the two types of instruments is that the AC meter does not integrate the signal, but rather measures the peak-to-peak amplitude, which, in the case of sinusoidal waves, is proportional to the RMS value. It is easy to see that such an instrument will give large errors when used in connection with, say, square waves or other types very different from a sine wave. There is little information available concerning its response to a random signal. Therefore, some comparisons were made between both instruments covering the whole range of voltages found in these experiments. The result is shown in fig. 3-29. A systematic deviation exists, the AC meter reading approximately 8% below the true RMS meter, whereas for sine waves, the agreement was within the 2% accuracy of this type of instrument. Therefore, a uniform correction was applied to the runs made with the AC meter (those in the rough pipe).

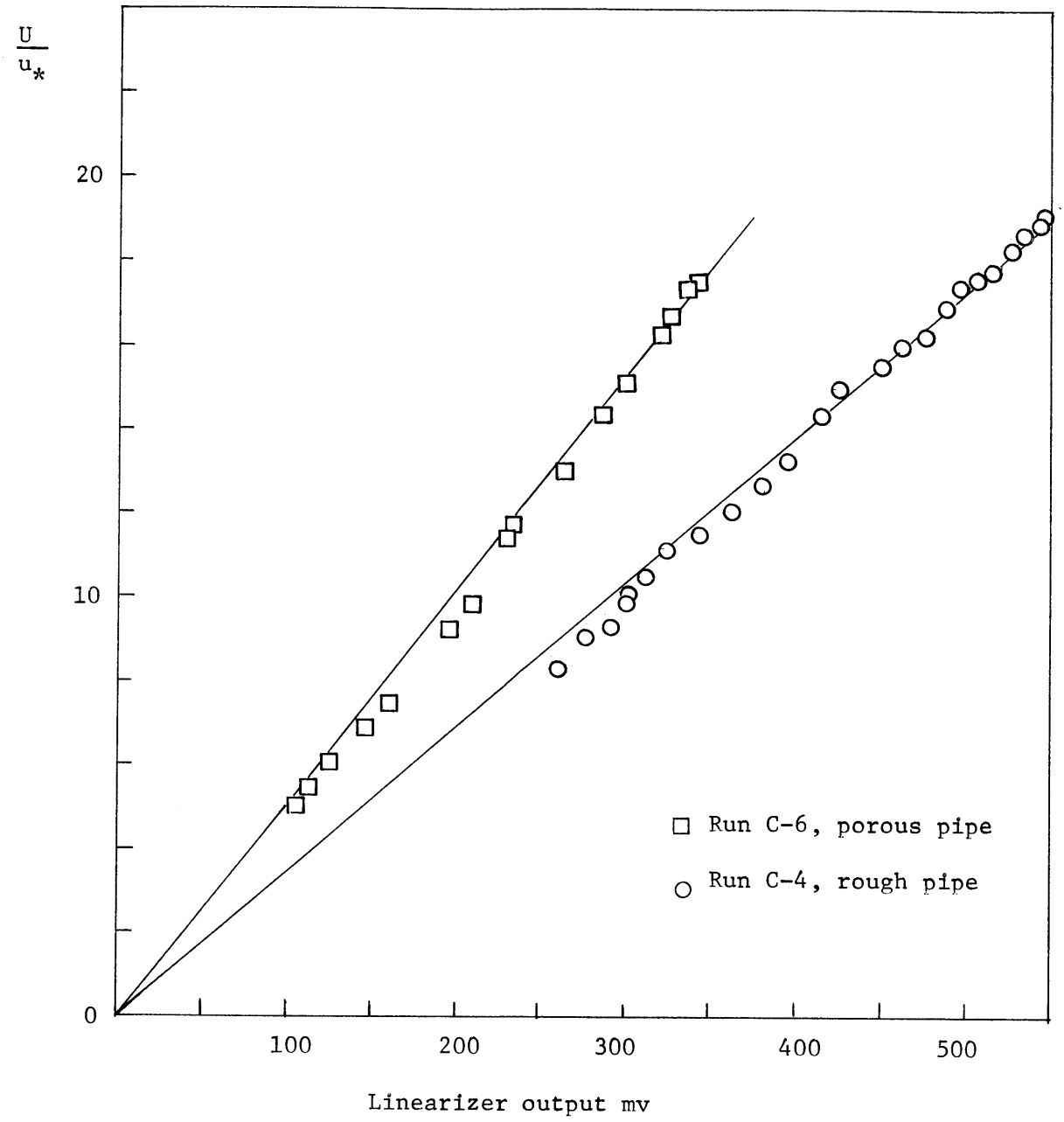

Fig. 3-27 Linearizer output versus mean velocity measured by the hot wire.

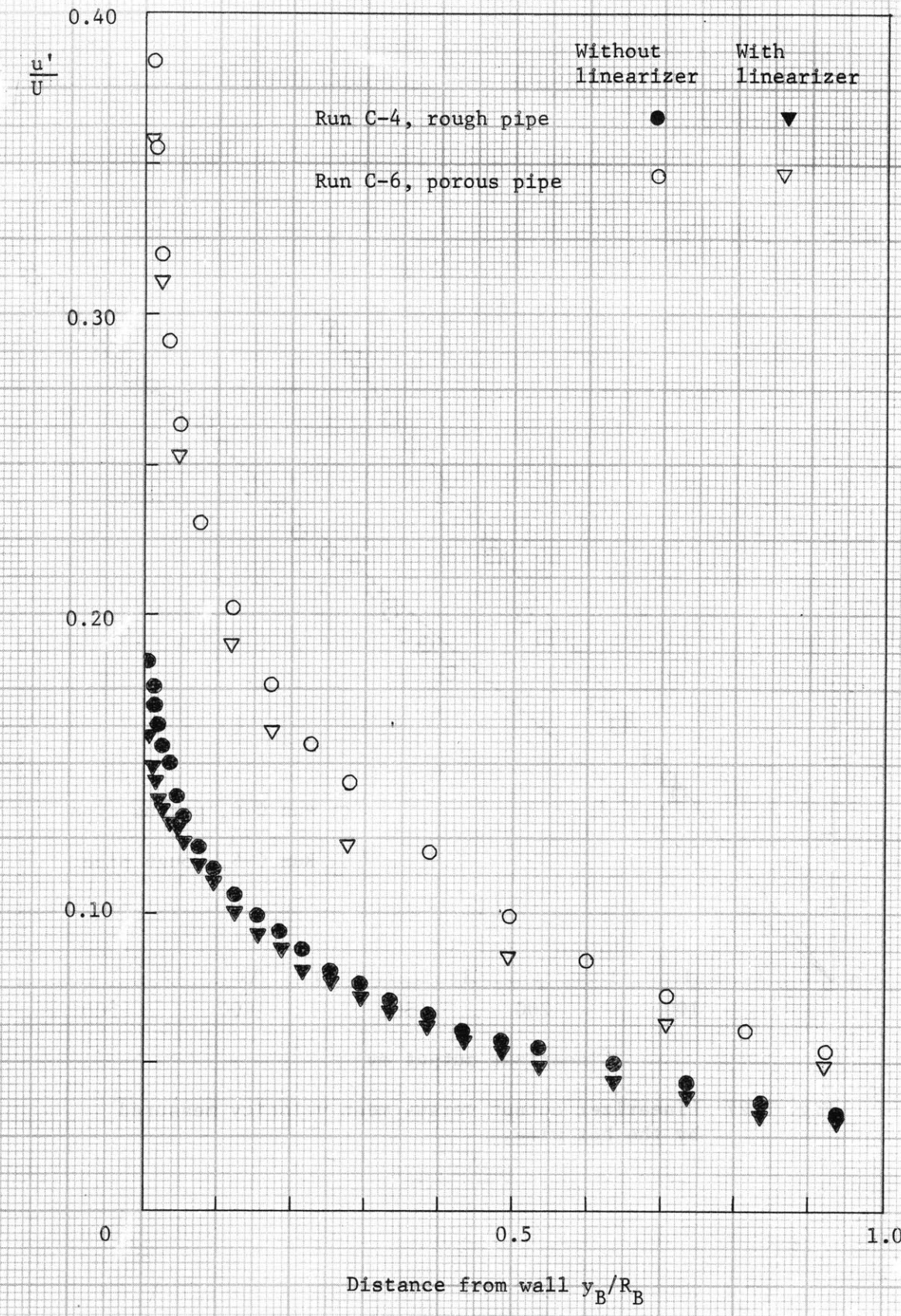

Fig. 3-28 Relative intensity of turbulence measured with and without linearizer.

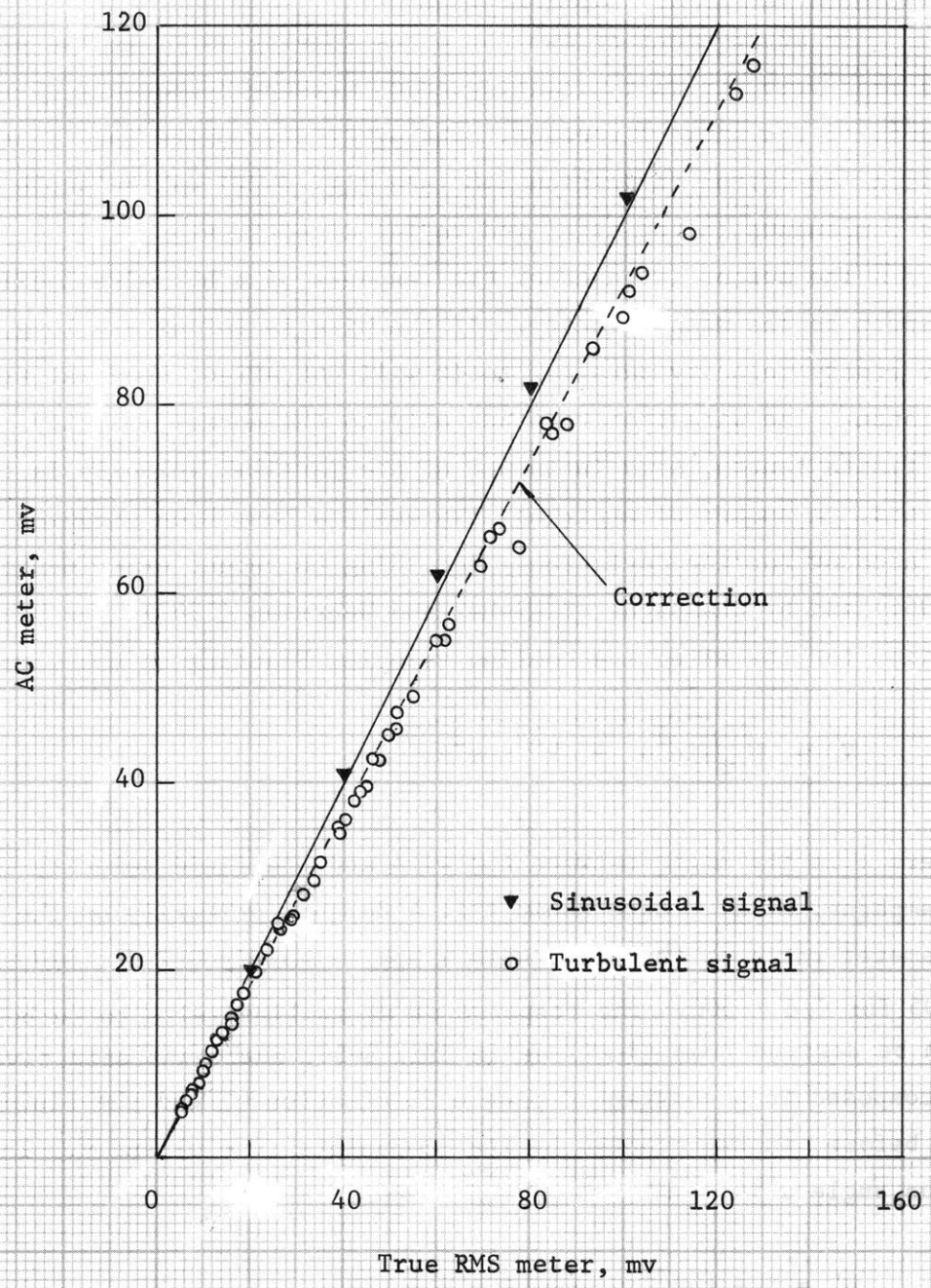

Fig. 3-29 Correction applied to AC voltmeter by comparison with true RMS meter

3.9 Operation of the X-Array Probe

An arrangement of two hot wires forming an X in the plane of the mean velocity is typically used to measure components of turbulence normal to the axial direction. The particular probe used in this investigation, described in Section 3.8 (see fig. 3-22) was suitable to measure the components in the axial and radial directions.

The method is based on the response of a hot wire inclined with respect to the mean velocity. If the wire is infinitely long, clearly any steady velocity parallel to it will not affect the heat transfer balance. The wire then responds only to the normal velocity. For wires of finite length, some influence of the parallel velocity is to be expected. A number of empirical expressions have been proposed in the past to account for the deviation. According to recent experiments by Delleur (1966) and by Champagne, Sleicher and Wehrmann (1967), the best representation for the effective cooling velocity V acting on the wire is given by

$$V = U\sqrt{\sin^2\alpha + k^2\cos^2\alpha} \qquad (3\text{-}27)$$

where α is the angle between the wire and the fluid velocity $\vec{U}$ (fig. 3-30). Champagne, et al., have shown that k depends primarily on the length-to-diameter ratio of the wire, with k approximately 0.2 for $\ell/d = 200$ and below 0.05 for $\ell/d > 500$. The response of an inclined wire to turbulent fluctuations can be derived from (3-27) as in fig. 3-30, where the effective velocity V is decomposed in a constant C plus a fluctuation c, and the fluid velocity, as before, is represented by its components (U + u) and v. The instantaneous angle α' is

$$\alpha' = \alpha + \tan^{-1}\frac{v}{U+u} \approx \alpha + \frac{v}{U}$$

Then, (3-27) can be written as

$$C\left(1 + \frac{c}{C}\right) = U\sqrt{1 + \frac{2u}{U} + \frac{u^2}{U^2} + \frac{v^2}{U^2}}\sqrt{\sin^2\alpha' + k^2\cos^2\alpha'}$$

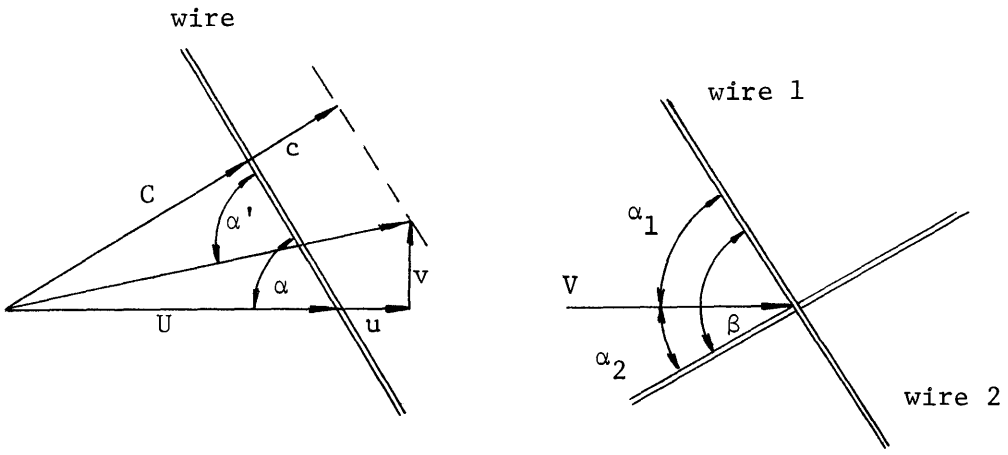

Fig. 3-30 Definition sketch for inclined and x-array wires

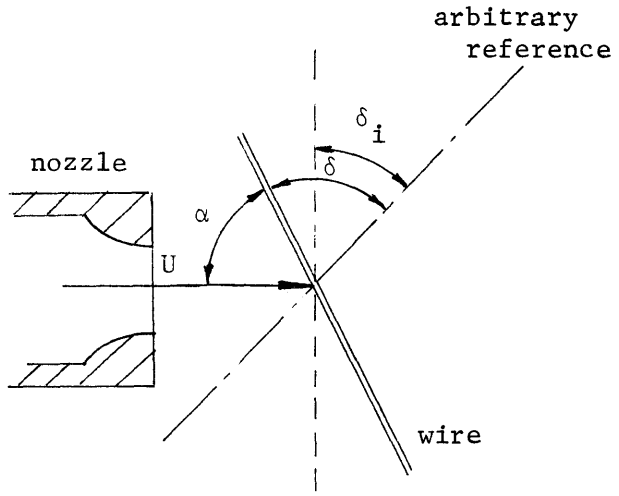

δ known (5 positions)

U known (3 values)

δ_i found by trial-and-error

Fig. 3-31 Definition sketch for angle calibration of the x-array probe

Assuming that u, v are small with respect to U, the quadratic terms can be neglected and, furthermore, sin $\frac{v}{U} \approx \frac{v}{U}$ and cos $\frac{v}{U} \approx 1$. Introducing the steady balance

$$C = U\sqrt{\sin^2\alpha + k^2 \cos^2\alpha}$$

the fluctuation of the effective cooling velocity is obtained as

$$\frac{c}{C} = \frac{u}{U} + \frac{v}{U} \frac{\left(1 - k^2\right) \sin\alpha\cos\alpha}{\sin^2\alpha + k^2 \cos^2\alpha} \tag{3-28}$$

Sometimes, instead of (3-27), the following expression for V is used:

$$V = U(\sin\alpha)^{\lambda}$$

where λ is a constant for each wire. This expression, after a similar development, leads to

$$\frac{c}{C} = \frac{u}{U} + \frac{v}{U} \frac{\lambda}{\tan\alpha} \tag{3-29}$$

Equation (3-28) can be transformed to read

$$\frac{c}{C} = \frac{u}{U} + \frac{v}{U} \frac{1}{\left[1 + \frac{k^2}{\left(1 - k^2\right)\sin^2\alpha}\right]\tan\alpha} \tag{3-30}$$

showing that the constant λ in (3-29) is equivalent to

$$\frac{1}{\lambda} = 1 + \frac{k^2}{1 - k^2\sin^2\alpha} \tag{3-31}$$

For convenience, in the following, (3-29) with (3-31) will be used.

Expressions for the operation of the X-array of hot wires can now

be written. Considerable simplification in the results arises from the assumptions that the wires are well-matched (i.e., they have the same calibration curve) and symmetrical with respect to the mean velocity U. However, it is very difficult to match the wires, an additional requirement being that the two electronic channels be also matched. Also, in the present case, there was no way of adjusting the position of the probe to have the wires symmetrical with respect to the flow. On the other hand, since all data reduction was to be done through a computer, the complexity of the equations posed no difficulty. The method used is explained in detail in Bulletin 68 (1962) of the manufacturer of the equipment, Flow Corporation. Here, the formulas are extended to the case of asymmetric wires. With reference to fig. 3-30, equation (3-29) is written for each wire,

$$\left.\begin{aligned} \frac{c_1}{C_1} &= \frac{u}{U} + \frac{1}{K_1}\frac{v}{U} \\ \frac{c_2}{C_2} &= \frac{u}{U} - \frac{1}{K_2}\frac{v}{U} \end{aligned}\right\} \qquad (3\text{-}32)$$

where

$$K_i = \frac{\tan \alpha_i}{\lambda_i} \qquad i = 1,2$$

in accordance with (3-29) and (3-31). Taking squares and averaging both equations of (3-32) plus their sum and their difference, the following result is obtained after a lengthy algebraic computation:

$$\frac{u'}{U} = \frac{\sqrt{\overline{u^2}}}{U} = \frac{1}{K_1 + K_2}\sqrt{K_1^2\frac{\overline{c_1^2}}{C_1^2} + K_2^2\frac{\overline{c_2^2}}{C_2^2} + 2K_1K_2\frac{\overline{c_1c_2}}{C_1C_2}} \qquad (3\text{-}33,\ i)$$

$$\frac{v'}{U} = \frac{\sqrt{\overline{v^2}}}{U} = \frac{K_1K_2}{K_1 + K_2}\sqrt{\frac{\overline{c_1^2}}{C_1^2} + \frac{\overline{c_2^2}}{C_2^2} - 2\frac{\overline{c_1c_2}}{C_1C_2}} \qquad (3\text{-}33,\ ii)$$

$$\frac{\overline{uv}}{U^2} = \frac{K_1 K_2}{\left(K_1 + K_2\right)^2} \left[K_1 \frac{\overline{c_1^2}}{C_1^2} - K_2 \frac{\overline{c_2^2}}{C_2^2} + K_2 - K_1 \frac{\overline{c_1 c_2}}{C_1 C_2} \right] \qquad (3\text{-}33,\ iii)$$

In (3-33), $\left(\overline{c_1^2}/C_1^2\right)$ and $\left(\overline{c_2^2}/C_2^2\right)$ are merely the intensities of turbulence indicated by each wire, computed by (3-25). The mean product $\overline{c_1 c_2}$ can be measured with a sum-and-difference circuit. From (3-24), the instantaneous velocity c is proportional to the current i for a fixed position of the probe in the flow (i.e., for a fixed mean velocity U), and, therefore, $\left(i_1 + i_2\right)$ and $\left(i_1 - i_2\right)$ are linear combinations of c_1 and c_2. A short computation shows that

$$R_{12} = \frac{\overline{c_1 c_2}}{\sqrt{\overline{c_1^2}}\sqrt{\overline{c_2^2}}} = \frac{1}{2} \frac{E_1^2 + E_2^2}{E_s^2 + E_d^2} \frac{E_s^2 - E_d^2}{E_1 E_2} \qquad (3\text{-}34)$$

where E_1, E_2, E_s, E_d are the RMS values of i_1, i_2, $\left(i_1 + i_2\right)$, $\left(i_1 - i_2\right)$, corrected for amplifier noise by

$$E = \sqrt{E^2_{\text{measured}} - E^2_{\text{noise}}}$$

With (3-34), equations (3-33) completely specify u'/U, v'/U and $\overline{uv}/U^2$, provided the constants K_1, K_2 are known. In fact, there are two constants for each wire, k and α. An accurate measurement of k is very difficult to perform, but is not necessary, as can be seen from equation (3-31), given that k is usually much smaller than 1. On the other hand, the accuracy in the determination of α can be critical. This can be seen from the structure of equations (3-33). Assuming that the ratio α_1/α_2 (where the subscripts 1 and 2 refer to each wire) is fixed, both v' and $\overline{uv}$ are roughly dependent on $\tan\left(\frac{1}{2}\beta\right)$, where $\beta = \alpha_1 + \alpha_2$ is the total angle between the wires. As β is approximately 90°, the percent error in v' and $\overline{uv}$ is slightly higher than the percent error in β, and β should be measured within $\pm$ 1° to keep the error below 2%. This is to say that the usual assumption that the angle between the wires is 90° can be accepted only if there is

reasonable certainty that this is satisfied within $\pm$ 1°. Otherwise, an experimental determination of the angle is necessary. This is relatively simple if the probe can be accurately rotated around an axis normal to the plane of the wires, but it was not feasible in the present case, because of the particular geometry of the probe. Therefore, a more elaborate method had to be used, as follows. First, each wire was independently calibrated by placing it normal to the flow in the calibration unit (fig. 3-23). From equation (3-27), the response of the wire is in this case insensitive to small angle variations, and it was accurate enough to locate the probe by eye. Afterwards, a second test was aimed at the determination of k and β, and finally, with the probe in the pipe, a third test served to define α_1 and α_2. To determine β, the probe was positioned at 5 different angles δ with respect to an arbitrary origin, as sketched in fig. 3-31 and 3 nozzle velocities were measured at each position. The position δ_i where each wire was normal to the flow was computed then by trial-and-error, searching for that angle δ_i that would minimize the measure of the error s_1 defined by

$$s_i^2 \left(\delta_i\right) = \frac{1}{(m - 1)} \sum_{1}^{m} \left(\frac{U_{meas} - U_{nozzle}}{U_{nozzle}} \right)^2 \qquad (3\text{-}35)$$

where U_{meas} is the flow velocity as measured by the wire in accordance with (3-27), U_{nozzle} is the known flow velocity at the nozzle, and m is the number of measurements. A typical calibration is shown in fig. 3-32 where s_1 is plotted as a function of the angle δ_i for various assumed values of k. In practice, the lowest values of s_1 always occurred for values of k in the vicinity of 0.12, which is the value of k predicted from the experiments by Champagne, et al., (1967) for the length-to-diameter ratio used in this investigation. Therefore, k = 0.12 was used throughout the calibrations. The total angle between the wires is finally found as $\beta = \delta_1 - \delta_2$.

The final step in the calibration was accomplished by locating the probe in the test section of the pipe and measuring with each wire

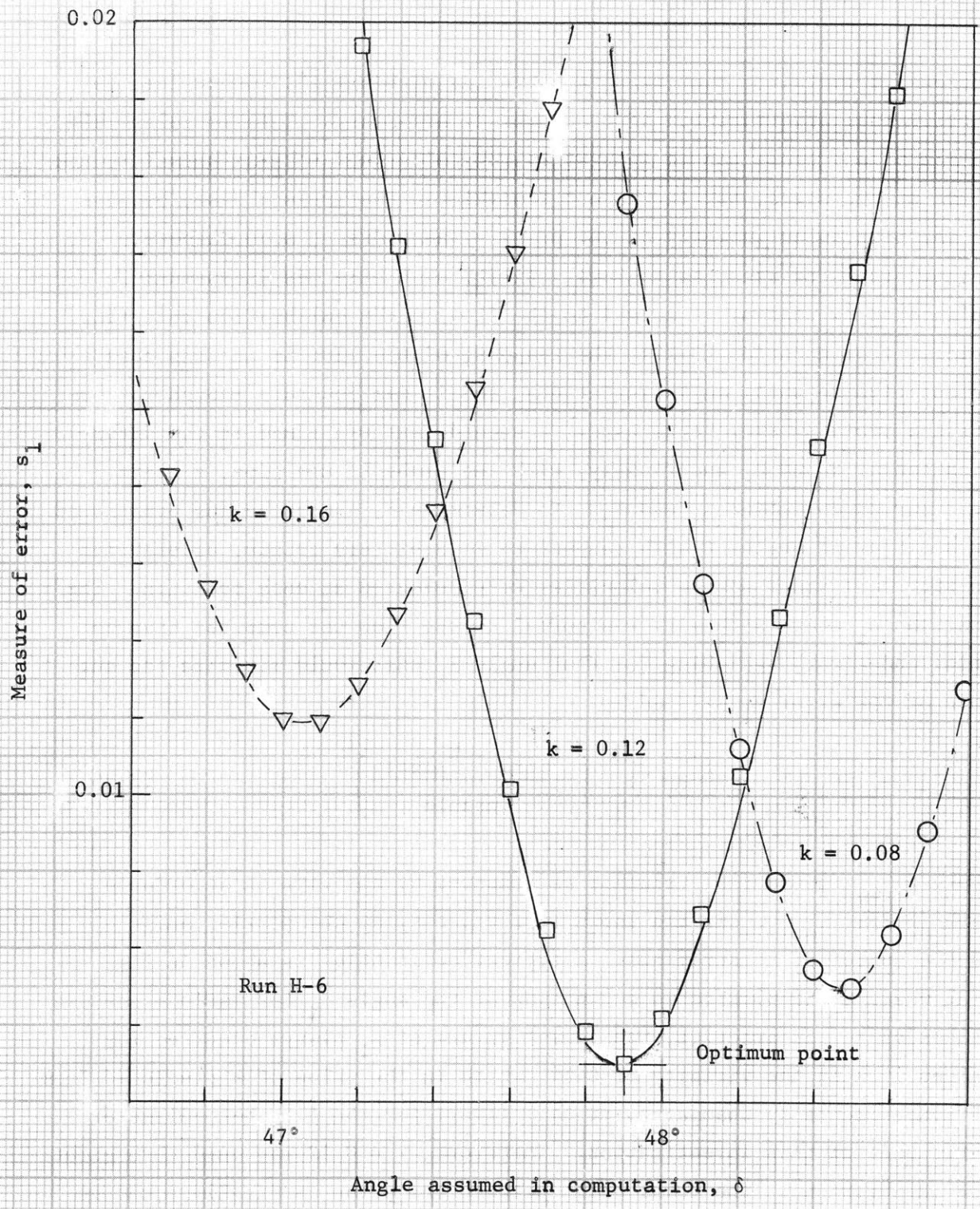

Fig. 3-32 Typical trial-and-error computation in calibration of angle of x-array probe

the mean velocity at a number of points. These were chosen in the core region of the flow, to reduce the error due to the turbulence. Again by trial-and-error, the angles α_1 and α_2 were determined from the condition that the velocities as measured by each wire should be equal, given $\alpha_1 + \alpha_2 = \beta$. The measure of the error to be minimized was defined by

$$s_2^2 \left(\alpha_1, \alpha_2\right) = \frac{1}{(m-1)} \sum_1^m \left[\frac{\left(U_1 - U_2\right)^2}{\frac{1}{2}\left(U_1 + U_2\right)} \right] \tag{3-36}$$

where U_1 and U_2 are the velocities computed from each wire reading, in accordance with (3-27). For the optimum condition, the difference between the velocities measured by each wire was in general about 2% of their average, with maximum deviations of 10%.

3.10 Velocity Spectrum Measurements

In order to obtain spectrum information, samples of the hot wire output were recorded using a Precision Instrument model PS-207A portable FM tape recorder, operating at 60 ips. The frequency response limit was of 5,000 cps. The signal was transferred to a continuous loop, with a total length equivalent to 45 seconds, and analyzed in a system consisting of a Sanborn-Ampex tape recorder model 2000, a Technical Products oscillator model TP-626 and analyzer model TP-627. The analyzer system has a frequency range from 2 to 25,000 cps and the hot wire anemometers were operated with a good frequency response up to 12,000 cps. Therefore, the limiting frequency in the spectral analysis was fixed by the recording procedure. Two electronic filters were available, with nominal bandwidths of 2 and 50 cps. The response of these filters to a sinusoidal signal is shown in fig. 3-33, from which the effective bandwidth has been determined as the width at which 50% of the total power (or 70.7% of the RMS value) is passed, with a result of 1.9 and 53 cps. Some of the samples were analyzed with both filters, in order to check their equivalence. Typical results are shown in fig. 3-34, which shows that both filters give essentially similar results, except of course at very low frequencies, where the wide filter is not

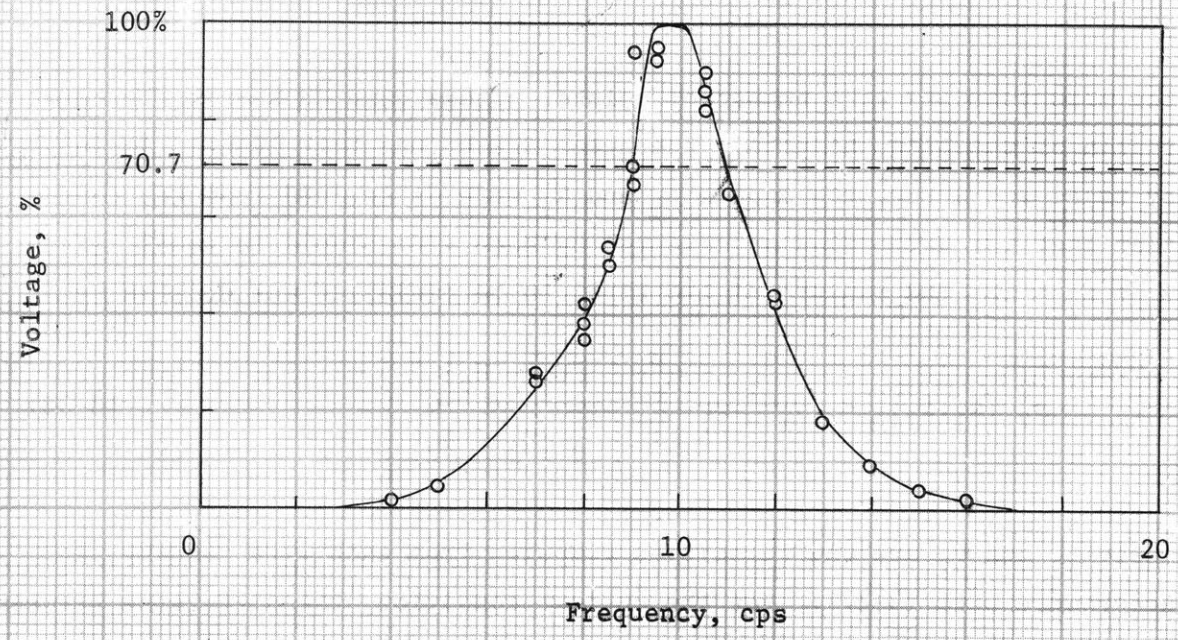

(a) Filter 1, nominal bandwidth 2cps

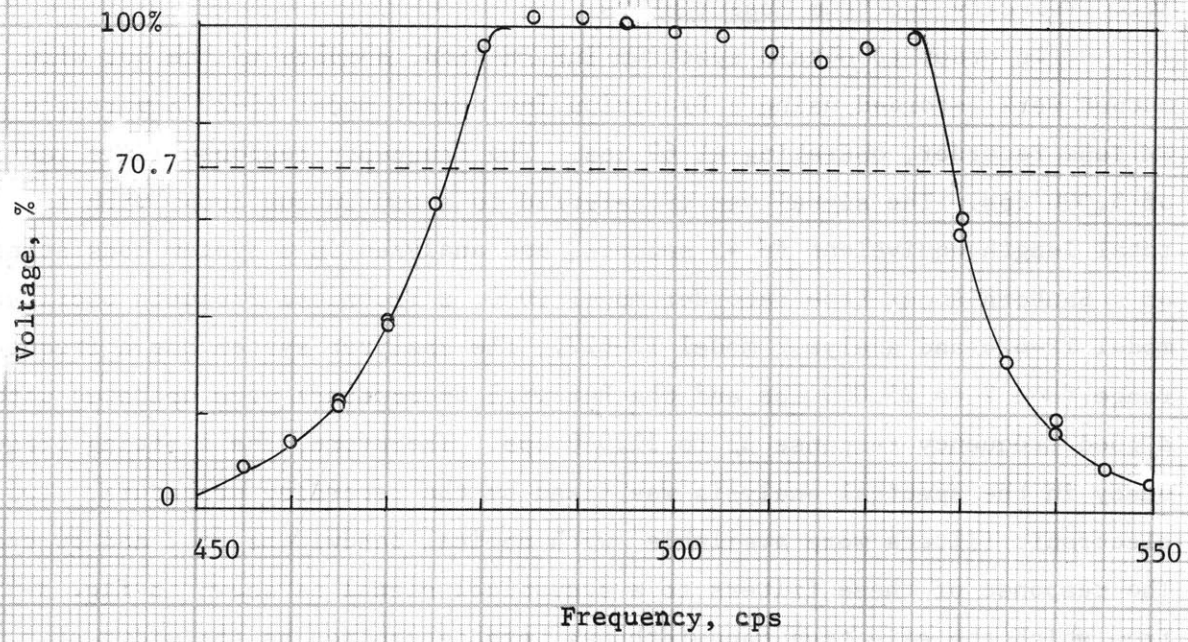

(b) Filter 2, nominal bandwidth 50 cps

Fig. 3-33 Bandwidth of filters used in energy spectrum analysis

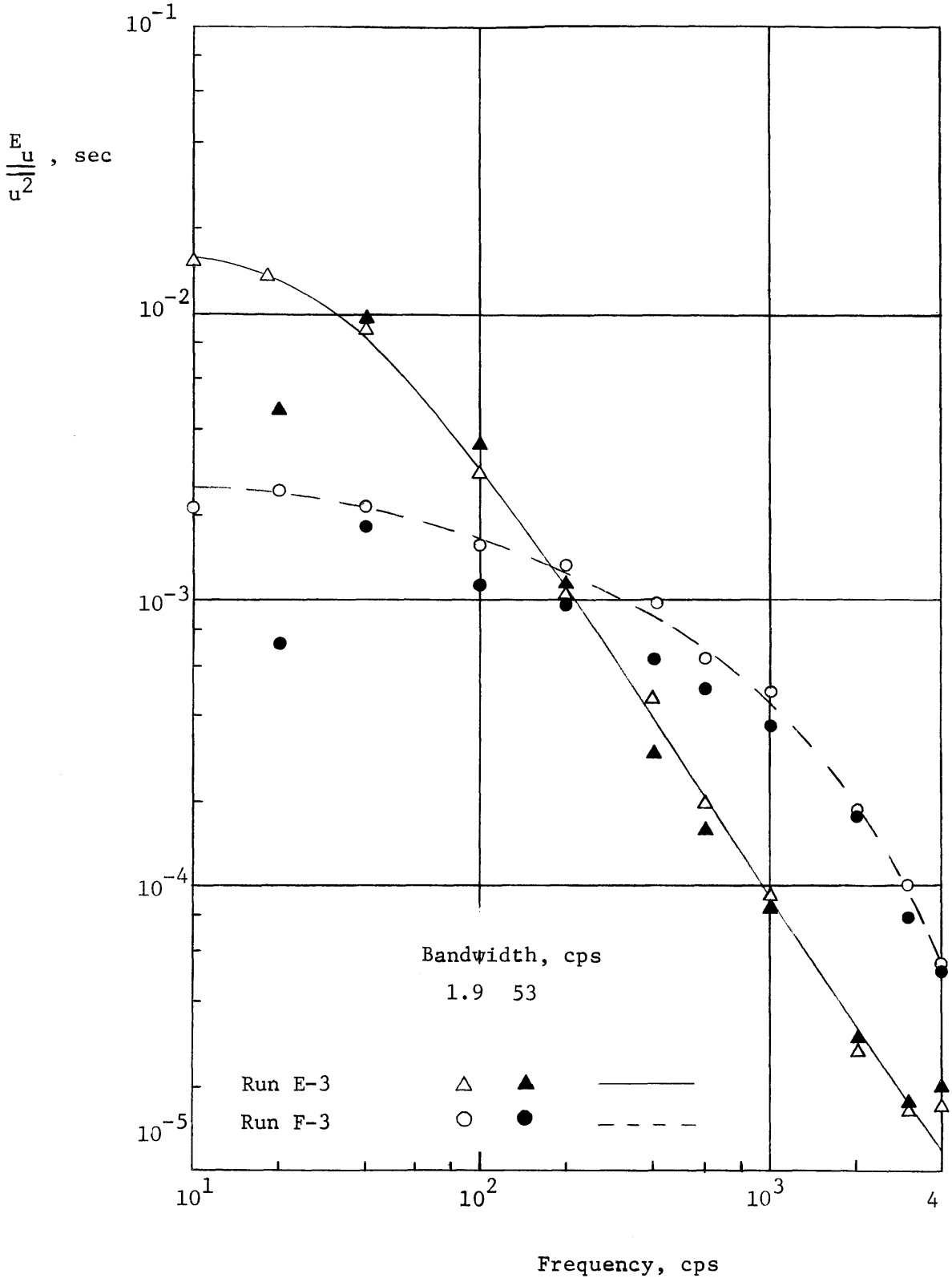

Fig. 3-34 Energy spectrum measured with two different bandwidth filters.

operative. As the most significant portion of the spectrum occurred at low frequencies, only the narrow filter was used throughout the measurements.

For the samples taken with the single wire probe, no further consideration is required, the measured spectrum corresponding to that of the fluctuating longitudinal velocity u. However, a difficulty arose in the use of the x-array probe, because the wires were not precisely matched. Equation (3-24) shows that the current $i/\bar{I}$ is proportional to the effective cooling velocity,

$$\frac{i}{\bar{I}} = \frac{1}{M}\,\frac{c}{C} \tag{3-37}$$

where the constant of proportionality M, of course, depends on I_o and $\bar{I}$. Combining (3-37) with (3-32) and rearranging,

$$\left.\begin{aligned} \frac{u}{U} &= \frac{1}{K_1 + K_2}\left(K_1 M_1 \frac{i_1}{\bar{I}_1} + K_2 M_2 \frac{i_2}{\bar{I}_2}\right) \\ \frac{v}{U} &= \frac{K_1 K_2}{K_1 + K_2}\left(M_1 \frac{i_1}{\bar{I}_1} - M_2 \frac{i_2}{\bar{I}_2}\right) \end{aligned}\right\} \tag{3-38}$$

Thus, if $M_1 = M_2$ and $K_1 = K_2$, that is, if the wires are well matched and symmetrical with respect to U, then the instantaneous fluctuations u and v are respectively proportional to the sum and difference of the hot wire output signals. This is not strictly the case, however, and the use of the sum and difference circuit in the CTA3 anemometer had to produce errors in accordance with (3-38). In the case of the spectrum of u', some indication of the magnitude of this error is obtained from the comparison shown in fig. 3-35 between measurements made with the single wire probe and with the x-array probe, since the first is not affected by this kind of error. The discrepancy is small, except at the very high frequencies, where the

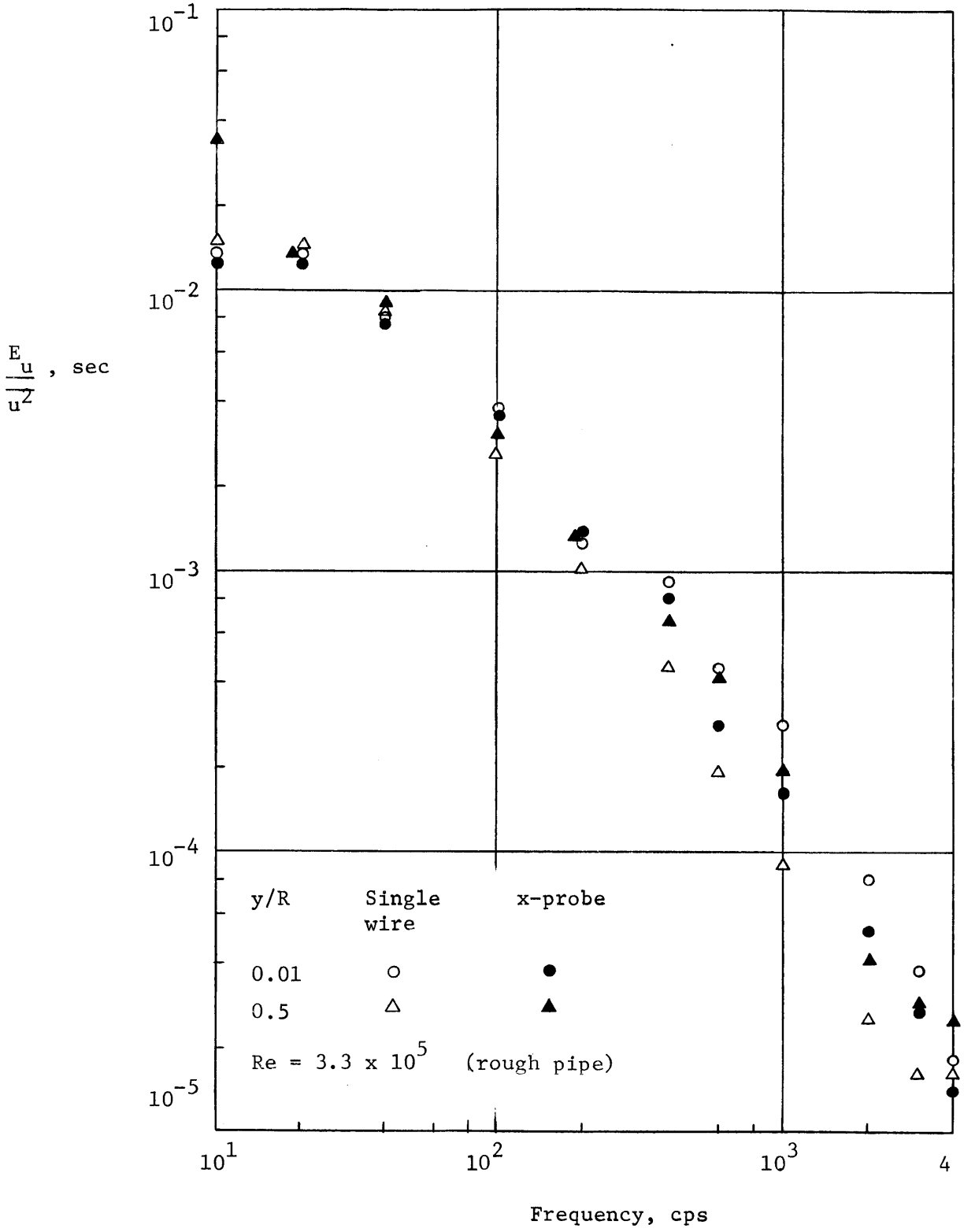

Fig. 3-35 Energy spectrum of the longitudinal velocity measured with single wire and x-array probes.

x-array measurements may have been affected by the noise of the amplifier of the sum-and-difference circuit. The spectrum of v' is, however, much more sensitive to the error represented by (3-38) and, unfortunately, there is no direct way of estimating the extent of the distortion. For reference, the values of the constants in equations (3-38) have been summarized in Table 3-2. At any rate, these tests can provide an estimate of the shape of the spectrum, and under this understanding, they will be presented in Chapter 4.

Table 3-2

Values of the Constants in Equations (3-38)
for Spectral Analysis of X-Array Signals

Pipe	Re	y_B/R_B	M_1	M_2
Rough	1×10^5	0.5	9.8	8.6
$K_1 = 0.96$				
$K_2 = 1.15$	3.5×10^5	0.03	8.6	8.2
		0.07	8.3	7.9
		0.5	7.6	7.2
		1.0	7.4	7.0
Porous	1×10^5	0.03	11.3	12.0
$K_1 = 0.84$		0.09	10.1	10.6
$K_2 = 0.96$		0.5	9.1	9.4
	2×10^5	0.03	10.0	9.8
		1.0	7.9	7.8
	4×10^5	0.03	8.5	8.5
		0.09	7.8	7.8
		0.5	7.1	7.0
		1.0	7.0	6.9

CHAPTER 4

EXPERIMENTAL RESULTS

The results obtained with both the rough and the porous pipes will be presented in parallel in this chapter. The gross characteristics of the flow, such as friction factor behavior and equivalent roughness, will be discussed first. Next, the details of the mean velocity distribution will be examined from the point of view of the law of the wall and of the velocity defect law. The turbulence measurements are presented in the last two sections.

4.1 Gross Mean Flow Description

The pressure variation along the rough pipe is shown in fig. 4-1 and along the porous pipe in fig. 4-2. In both cases, a constant pressure gradient is established much earlier than a fully developed velocity profile (compare fig. 4-1 with fig. 3-7). In fig. 4-2, a larger pressure gradient seems to exist at the downstream end, which probably is produced by the ending of the porous lining. However, such disturbance does not affect the flow in the test section. From these plots, a friction factor f was computed, as defined by

$$\frac{dp}{dx} = \frac{f}{D} \frac{1}{2} \rho \bar{U}^2 \qquad (4\text{-}1)$$

where $\bar{U}$ is the average velocity in the pipe and D the effective diameter defined in section 3.5. The friction factor is plotted in fig. 4-3 as a function of the Reynolds number $Re = \bar{U}D/\nu$. For the rough pipe, the friction factor follows very closely the well-known behavior of grain-type roughness. For high Reynolds number, a fully rough condition is approached, corresponding to a relative roughness of approximately 0.008. With a pipe diameter of 9.54", the equivalent roughness size k_s is 0.075", which is about one half of the size of the spherical elements. This result seems reasonable, as a closely packed bed of spheres conforms to a much smoother surface than a bed of angular sand grains of the same size. The porous pipe, however, exhibits a quite different behavior, with the friction factor continuously

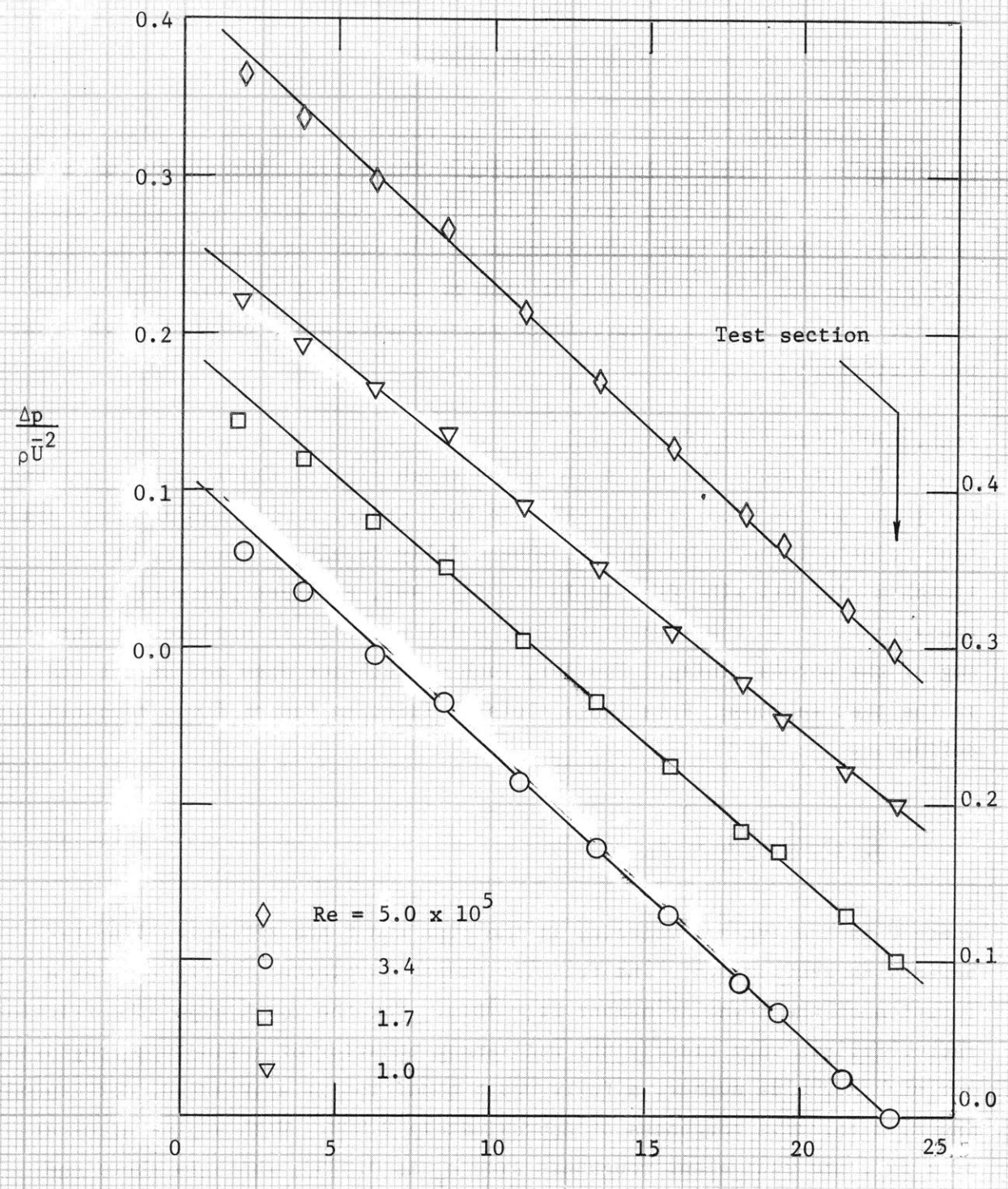

Fig. 4-1 Pressure gradient along rough pipe (scales are displaced in 0.1 for each run)

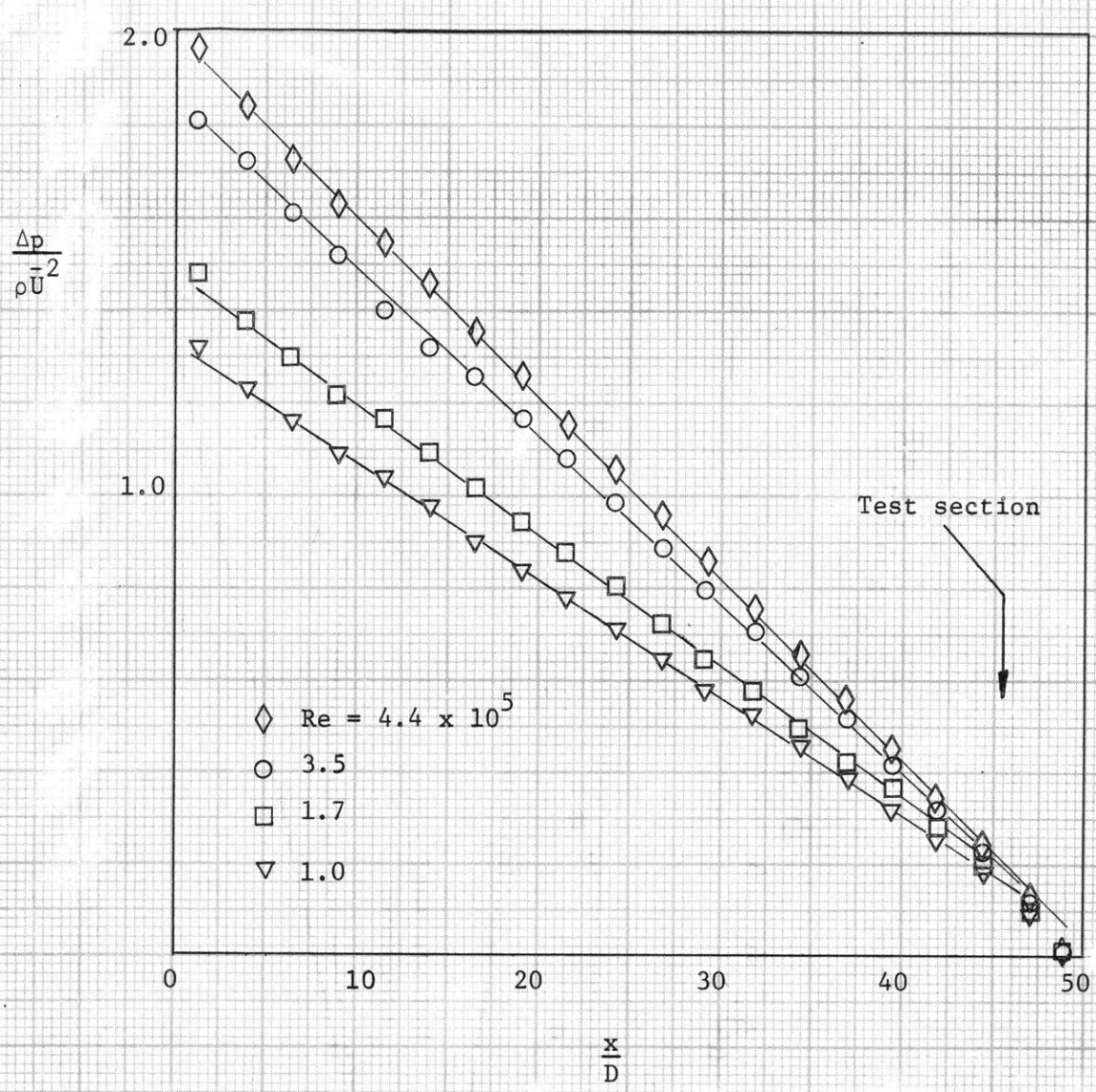

Fig. 4-2 Pressure gradient along the porous pipe

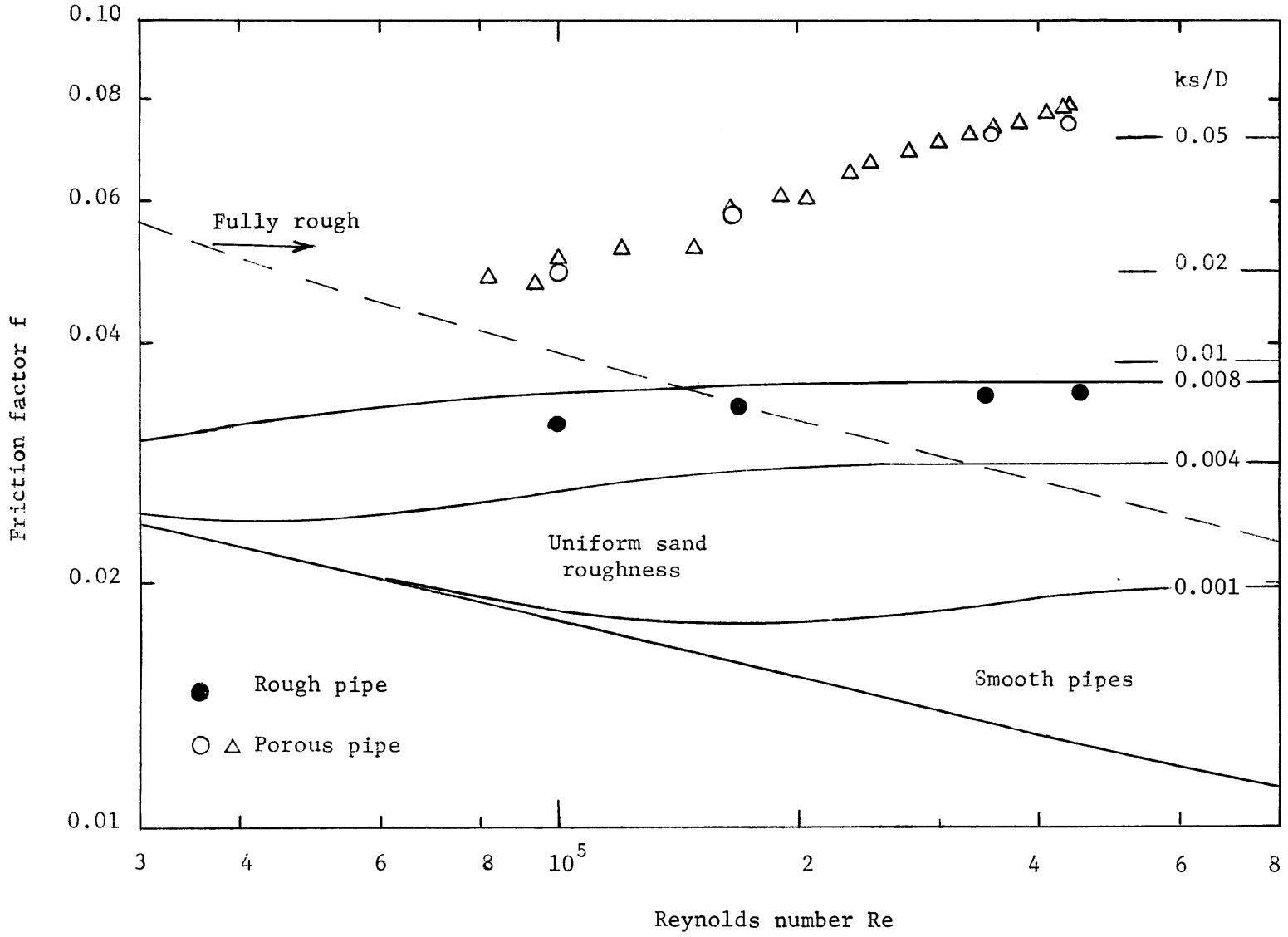

Fig. 4-3 Friction factor vs. Reynolds number.

increasing with Reynolds number, in spite of the fact that the flow is well within the usual fully rough regime. To check this behavior in more detail, a number of short measurements were taken in addition to the pressure gradient runs shown in fig. 4-2, using only two piezometer sections. These measurements are also shown in fig. 4-3 and they prove the general consistency of the results. It must be noted that, in the computation of the mean velocity, the total inlet discharge is assumed to flow through the open section of the pipe. Therefore, if a substantial fraction of the flow were to occur within the porous wall, there would be an error in the computed friction factors. In order to examine this point, the specific discharge q through the porous medium has been computed from (3-4) with 0.13 for the constant for each measured pressure gradient. The values of q are presented in Table 4-1, together with the corresponding discharge in the porous material and the

Table 4-1

Computation of the Discharge Through
the Porous Lining in Accordance with (3-4)

Q_{inlet} cfs	$\bar{U}$ fps	q fps	r	Q_{porous} cfs	Q_{porous}/Q_{inlet}
9.90	20.7	0.10	10.8	0.028	0.003
16.4	34.2	0.29	3.7	0.082	0.005
34.2	71.5	1.01	1.1	0.29	0.009
42.6	89.5	1.44	0.75	0.41	0.010

ratio r between the linear and the quadratic terms in the modified Darcy's equation (2-26). Table 4-1 shows that any correction in the friction factor to take account of the flow through the porous medium would be negligible. Further evidence in the same respect is provided in fig. 3-19, where the discharge integrated from the velocity profile under the assumption of no flow in the porous medium is shown to be in good agreement with the calibration of the inlet contraction.

Two unusual features of the friction factor of the porous pipe in fig. 4-3 are the very high equivalent relative roughnesses k_s/D, between 0.018 and 0.06, and the continuous increase of f with Reynolds number. Introducing D, k_s is seen to vary between 0.17" and 0.56", and it is obvious that such effects cannot be explained by the surface texture of the material, but must be associated with the flow occurring in the porous medium. A speculative explanation for the variation of f with Reynolds number can be given with reference to the modified Darcy's equation (2-26). For low rates of flow, the linear term, dependent on viscosity, is dominant over the quadratic term, their ratio r being much larger than 1. As the Reynolds number increases, the influence of the linear term gradually diminishes and eventually the equation becomes independent of viscosity as r becomes much smaller than 1. This gradual change in the form of the governing equation for the turbulent motion within the porous medium should be reflected in the characteristics of the pipe flow. Considering the curves presented in fig. 3-11, the mean velocity in the porous medium is seen to be the determinant factor in defining the relative importance of the two terms in equation (2-26) and, therefore, the values of r in Table 4-1 can be taken as representative of the flow regime in the porous medium. It is thus conceivable that the increase of the pipe friction factor with Reynolds number may reflect this change of regime of the flow in the porous medium shown in Table 4-1. If such is the case, the friction factor will become constant only when equation (2-26) is practically independent of the viscosity at sufficiently high permeability Reynolds numbers. However, no direct proof for this explanation can be given now, and it must be taken as a tentative proposition.

4.2 Mean Velocity Distribution

The same features exhibited by the friction factor behavior are present in the mean velocity profile, as evidenced by fig. 4-4, where U/U_{max} is plotted as a function of position. For the rough pipe, there is little variation with Reynolds number, whereas the increase of friction factor with Reynolds number is reflected by the displacement of the porous pipe

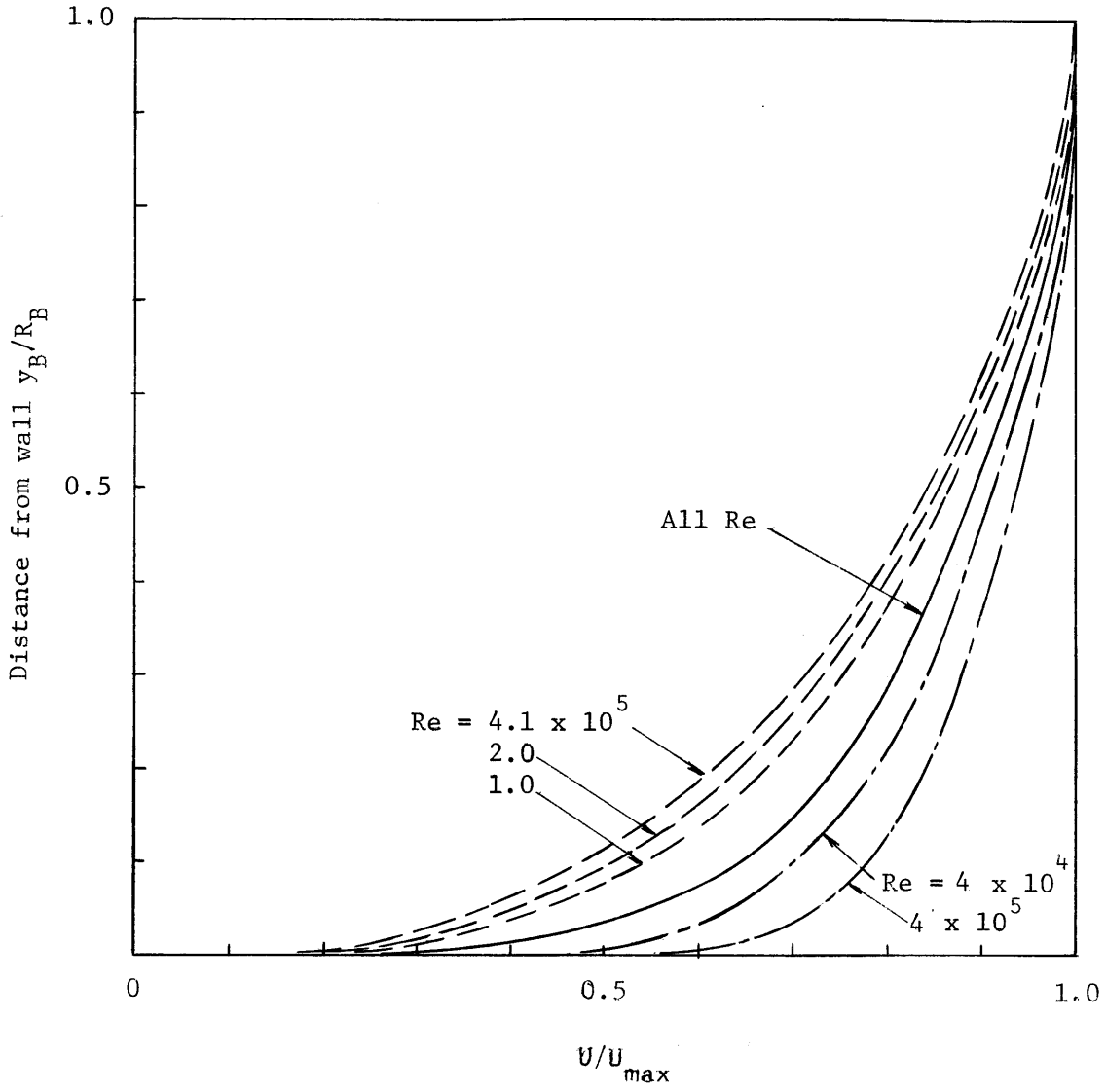

Fig. 4-4 Mean velocity distribution.

velocity distribution.

As discussed in Chapter 2, the analysis of the mean velocity distribution can be made from two different points of view: the law of the wall, equation (2-4), and the velocity defect law, equation (2-10), each one with its own zone of validity. In order to plot the data in terms of the law of the wall parameters, some decision had to be made in regard to the origin of the geometrical coordinate, as discussed in Chapter 2. There is an inherent ambiguity in this process, because it is not known in advance how far away from the wall the semi-logarithmic law should extend. Therefore, the evaluation of the best location for the effective origin and the resulting slope $1/\kappa$ of the semi-logarithmic straight line will be affected by the width of the zone where a good fit to the data is required. As long as the eventual variations of y_o remain small, some fairly definite conclusions can be reached. Such is the case for the rough pipe. The origin was selected using three complete traverses, that is, six profiles at different orientations, at the same Reynolds number, 3.2×10^5. All the data were plotted together and an average curve was drawn through them. By trial-and-error, an origin 0.105" from the aluminum pipe. i.e., 0.032" below the top of the roughness elements, was found to give the best fit to a straight line. With such an origin, the semi-logarithmic velocity distribution is plotted in fig. 4-5 for four Reynolds numbers. A reasonable fit to parallel straight lines can be obtained, with a slope A = 6.15 for equation (2-4), corresponding to $\kappa = 0.375$. The deviation $\Delta U/u_*$ from the smooth law, defined in equation (2-7), has been evaluated at the center portion of the profiles and is compared in fig. 4-6 with the information compiled by Clauser (1956). For the roughness height k_s, the same equivalent size found from the friction factor diagram was used, namely, $k_s = 0.075"$. The agreement with the curve corresponding to Nikuradse's sand roughness experiments is satisfactory, confirming the consistency of this series of observations with the classical characteristics of grain-type roughness. It is interesting to note the tendency of the points in fig. 4-6 to follow a line with the same slope A = 6.15 of the semi-logarithmic velocity distribution. Of course, no definite conclusion

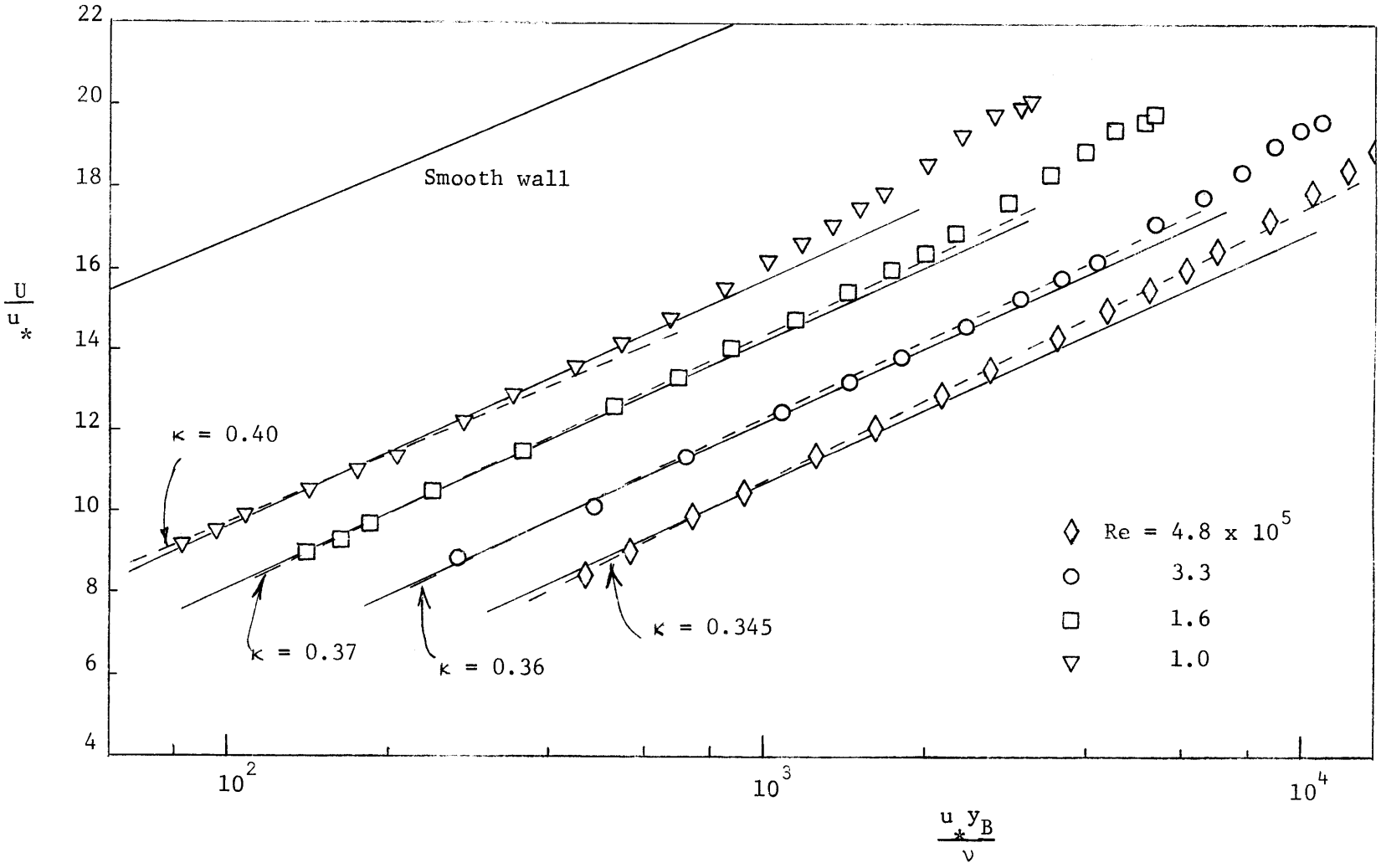

Fig. 4-5 Law of the wall in rough pipe, κ = 0.375

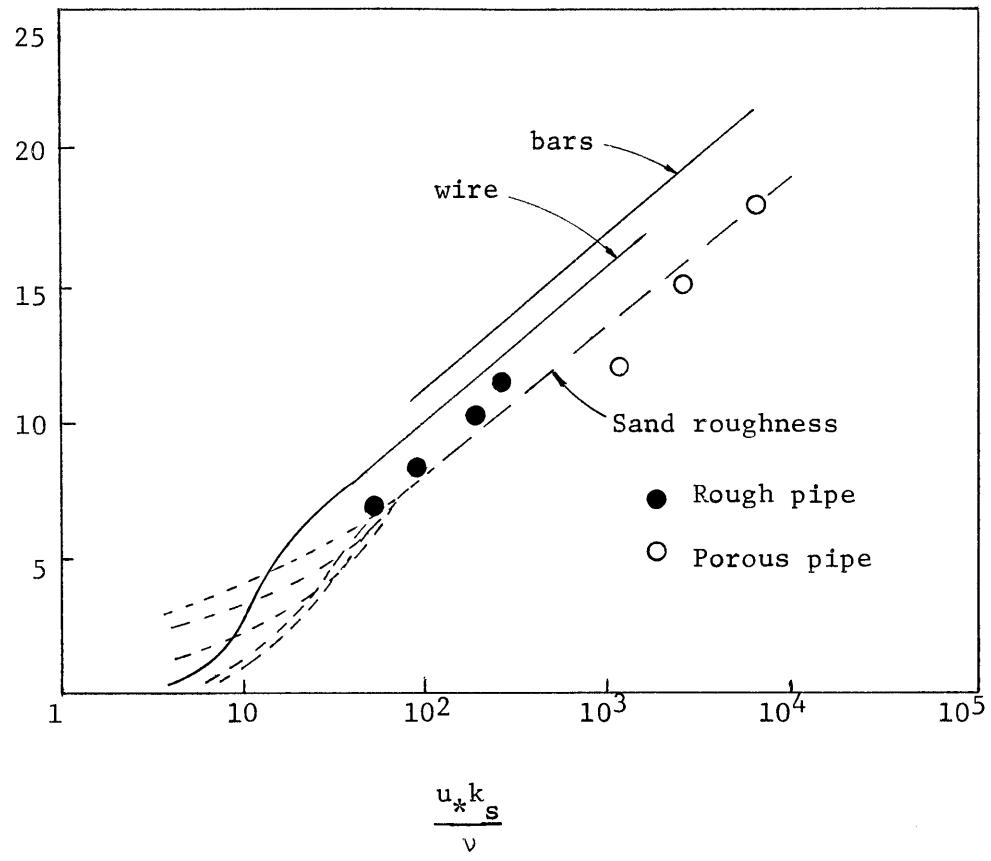

Fig. 4-6 Shift in the velocity profile for rough walls, according to Clauser (1956)

in this regard can be reached on the basis of only four points.

A more careful observation of the data in fig. 4-5 indicates, however, that some systematic deviations exist. If the best straight line is drawn separately for each run (the segment lines in fig. 4-5), κ is seen to decrease from 0.40 at Re = 1.0×10^5 to 0.345 at Re = 4.8×10^5. This result is not unusual. Hinze (1962) has re-examined many smooth pipe experiments plus the rough pipe tests of Nikuradse, and he reports large variations, up to 20%, in κ. However, it is difficult to establish whether such variations are systematic, because the scatter is considerable. In this connection, the present experiments in the porous pipe provide a better perspective of the problem, due to the large apparent roughness, which accentuates the usually small departures from the universal behavior. In fig. 4-7, the mean velocity profile is plotted in terms of the distance y from the surface of the porous material, without any origin correction, and little evidence can be found of a tendency for the measurements to follow a semi-logarithmic straight line. It is possible to obtain such a straight line by introducing suitable displacements of the origin, y_o, but the process does not have a clearly defined solution.

In order to show how the results depend on the particular value of y_o selected, two different interpretations have been made of the same data. In the first case, shown in fig. 4-8, a displacement $y_o = 0.08"$ has been chosen so as to obtain a fitting to straight lines with slope approximately given by $\kappa = 0.40$. As in the rough pipe case, the average of six profiles at the same Reynolds number was used to find the amount of the correction. A very thin logarithmic region is found, extending to not more than 0.35" from the surface of the porous material, which is less than 10% of the radius of the pipe. There is some indication that the displacement y_o should be smaller as the Reynolds number decreases. The deviation $\Delta U/u_*$ from the smooth wall case has been measured from fig. 4-8. In order to compare it with the curves of fig. 4-6, an equivalent roughness height k_s has been estimated from the condition that, for the highest Reynolds number, the point should fall in the fully rough curve for sand roughness. This is an arbitrary criterion, but it serves the purpose of a relative comparison.

The resulting k_s is approximately 1.2", that is, it is equal to the thickness of the porous layer. This value seems surprisingly large, but inspection of the friction factor diagram in fig. 4-3 shows that the fully rough condition will probably imply an equivalent relative roughness of about 0.10, that is, k_s of the order of 1".

A second, alternative correction is presented in fig. 4-9, where an effort was made to extend a reasonable fit to a straight line up to 0.2 of the radius, regardless of the resulting slope. After a uniform correction $y_o = 0.21"$, parallel straight lines can be more or less fitted to the data, with $\kappa = 0.26$. Again, there are strong indications that the displacement changes with Reynolds number. Fig. 4-10, with displacements ranging from 0.14" to 0.21", shows a better fit, while κ still is 0.26. For purposes of comparison, all the curves shown in figs. 4-5, 4-7, 4-8 and 4-10 have been summarized in fig. 4-11, where the experimental points have been omitted for simplicity.

In summary, both the slope $1/\kappa$ and the width of the semi-logarithmic profile are seen to vary as a function of the chosen displacement y_o in the distances from the wall. In a way, the problem under consideration reduces to the recurring question of whether κ is truly a universal constant. It is convenient to examine this point on the basis of the concepts discussed in section 2.1. The parameter $\kappa(y_o + y)$ was interpreted as a turbulence scale for a universal mechanism characterized by the equilibrium between production and dissipation of turbulent energy, which ultimately leads to a logarithmic mean velocity distribution. If such a turbulence scale has a physical reality, it follows that the measurements should define a unique value for $\kappa(y_o + y)$ at any particular location; hence, the inverse type of relationship between κ and y_o found in the computations.

In fact, the presence of two empirical constants, κ and y_o, allows for the arbitrary determination of one of them, and it will be shown in the following that the acceptance of κ as a universal constant brings as a consequence a very general universal description of the flow in the wall region. One important characteristic of the flow is the production of turbulent energy, which, in accordance with the implicit postulate of fig. 2-2, should

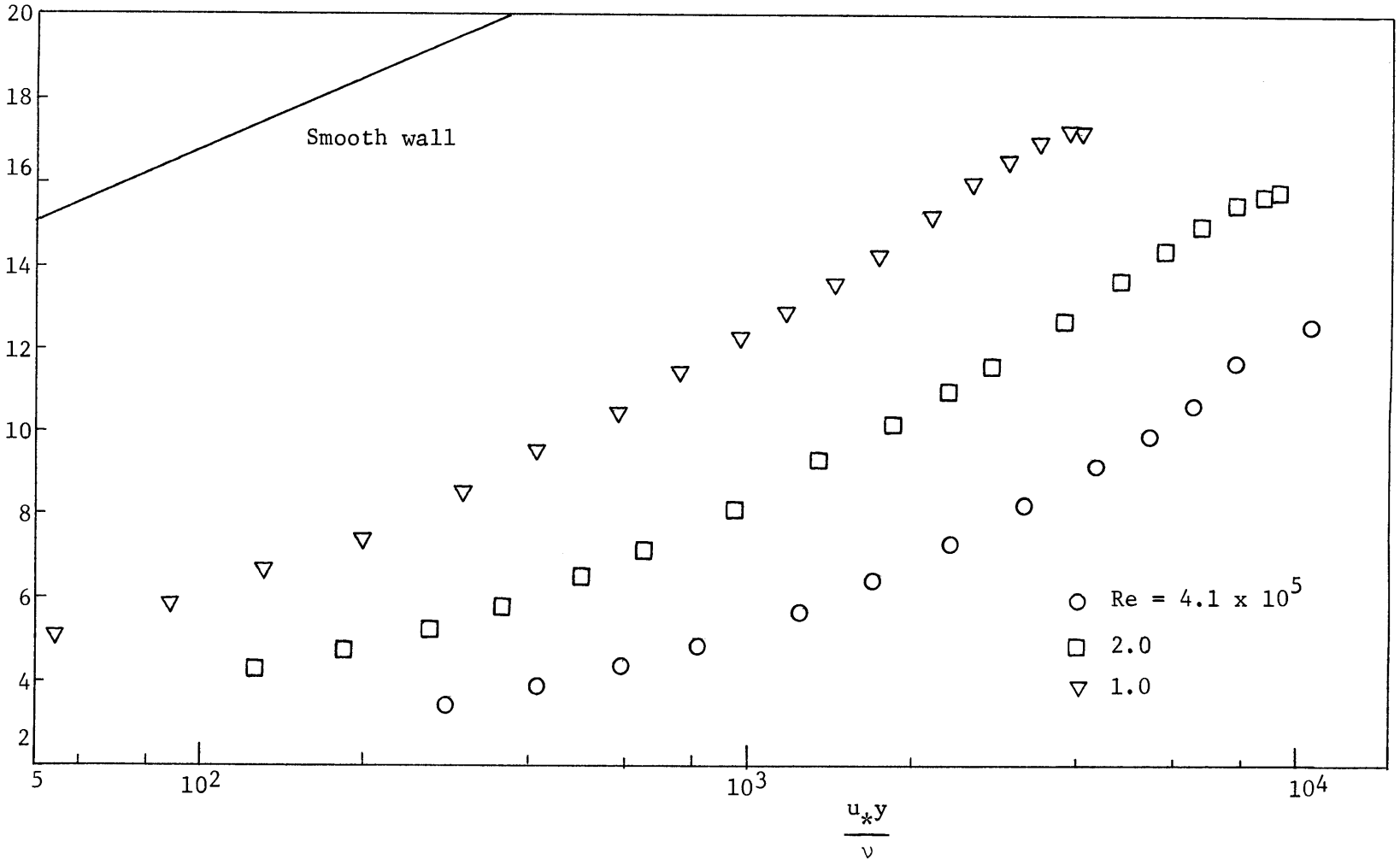

Fig. 4-7 Velocity measurements in porous pipe

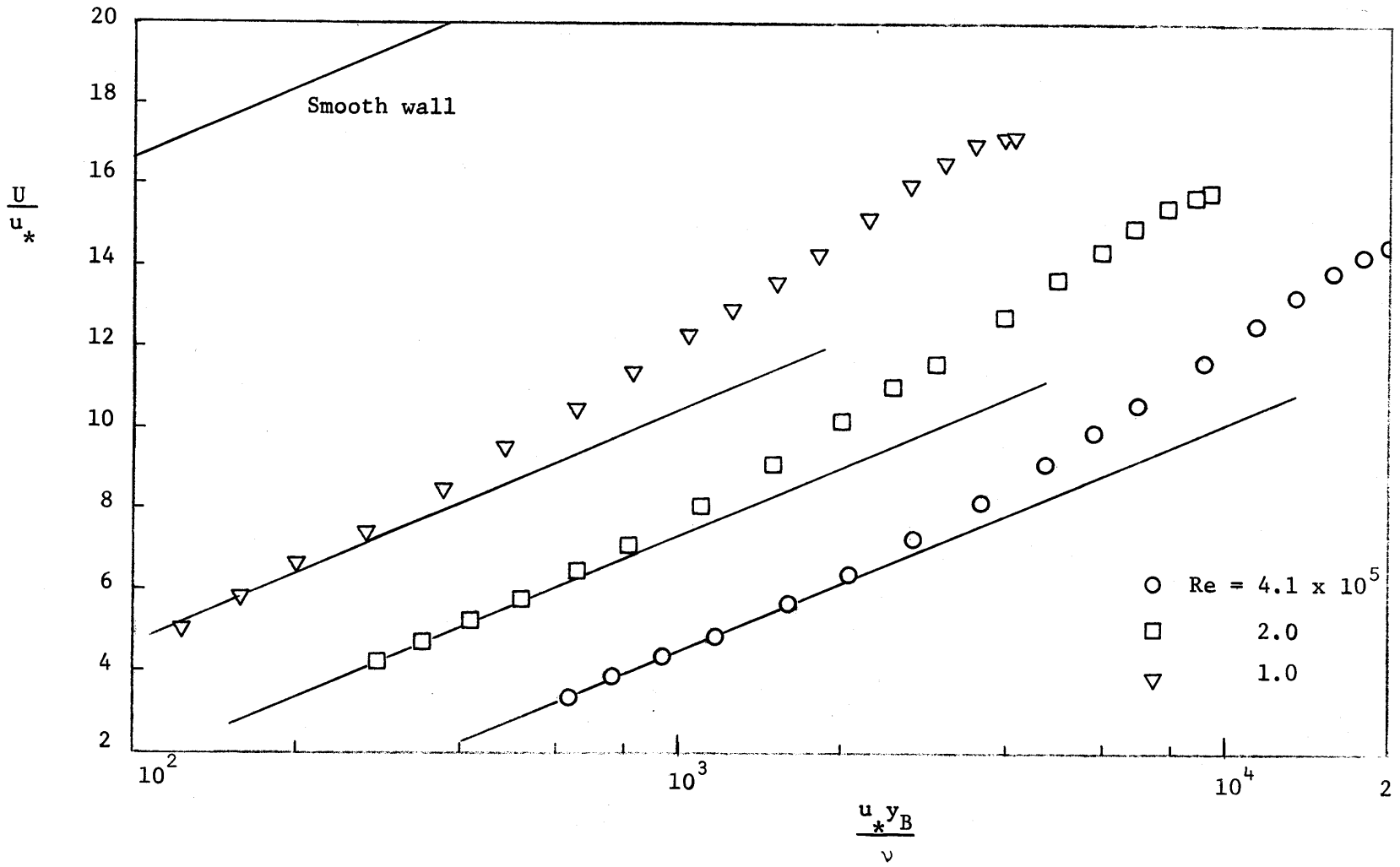

Fig. 4-8 Law of the wall in porous pipe, y_o = 0.08", κ = 0.40

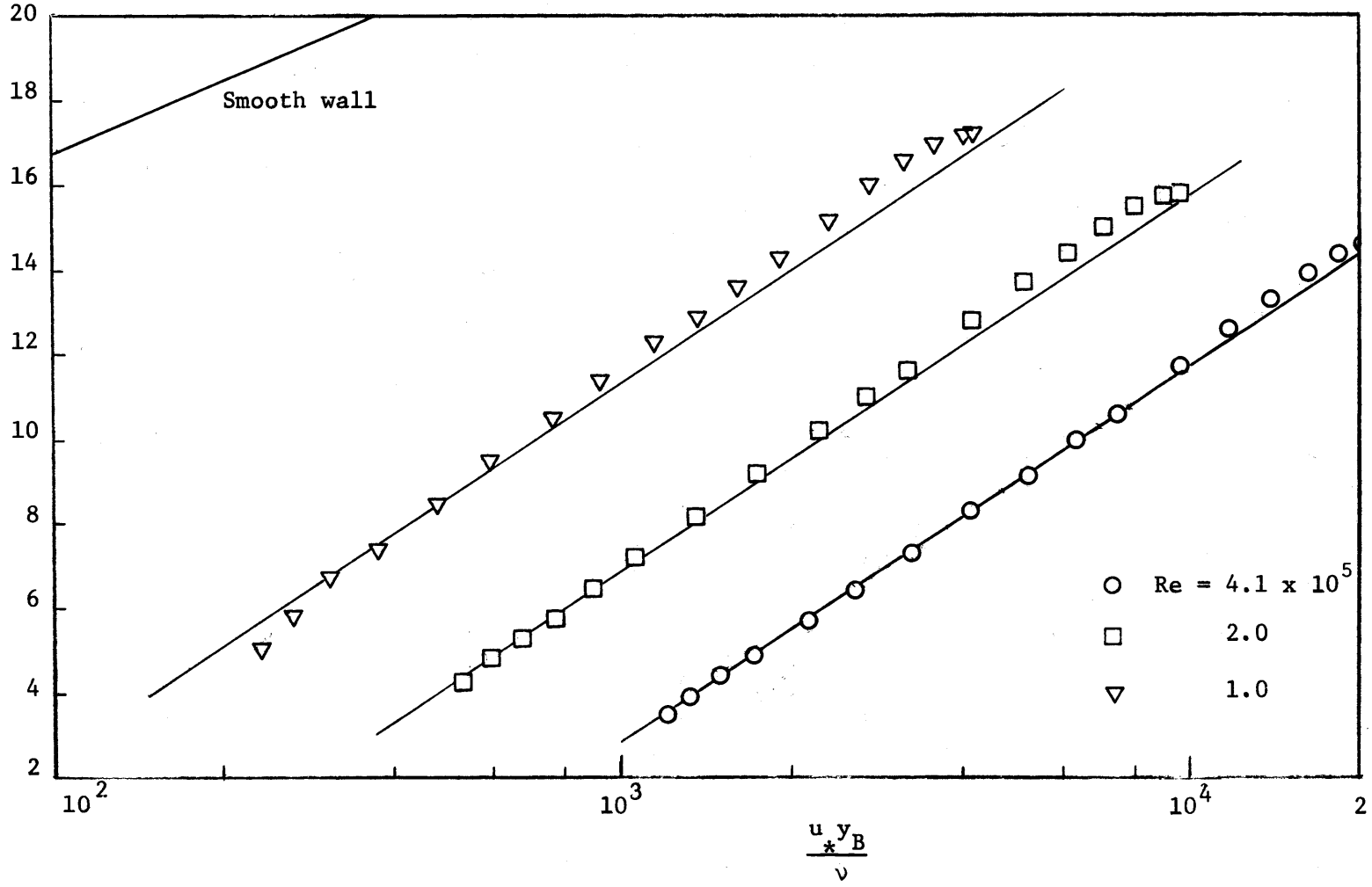

Fig. 4-9 Law of the wall in porous pipe, y_o = 0.21", κ = 0.26

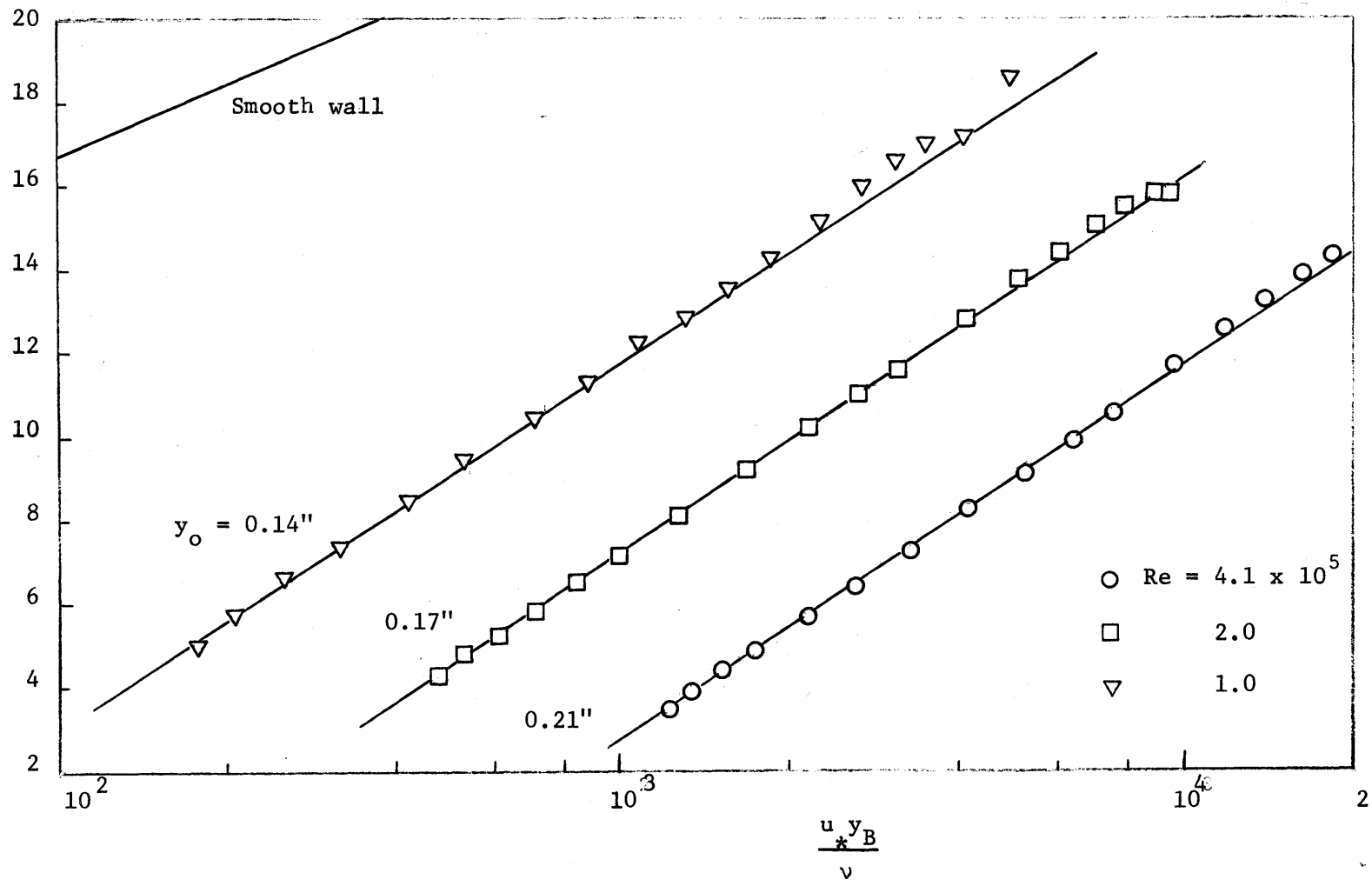

Fig. 4-10 Law of the wall in porous pipe, y_o variable from 0.14 to 0.21", $\kappa = 0.26$

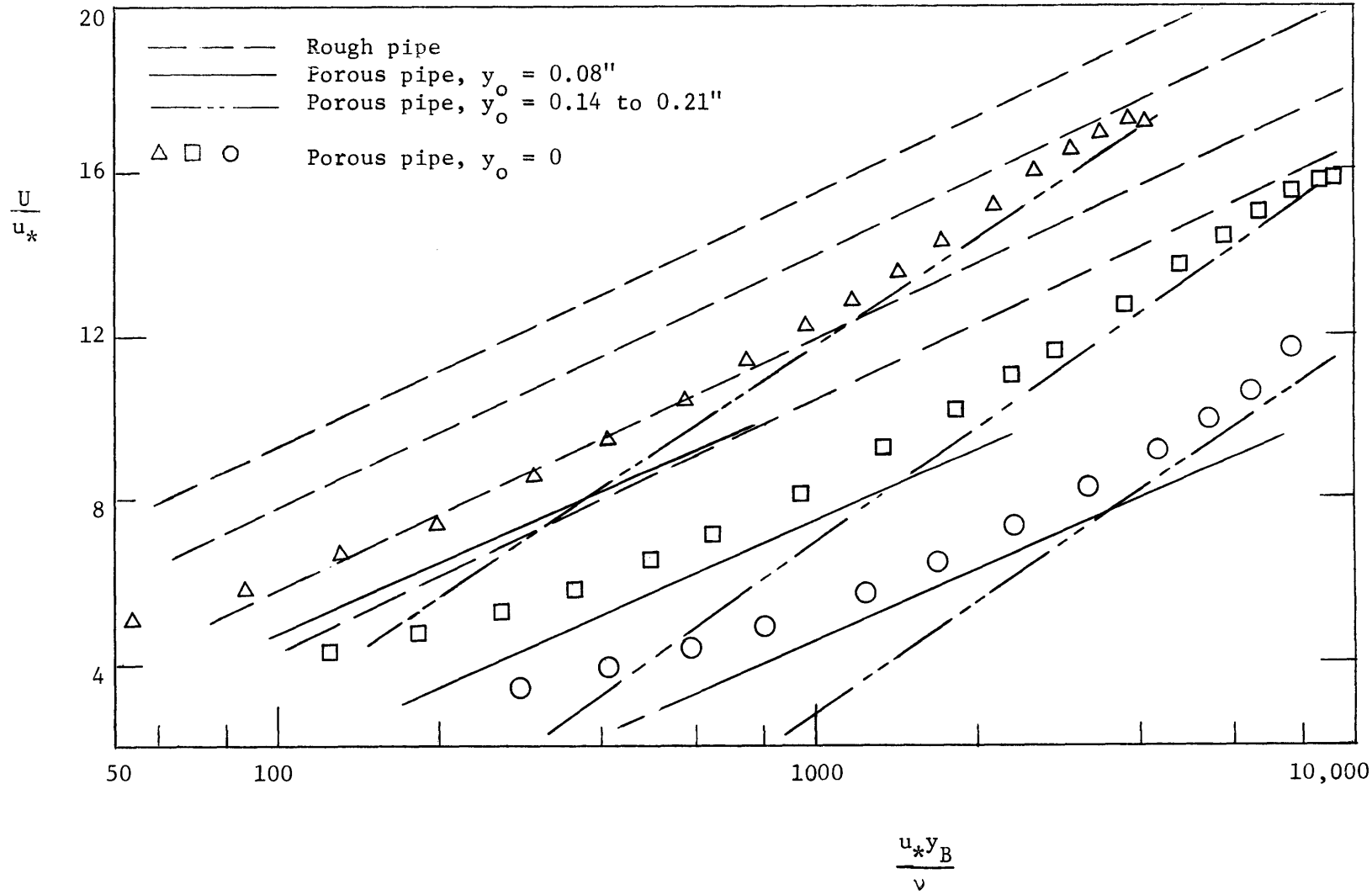

Fig. 4-11 Summary of mean velocity analysis in terms of law of the wall

have a universal distribution in the equilibrium layer in terms of the coordinate $(y_o + y)$. In this region, the logarithmic velocity law holds and, therefore,

$$\frac{dU}{dy} = \frac{u_*}{\kappa\left(y_o + y\right)} \tag{4-2}$$

Assuming a constant stress layer near the wall, the normalized production of turbulent energy is

$$\frac{-\overline{uv}}{u_*^4}\frac{dU}{dy}\frac{\nu}{} = \frac{1}{\kappa\frac{u_*\left(y_o + y\right)}{\nu}} \tag{4-3}$$

Thus, the constancy of κ implies that (4-3) has a universal distribution.

Another way of analyzing these data is in terms of the eddy viscosity ε defined in (2-13). With the same assumptions of constant stress and a logarithmic velocity distribution,

$$\frac{\varepsilon}{u_*\left(y_o + y\right)} = \kappa \tag{4-4}$$

or

$$\frac{\varepsilon}{\nu} = \kappa\frac{u_*\left(y + y_o\right)}{\nu} \tag{4-5}$$

showing again that ε/ν will have a universal distribution if κ is constant. It is more convenient to transform (4-5) to

$$\frac{\varepsilon}{u_* R} = \frac{\kappa\left(y_o + y\right)}{R} = \kappa\zeta \tag{4-6}$$

with $\zeta = \left(y_o + y\right)/R$, because in this form the same dimensionless parameters describe the flow over the whole pipe. The eddy viscosity has been computed using a semi-logarithmic plot of the velocity defect

$$\eta = \frac{U_{max} - U}{u_*}$$

versus ζ. From the definition of ε in (2-13) and a linear shear stress distribution, it follows that

$$\frac{\varepsilon}{u_* R} = \frac{\zeta\,(\zeta - 1)}{\frac{d\eta}{d(\ln \zeta)}} \tag{4-7}$$

and, as the semi-logarithmic plot is fairly close to a straight line, a graphical evaluation of (4-7) can be conveniently done. The computation of ε has been carried out for the two values of y_o, 0.08 and 0.21", and the results are shown in fig. 4-12. As expected, the points lie very close to equation (4-6), with the same values of κ as in the mean velocity plots. It seems, therefore, that the most reasonable interpretation is to treat κ as a universal constant, approximately 0.40, since in this way a universal distribution of ε is obtained near the wall. The point of departure from the universal distribution marks the end of the zone of validity of the logarithmic law. Fig. 4-13 presents the distribution of ε for both the rough and the porous pipes, in the latter case assuming $y_o = 0.08"$, together with the values computed by Hinze (1959) from smooth pipe measurements by Laufer and Nunner and the empirical curve found by Reichardt (1951) in a smooth rectangular channel, given by

$$\frac{\varepsilon}{u_* R} = \frac{\kappa}{3}\left[0.5 + \left(1 - \frac{y}{R}\right)^2\right]\left[1 - \left(1 - \frac{y}{R}\right)^2\right] \tag{4-8}$$

The agreement close to the wall is quite good. In the central core region, however, there are systematic variations which cannot be explained by mere experimental scatter. The values of $\varepsilon/u_* R$ seem to decrease with increasing effective relative roughness.

From the definition of ε, it is clear that a universal velocity defect law implies a universal distribution of ε, as can be seen explicitly in

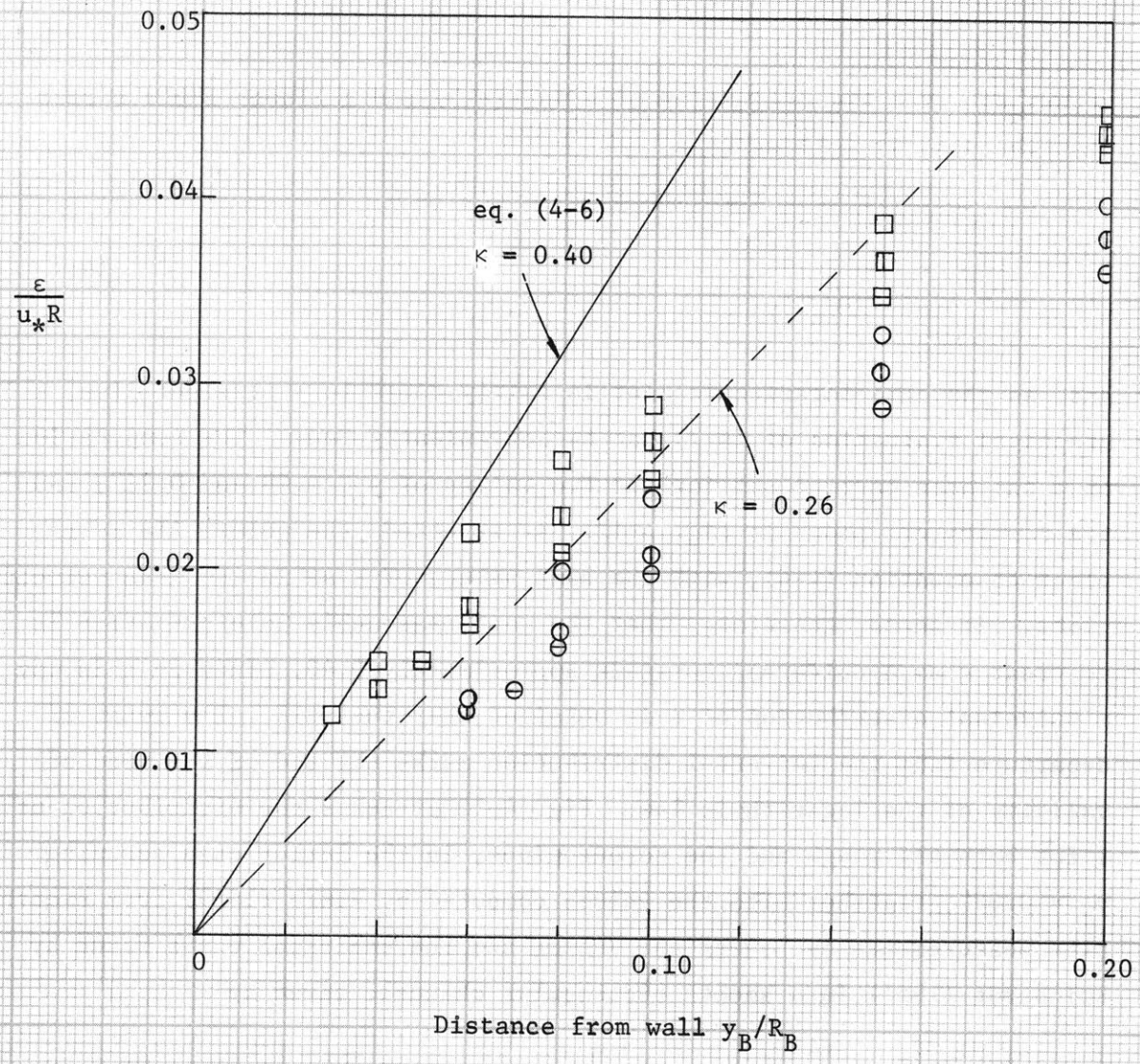

	$y_o = 0.08''$	$y_o = 0.21''$
$Re = 4.1 \times 10^5$	□	○
2.0	⊞	⊕
1.0	⊟	⊖

Fig. 4-12 Eddy viscosity distribution near the porous wall, with two alternatives values of y_o

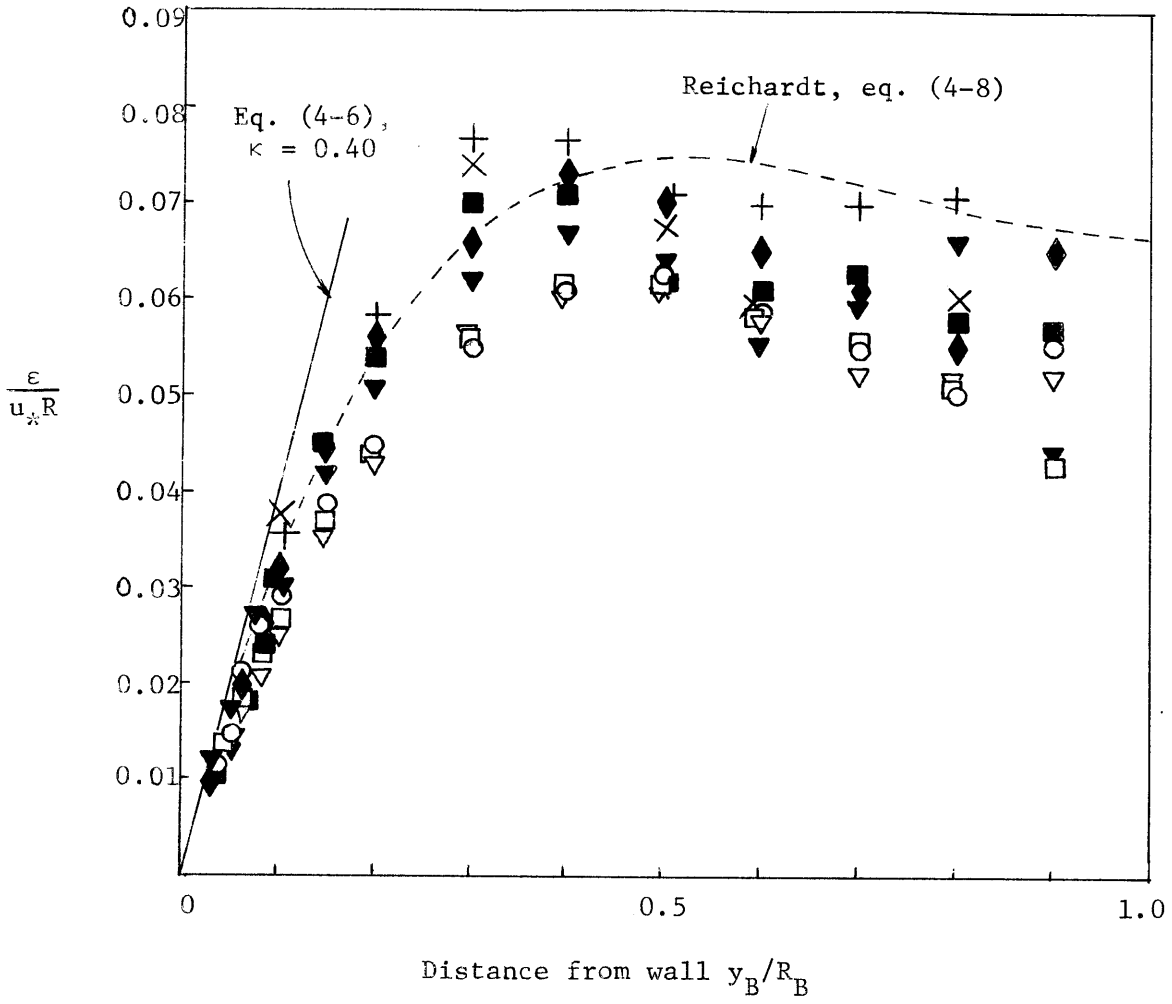

Fig. 4-13 Eddy viscosity distribution in rough and porous pipes

equation (4-7). Therefore, fig. 4-13 suggests systematic variations in the velocity defect profile. That such is, in fact, the case is shown in fig. 4-14 where the velocity defect is plotted as a function of position for both the rough and porous pipes. No substantial variation with Reynolds number is apparent, but there is a net displacement between the two series and also with respect to the smooth wall data represented by Laufer's measurements in a smooth pipe. Several proposed expressions for the velocity defect law are also shown in fig. 4-14, namely, the commonly used logarithmic equation (2-11), Lettau's equation (2-19) and the expression derived by Reichardt from his empirical equation (4-8) for the eddy viscosity

$$\frac{U_{max} - U}{u_*} = \frac{1}{\kappa} \ln\left[\frac{1 + 2\left(\frac{1-y}{R}\right)^2}{1 - \left(\frac{1-y}{R}\right)^2} \right] \qquad (4\text{-}9)$$

In all these expressions, κ has been taken as 0.40. The logarithmic equation shows a rather poor agreement with the data, even for smooth wall, whereas the empirical expressions of Lettau and Reichardt represent very well the smooth wall data. It is interesting to note that the same ambiguity encountered in the interpretation of the law of the wall is found here. For an expression like (4-9) can be made to fit the present data for rough or porous walls if a suitable κ is chosen. But then this constant would not be equivalent to the one appearing in the law of the wall. In fact, such a procedure would render κ meaningless. It must be concluded, therefore, that a strictly universal velocity defect law does not seem to exist for all kinds of wall conditions.

4.3 Turbulence Intensity

As a first indication of the reliability of the measurements, the normalized distribution of the Reynolds stress $-\overline{uv}/u_*^2$ is presented in fig. 4-15 for both pipes and compared with the theoretically known linear distribution. The agreement is typical of this kind of measurement and can be accepted as fair, considering that the computation is done by taking

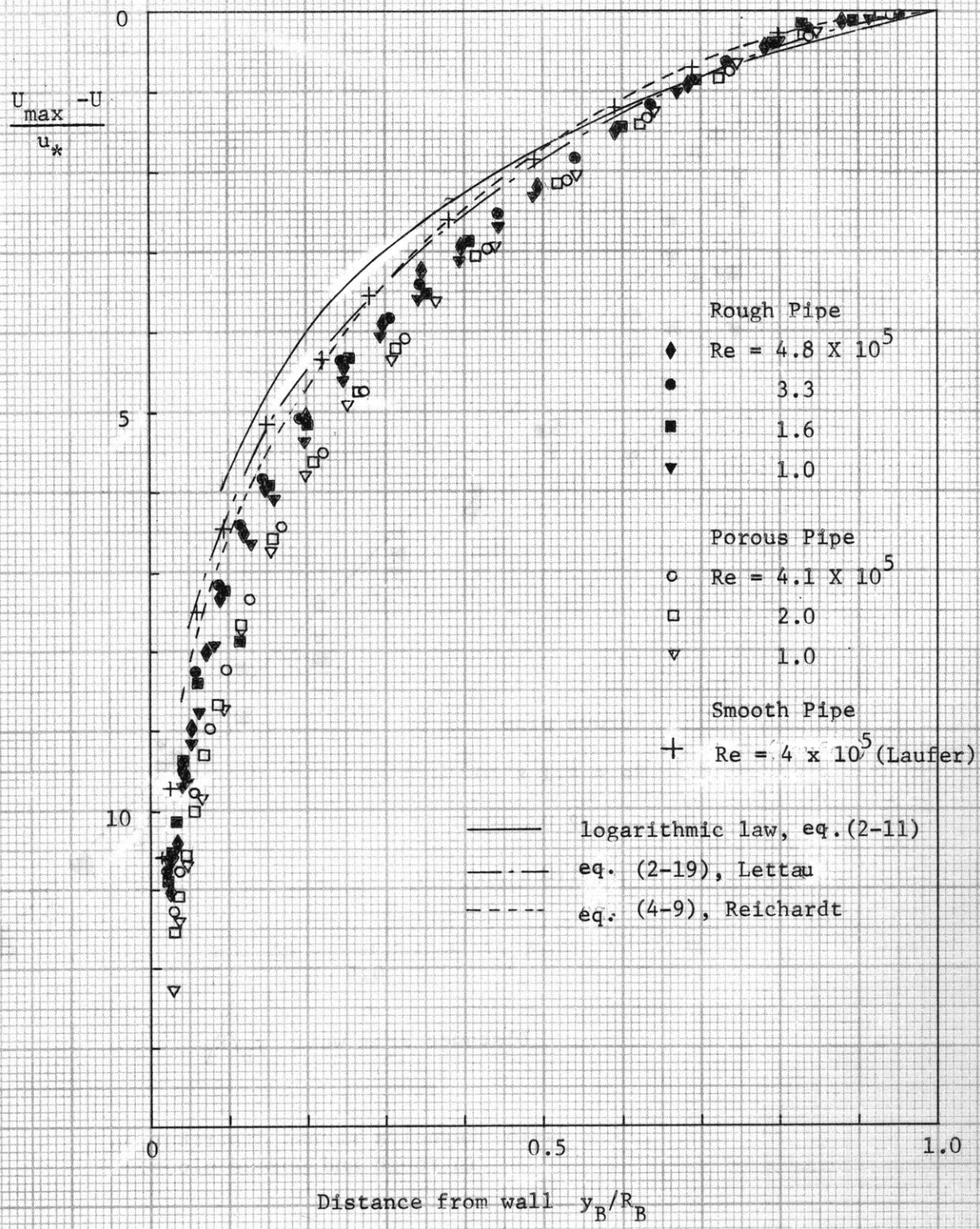

Fig. 4-14. Velocity defect distribution in rough and porous pipes.

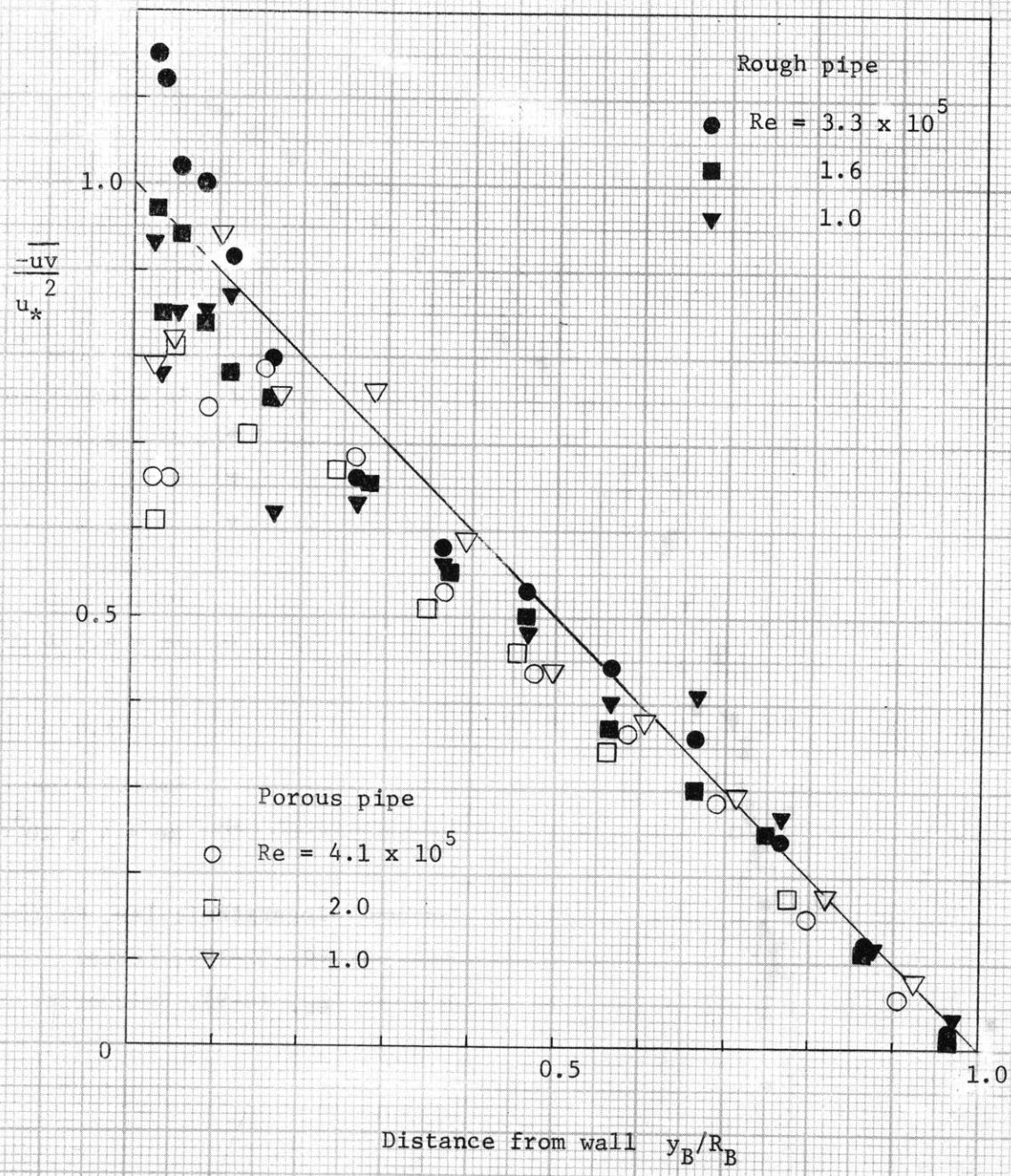

Fig. 4-15 Reynolds stress distribution in rough and porous pipes.

the difference of the squares of two measured quantities, as shown by equations (3-33). The same equations show that the intensities u' and v' are much less sensitive to random experimental errors, and therefore, their measurements should be expected to be substantially more accurate.

The axial and radial intensities of turbulence relative to the local velocity are plotted in figs. 4-16 and 4-17. In fig. 4-16, a comparison is made between the measurements of u'/U taken with the single wire and with the x-array probe. The four runs made with the single wire in the rough pipe exhibit a remarkable consistency, especially close to the wall, whereas similar measurements with the x-array probe are some 15% higher and show a distinct variation with Reynolds number. No explanation was found for the disagreement between the two probes. At first glance, the single wire measurements could be taken as more reliable. However, it must be recalled that the same probe failed to measure satisfactorily the mean velocity and it may be that the same instrumental errors have affected the turbulence measurements. On the other hand, in the case of the x-probe, the wires are much less exposed to interference from the probe stem. Therefore, there is no clear reason to prefer one of the probes as more reliable. The disagreement is somewhat smaller in the porous pipe runs, but there is more variation with Reynolds number in the x-array results. However, the accuracy of the measurements is not enough to assign a special significance to these variations. The most relevant feature of the relative intensities is, of course, their considerable increase with roughness. This is especially so of the intensity normal to the wall v'/U, which, for smooth walls, is fairly uniform throughout the pipe, but shows a continuous increase when approaching the rough and the porous walls.

However, when the same data are normalized with respect to the shear velocity u_*, the agreement with the smooth wall measurements is striking, as shown in figs. 4-18 and 4-19. This fact has been pointed out before, as was discussed in section 2.2. Considering the wide variations in the distributions of mean velocity and relative intensity of turbulence found in the present experiments, the final agreement must be taken as a strong proof of the existence of a universal distribution of the normalized inten-

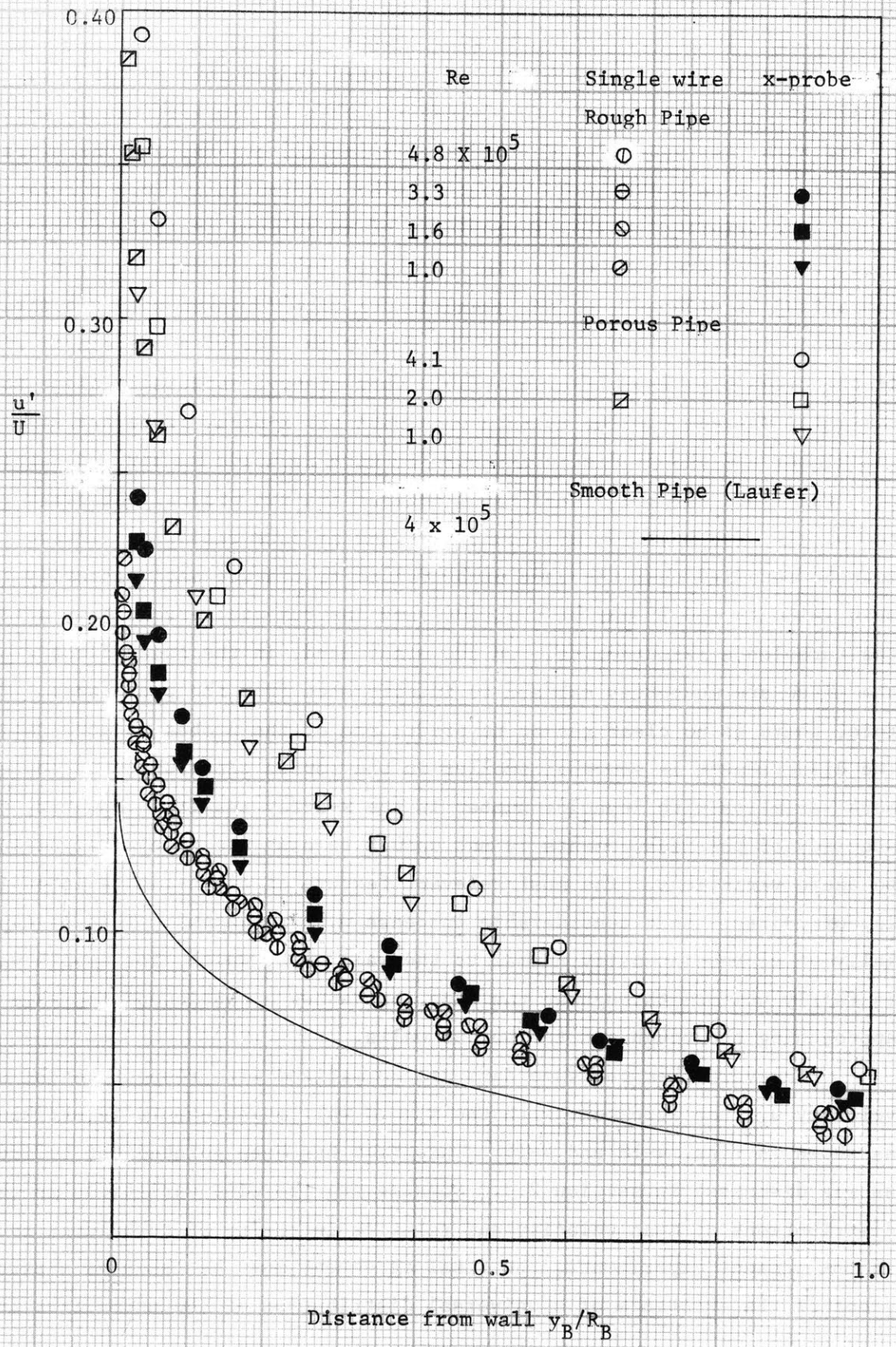

Fig. 4-16 Longitudinal intensity of turbulence relative to local velocity in rough and porous pipes.

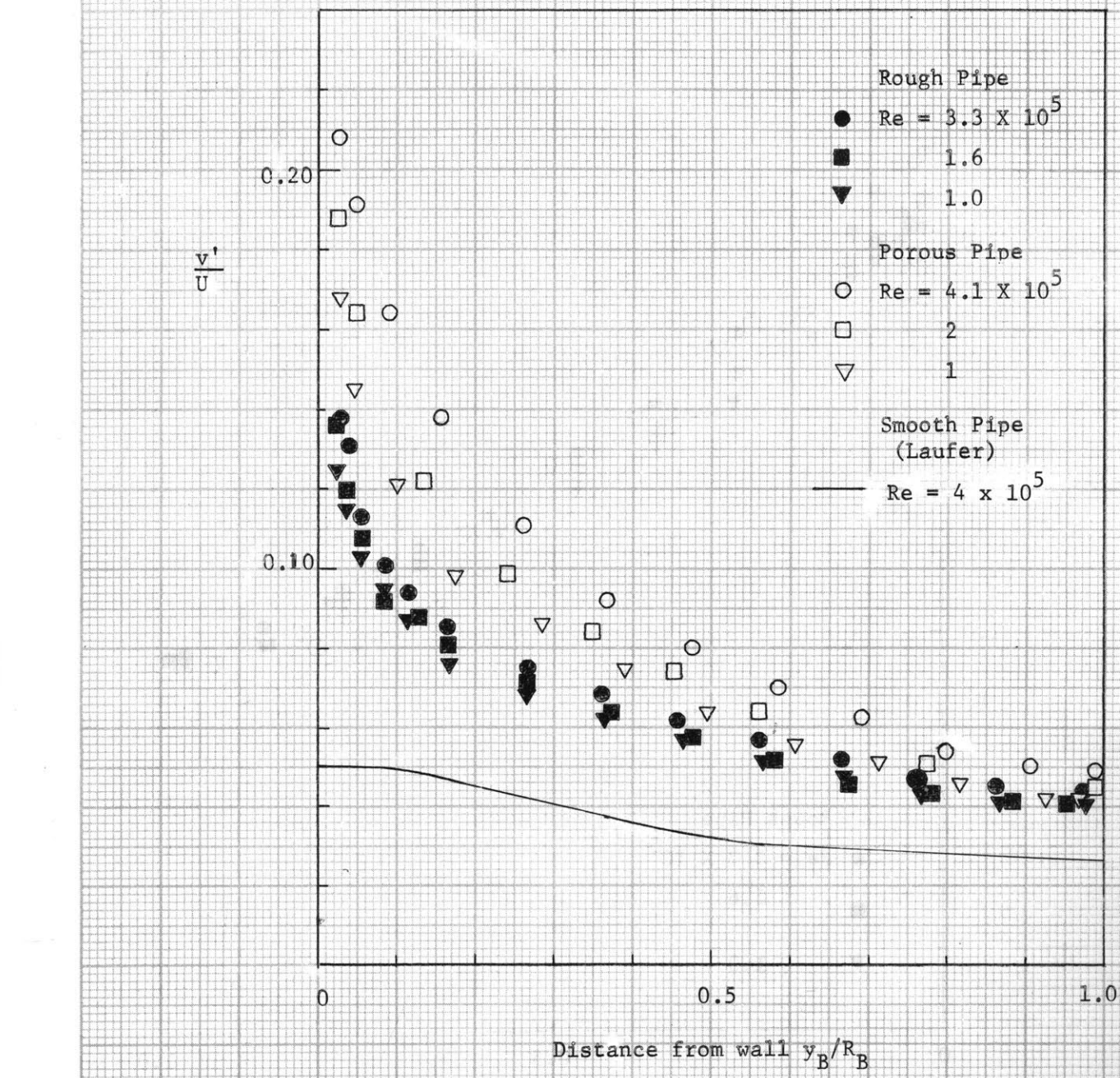

Fig. 4-17 Radial intensity of turbulence relative to local velocity in rough and porous pipes.

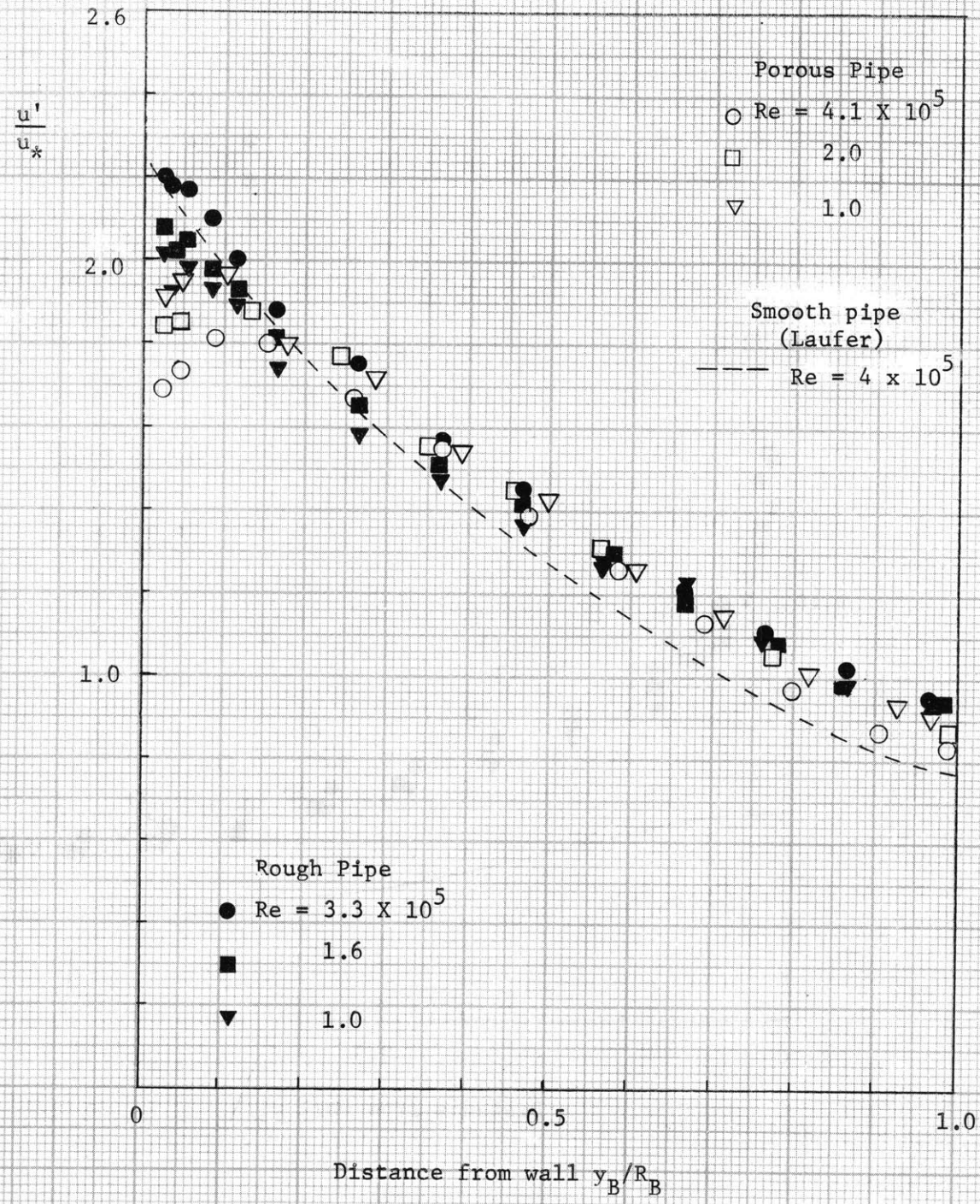

Fig. 4-18 Longitudinal intensity of turbulence relative to shear velocity in rough and porous pipes.

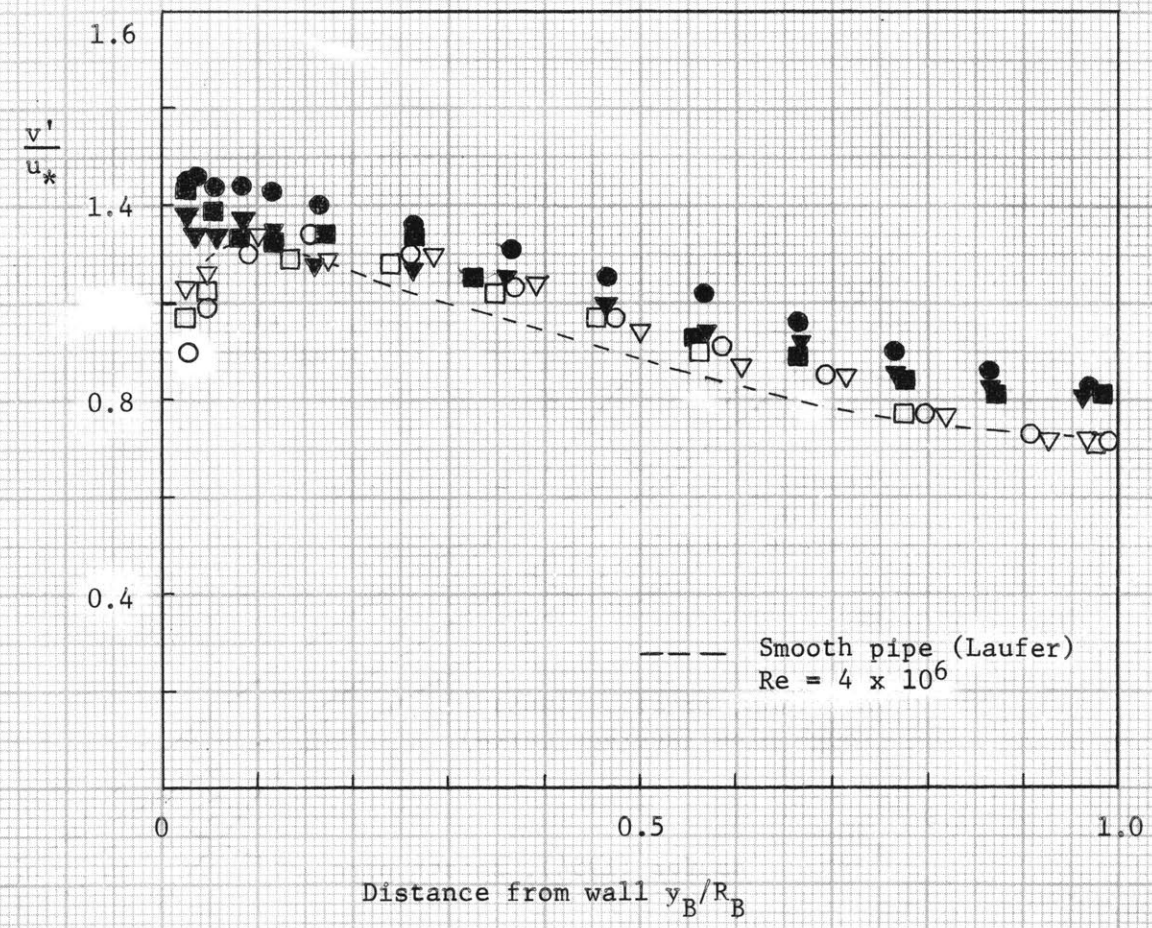

Symbols

Rough Pipe		Porous Pipe	
●	Re = 3.3 X 10^5	○	Re = 4.1 X 10^5
■	1.6	□	2.0
▼	1.0	▽	1.0

Fig. 4-19 Radial intensity of turbulence relative to shear velocity in rough and porous pipes.

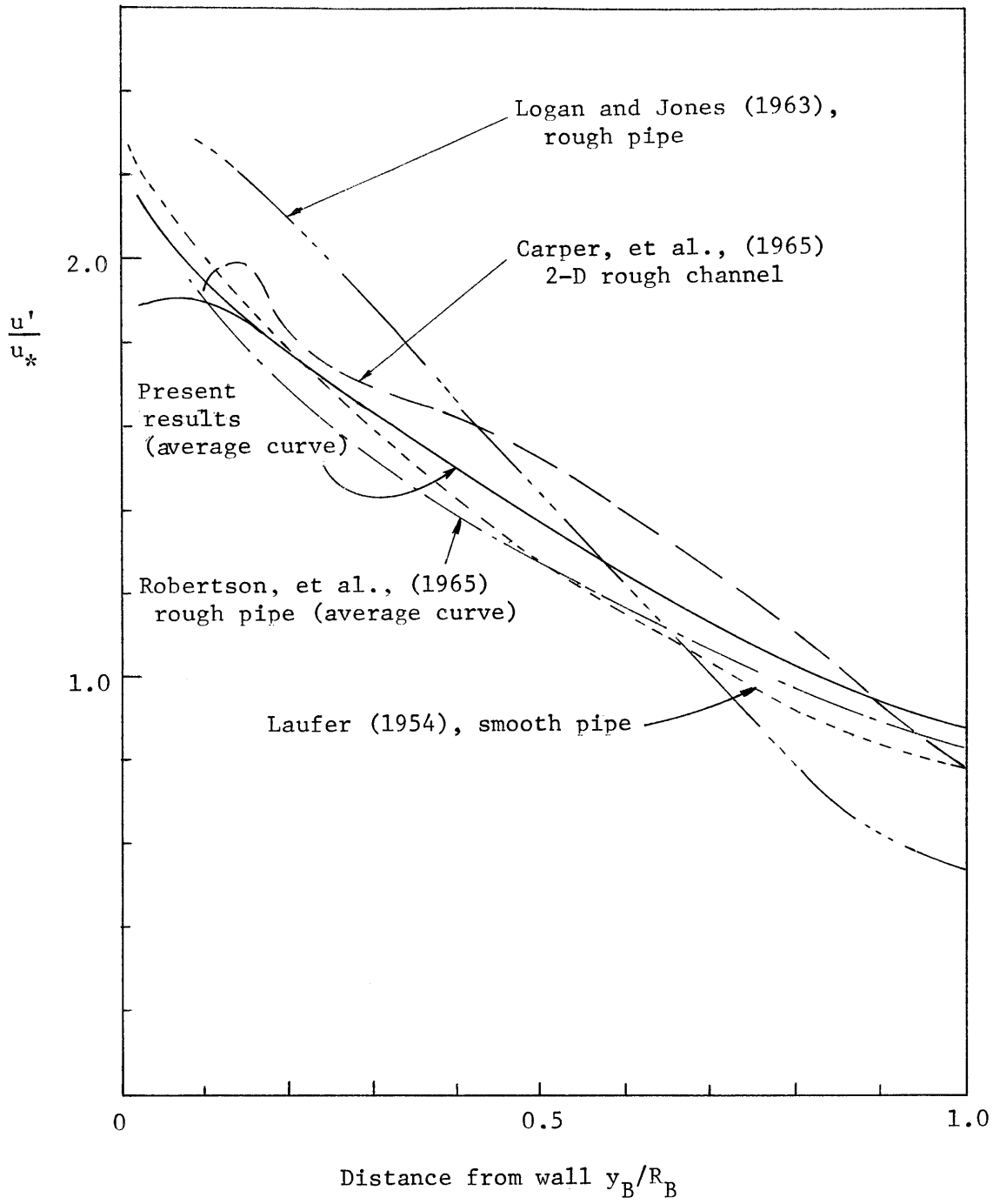

Fig. 4-20 Comparison of the measured intensity of turbulence with other data.

sities, independent of the nature of the wall. There are some minor variations close to the wall, the rough wall results being slightly higher than those for the porous wall. A similar trend of a decrease in u'/u_* with increasing roughness was found by Arndt and Ippen (1967) in a boundary layer. However, in the present case the variation is much less obvious, and it is contradicted by a comparison with the smooth wall results by Laufer, which are, if anything, below those for the rough wall. It seems, therefore, that the departures from a universal distribution found in this investigation should not be deemed significant. As explained before, there is little available information with which the present results may be compared. A summary is presented in fig. 4-20. The results of Robertson, Burkhart and Martin (1965) for u'/u_* and v'/u_* are represented by the average trend curve. The deviations of the individual observations are not large, less than 15%, if two runs notoriously out of line are eliminated. In addition, the distributions of u'/u_* measured by Logan and Jones (1963) in a rough pipe and by Carper, Heilhecker and Logan (1965) in a rough rectangular channel are shown. It must be recalled that, in these last two cases, the profile had not reached the fully developed condition. In particular, the data by Logan and Jones weretaken at 12.75 diameters from the beginning of the roughness. Reference to fig. 3-8 shows that the intensity of turbulence distribution differs appreciably at this station from the final profile. Thus, these data are presented only to compare the general order of magnitude. The data of Carper, et al., were taken at 20 times the height of the channel, and they seem to be much closer to a fully developed profile. Data for rough boundary layers are not included in fig. 4-20, since the distribution of intensity is different, but, as shown by Arndt and Ippen (1967), the maximum values of u'/u_* close to the wall are in the same general range as in a pipe, i.e., between 1.6 and 2.1.

The anisotropy ratio v'/u' is presented in fig. 4-21. Over most of the pipe, there is general agreement, regardless of the nature of the wall. However, close to the wall, the ratio tends to a constant value, approximately 0.6, in the present experiments, whereas for a smooth wall there is a sharp drop to a value around 0.25 at the edge of the viscous sublayer.

Conversely, at the centerline, the ratio v'/u' for rough and porous walls is somewhat lower than in the smooth wall case.

4.4 Turbulent Energy Spectra

The energy spectrum functions E_u for u and E_v for v are defined by

$$\left.\begin{aligned} \int_o^\infty E_u(f)\, df &= \overline{u^2} \\ \int_o^\infty E_v(f)\, df &= \overline{v^2} \end{aligned}\right\} \qquad (4\text{-}10)$$

where f is the frequency measured in cps. The data have been normalized by

$$\left.\begin{aligned} \phi_u &= \frac{E_u\, U}{\overline{u^2}\, D} \\ \phi_v &= \frac{E_v\, U}{\overline{v^2}\, D} \\ f' &= f\,\frac{D}{U} \end{aligned}\right\} \qquad (4\text{-}11)$$

where U is the local mean velocity and D the diameter of the pipe. In this way,

$$\int_o^\infty \phi_u(f')\, df' = \int_o^\infty \phi_v(f')\, df' = 1.$$

It is interesting to note that, by Taylor's hypothesis, the wave number k is given by

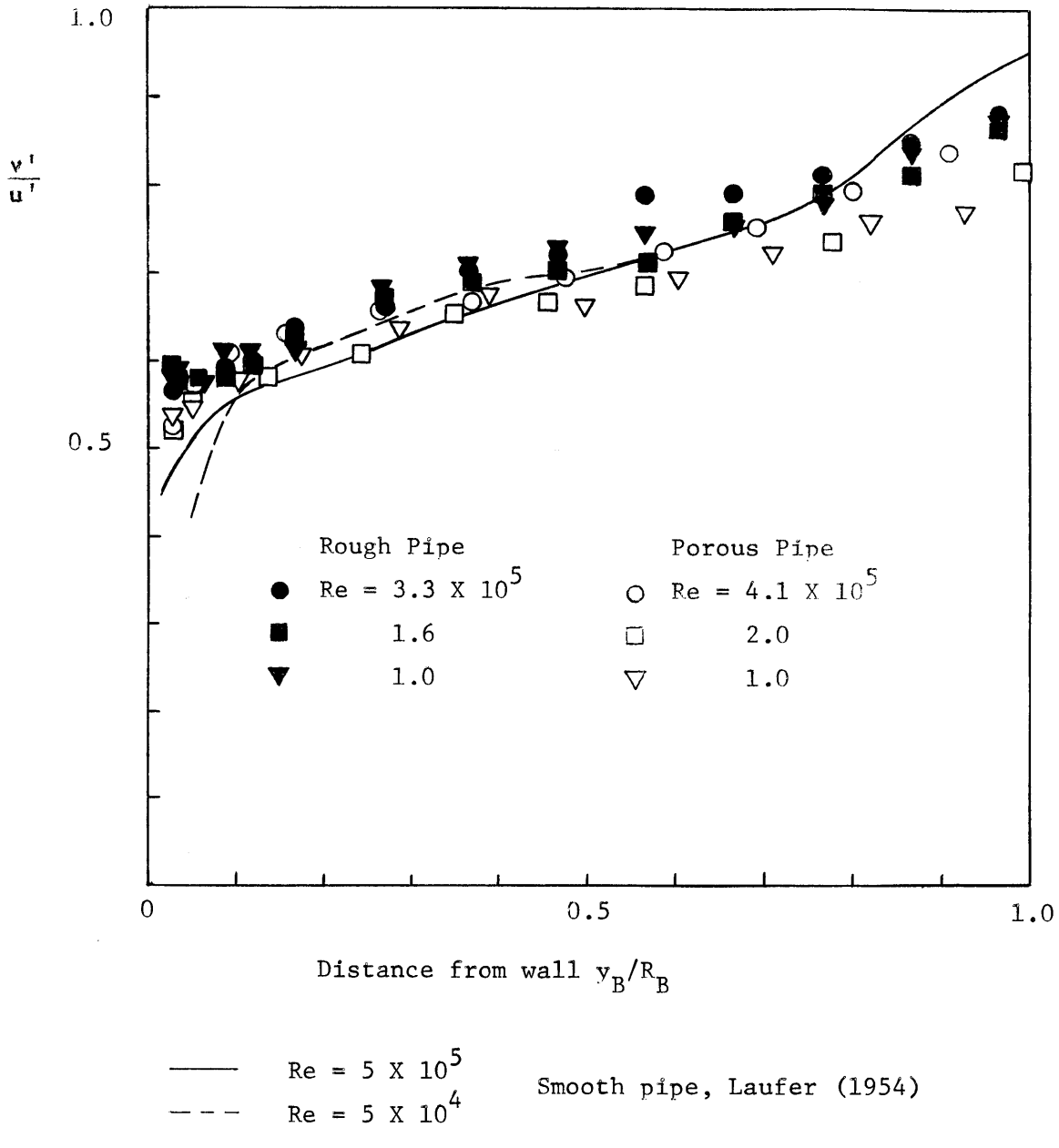

Fig. 4-21 Turbulence anisotropy ratio v'/u'.

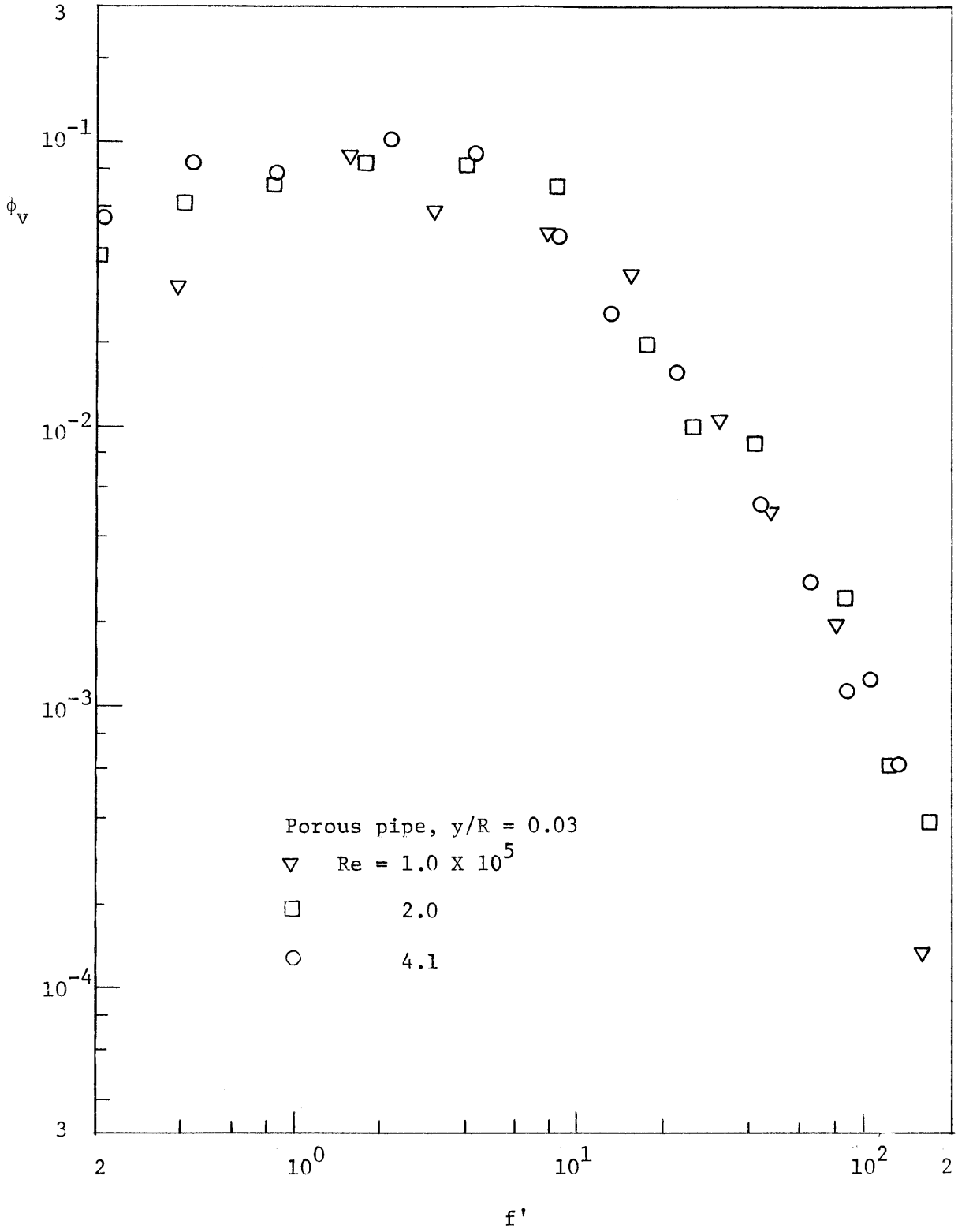

Fig. 4-22 Variation of normalized energy spectrum Φ_v with Reynolds number.

$$k = \frac{2\pi f}{U} \tag{4-12}$$

and it follows that

$$f' = \frac{kD}{2\pi} = \frac{D}{L} \tag{4-13}$$

if L is the wavelength at the frequency f.

The dependence of the normalized energy spectra ϕ_u and ϕ_v on Reynolds number and distance to the wall was studied in both the rough and the porous pipe. No significant variation with Reynolds number was found. A typical example is offered in fig. 4-22, which shows ϕ_v at the position closest to the wall in the porous pipe.

In fact, a fairly universal behavior can be detected in both ϕ_u and ϕ_v, as evidenced by the composite plots of figures 4-23 and 4-24, which include the total of the spectral observations. In each run, the lowest frequency shown is 5 cps and the highest 5,000 cps, which is the nominal frequency response limit of the recording system. The average trend curves for ϕ_u and ϕ_v are shown in both graphs to emphasize the consistent difference in shape between the two functions.

There are, however, some systematic variations with distance from the wall. In fig. 4-25, a comparison is made between ϕ_u measured at the centerline and at the smallest distance from the wall, for both pipes. The spectra measured by Laufer at corresponding positions in a smooth pipe are also shown in fig. 4-25. The most noticeable effect is the decrease of the spectrum at the wall with respect to that at the centerline for the low frequencies, especially so in the porous pipe. Even though at these low frequencies the measurements are more subject to instrumental errors, the variation is deemed significant. It was noticed that the shape of ϕ_u in the porous pipe hints at some similarity with the theoretical spectrum of the velocity fluctuation at the surface of the porous medium, as presented in fig. 2-8. Although the significance of this similarity is difficult to judge, it is interesting to note that, for the experimental conditions,

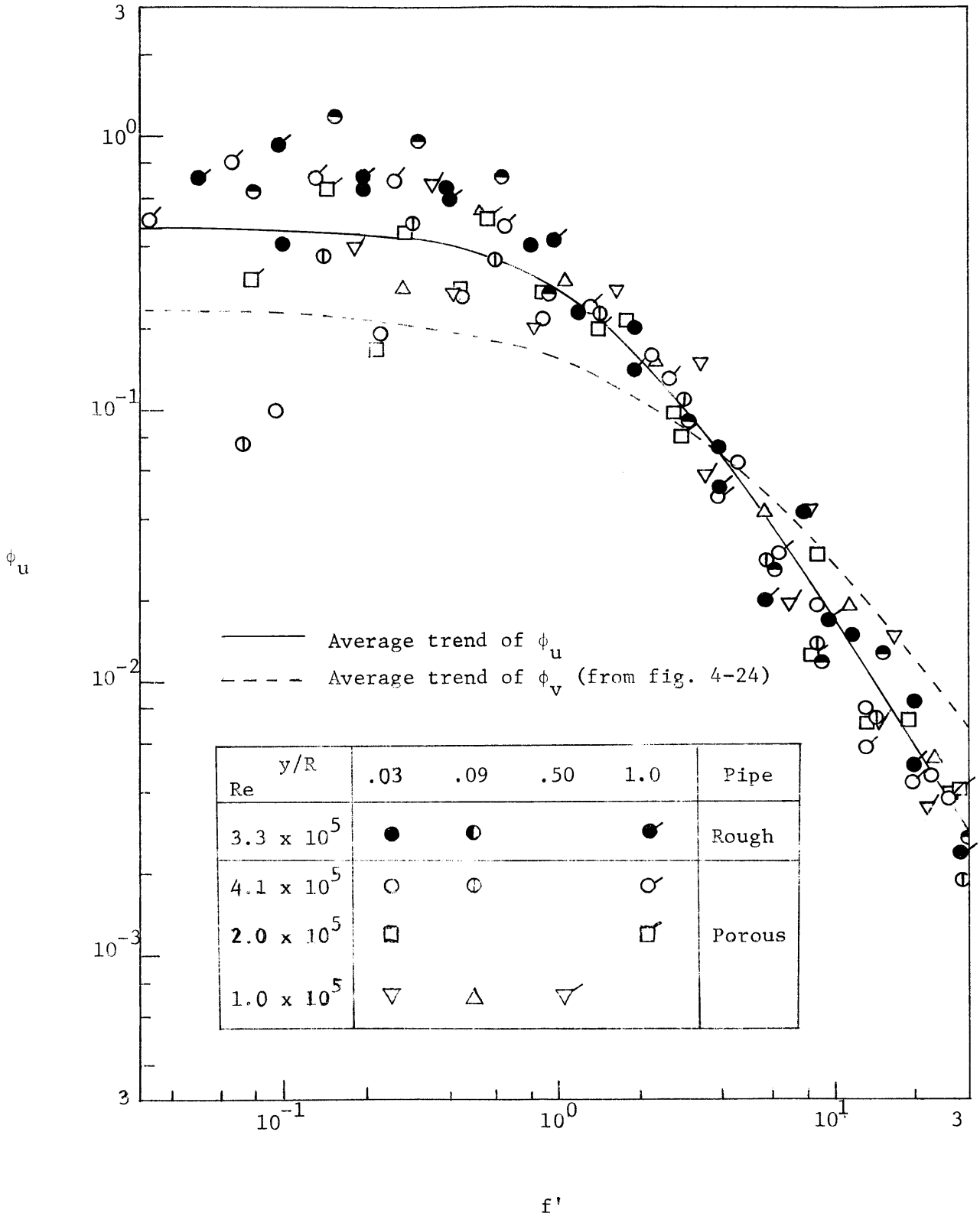

Fig. 4-23 Universal plot of spectrum analysis of the longitudinal velocity fluctuation

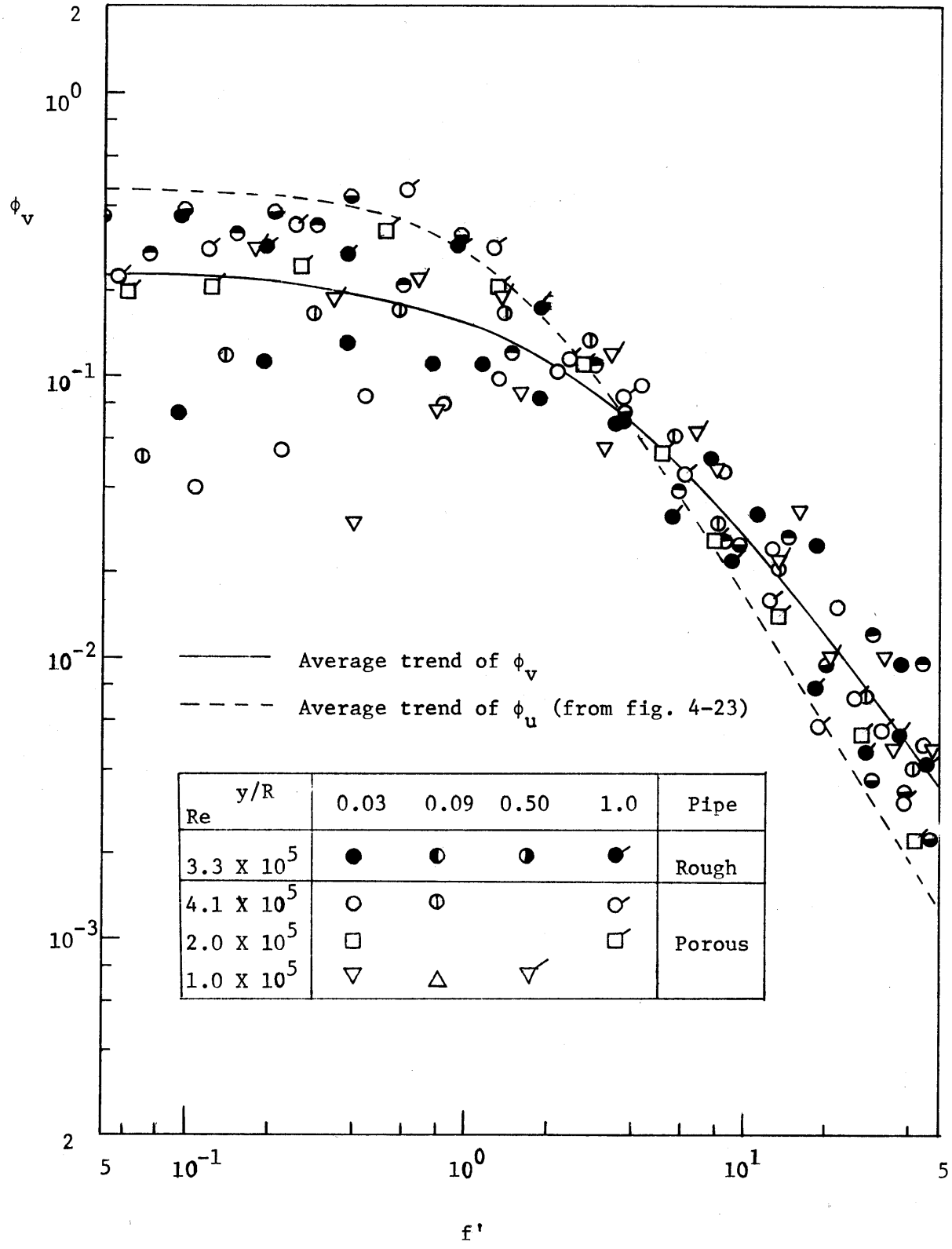

Fig. 4-24 Universal plot of spectrum analysis of the radial velocity fluctuation.

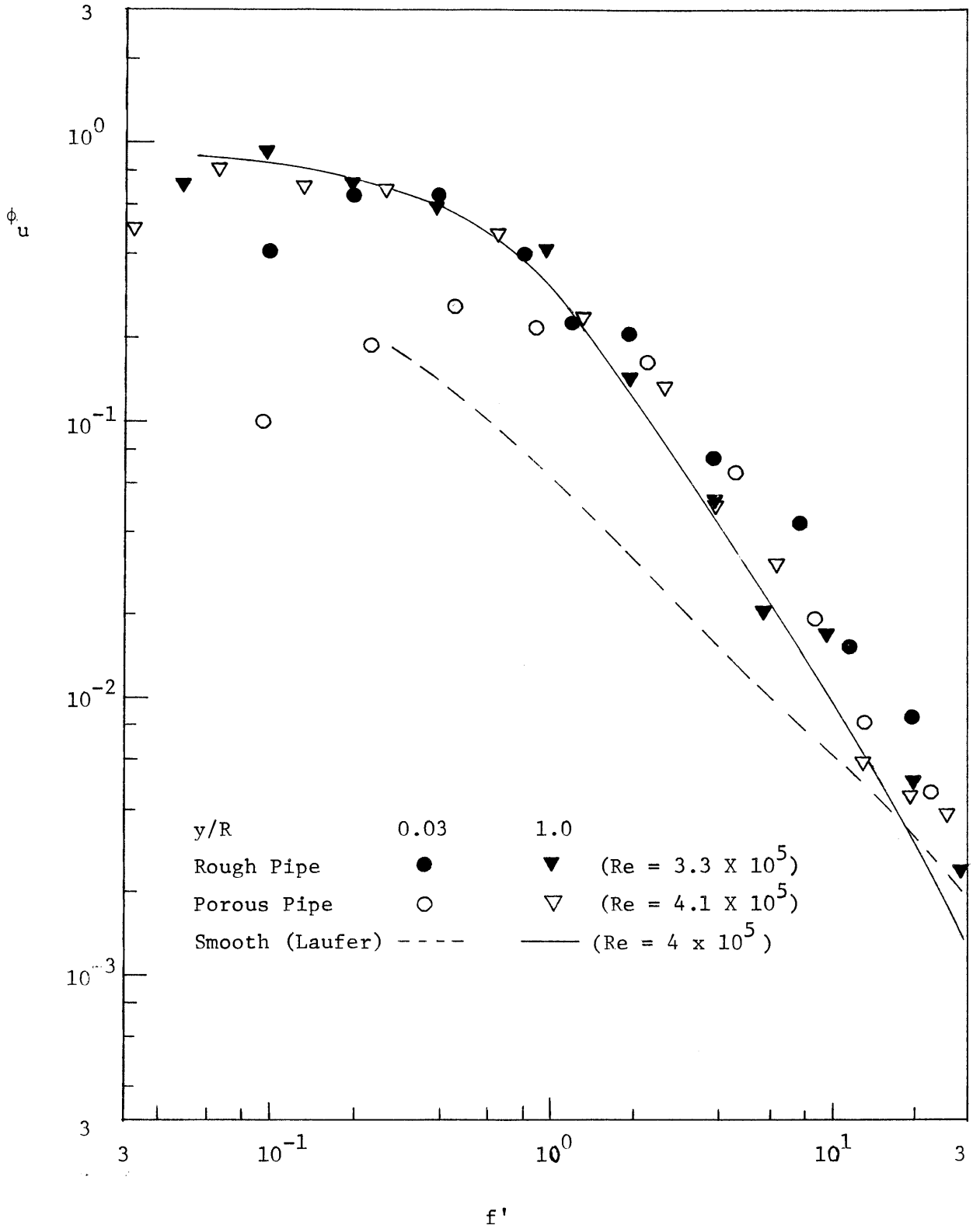

Fig. 4-25 Variation of energy spectrum ϕ_u with distance to wall.

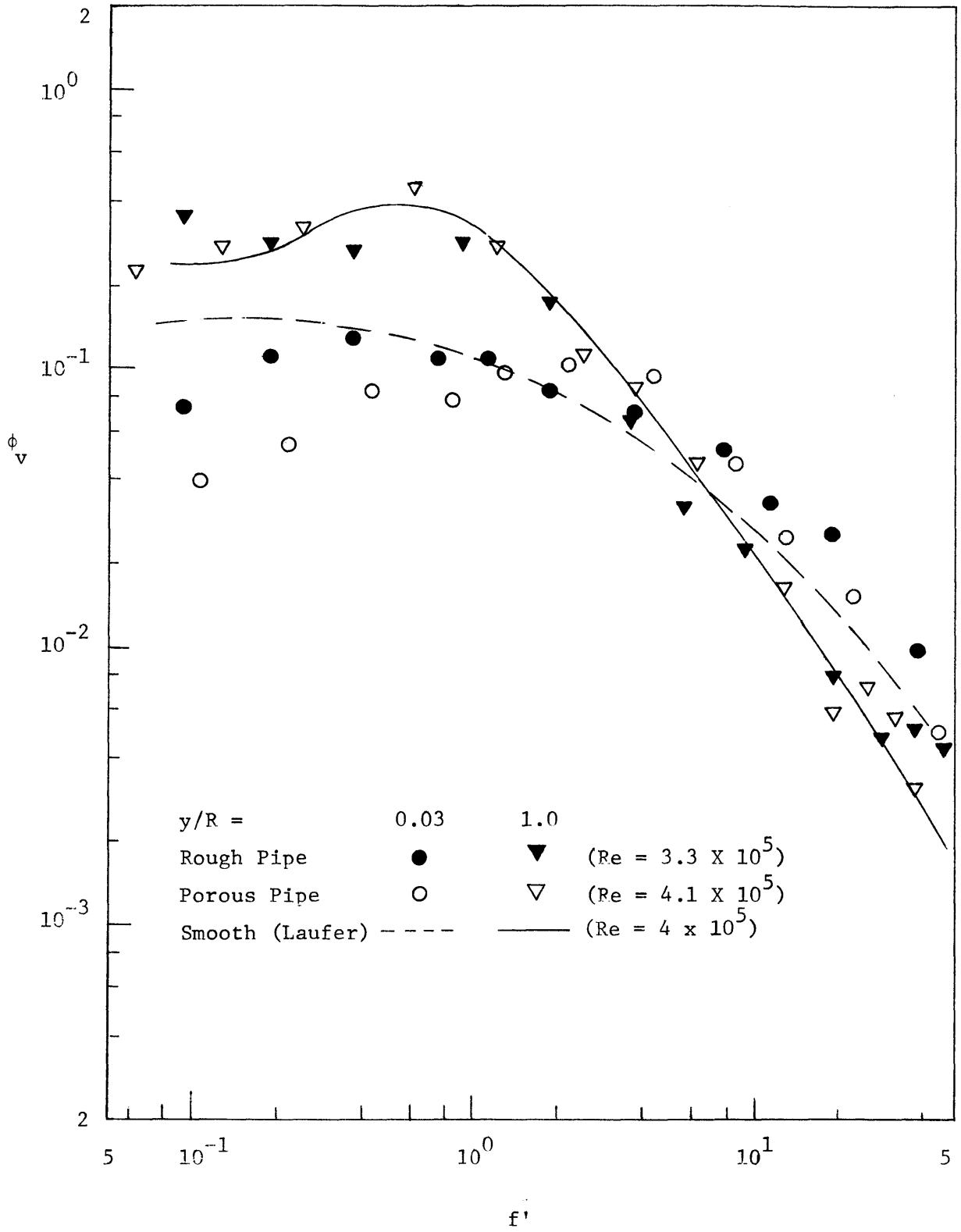

Fig. 4-26 Variation of energy spectrum ϕ_v with distance to wall.

σ is approximately 0.8, which corresponds in fig. 2-8 to a peak of the spectrum at $\Omega = 2\pi f\ D/\bar{U} = 0.8$, and therefore, $f' \approx 0.25$, which is not far from the suggested experimental peak in fig. 4-25.

At the higher frequencies, the spectrum at the wall tends to become larger than that at the centerline, in accordance with the notion that the size of the eddies increases towards the centerline of the pipe. In general, the measurements at the centerline for the three wall cases are in good agreement, but significant variations are encountered close to the wall.

A similar analysis for ϕ_v is presented in fig. 4-26, which shows the same features as in the case of ϕ_u in fig. 4-25. The spectrum at the wall is substantially smaller than that at the centerline for the low frequencies, and slightly higher for high frequencies. The low frequency departure is more accentuated in the porous pipe than in the rough pipe. The agreement with Laufer's data is better than in the case of ϕ_u.

CHAPTER 5
SUMMARY AND CONCLUSIONS

A study of the turbulence characteristics in pipe flow with rough and porous walls has been made, with the ultimate purpose of developing a more complete understanding of the mechanics of sediment transport. The main conclusions are summarized in the following.

5.1 Theoretical Analysis of the Flow in the Porous Wall

Turbulent pipe flow produces wall pressure fluctuations, which in the case of a porous wall will be transmitted into the fluid in the porous medium and generate a turbulent motion therein. An analysis of this flow has been made, assuming the validity of a linearized, Darcy-type equation of motion with inclusion of the local acceleration term. As boundary condition at the wall surface, the pressure is assumed to be of essentially the same form as the wall pressure in a smooth pipe. Two different specifications for the wall pressure have been applied, one as a random function of space and time and the other as a sinusoidal pressure wave. Important features of the solutions are:

a) The normalized intensity of the longitudinal velocity fluctuations at the wall surface u'/u_* tends to an asymptotic value of 0.38 as the permeability increases. This value is deemed large enough to produce substantial effects on the pipe flow, although it is smaller than the measured intensities in shear flows near a wall, which are of the order of 2 u_*.

b) The ratio of the viscous energy dissipation in the porous medium to the total dissipation in pipe flow has a maximum for a particular combination of permeability, viscosity and average velocity. The maximum can be as high as 5% in the case of infinite thickness of the porous layer. For the present experimental conditions, it was close to 1%.

c) The sinusoidal wave formulation of the problem provides an approximate solution in fairly good agreement with the more complicated spectral approach if a suitable wave length, of the order of 10 pipe diameters, is used.

d) The Reynolds stress $-\overline{uv}$ derived from this linearized analysis is

identically zero throughout the porous medium.

e) The computation of the spectrum of the velocity fluctuation at the surface of the porous layer shows that the porous medium acts as a filter, with the components at the low frequencies (i.e., at large wave lengths) being severely attenuated. A resonant peak is found at a characteristic frequency which depends on the permeability, the viscosity and the time integral scale of the wall pressure.

Although it was not possible to evaluate the modifications produced in the pipe flow by the feedback effects from the porous medium flow, the analysis proved useful in the selection of the experimental conditions.

5.2 Mean Flow Characteristics

Measurements of friction factor and mean velocity distribution were conducted in two pipes, approximately 10" in diameter, one with 1/8" spherical roughness elements and the other with a 1.20" thick porous lining. The Reynolds number based on pipe diameter and average velocity ranged from 1×10^5 to 5×10^5. No measurements were taken within the porous layer.

The rough pipe behaves in every respect in accordance with the classical experiments of Nikuradse for particulate roughness.

The most obvious difference found in the porous pipe is the very high friction factor and its continuous increase with Reynolds number throughout the range of the experiments, even when, under normal conditions, the flow would have been in the fully rough regime. The displacement of the logarithmic velocity distribution with respect to the smooth wall law is consistent with the friction factor behavior, both indicating an equivalent roughness of the same order as the thickness of the porous lining.

Alternative interpretations of the Kármán constant κ have been examined. A consistent description of the mean velocity distribution is obtained by accepting κ as a truly universal constant, approximately 0.40. The position of the effective origin for the logarithmic profile changes with Reynolds number. The distance from the wall up to which the logarithmic law holds is smaller for the porous pipe than for the rough pipe.

The eddy viscosity follows a universal behavior near the wall, but systematic variations are present towards the center of the pipe. The normalized eddy viscosity is smaller in the rough wall case than in smooth pipes, and even more so for the porous pipe. These variations are reflected in the velocity-defect distribution, which is not strictly a universal function of position.

5.3 Turbulence Characteristics

The distributions of the intensities of turbulence u' and v' in the axial and radial directions, as well as the corresponding Reynolds stress were measured in each pipe using constant temperature hot wire anemometers. The relative intensities u'/U and v'/U are higher in the rough case than in the smooth case throughout the pipe, and much higher in the porous pipe. Of special significance is the change in v'/U, which for a smooth wall is roughly constant, except in the immediate vicinity of the wall where it drops to zero; whereas, for the rough wall, and even more so for the porous case, it steadily increases as the wall is approached. As a consequence, the ratio v'/u' remains at the same constant level in the presence of rough and porous walls, without any sign of the sharp decrease shown by smooth wall data.

When normalized with respect to shear velocity, a universal agreement is found between intensity data for smooth, rough and porous walls.

The energy spectrum of the velocity fluctuation u in the axial direction shows a fairly universal shape, independent of the wall condition, for smooth, rough and porous walls. The same is true of the spectrum of the radial component v of the fluctuation. No dependence on Reynolds number was found. A systematic variation with distance from the wall is present in the spectra for both u and v. At low frequencies, the spectrum near the wall is lower than at the centerline, whereas at high frequencies the opposite trend holds. This variation is more pronounced in the case of the porous wall. For the rough pipe, the variation is clear only in the spectrum of v.

5.4 Recommendations

It is believed that the present study has provided the needed background

information to guide a more comprehensive evaluation of porous boundary effects. One obvious extension of the experimental work is the systematic testing of different porous boundaries, with varying permeability, porosity, thickness and surface texture. In particular, it has been suggested that the flexibility of the material used in this investigation might have had a significant role in the observed effects. Only a comparative test can provide a definite conclusion in this respect. These kind of experiments could be more conveniently conducted in a rectangular channel.

From the theoretical point of view, an attempt should be made to analyze the flow in the porous medium using the complete, nonlinear equation of motion. If a non-zero Reynolds stress were found, perhaps the coupling between the pipe and the porous medium flows could be achieved through a mixing length formulation. In this regard, it would be useful to have experimental information about the balance of turbulent energy near rough and porous walls. These are not easily accomplished tasks, but substantial progress in such difficult problems as the theory of sediment transport can be achieved only through a much deeper insight into the nature of wall turbulence.

REFERENCES

1. Arndt, R.E.A. and Ippen, A.T., "Cavitation Near Surfaces of Distributed Roughness", M.I.T. Hydrodynamics Laboratory Technical Report No. 104, June 1967.

2. Bachmat, Y., "Basic Transport Coefficients as Aquifer Characteristics", Int. Assn. Sci. Hydrology, Symposium on the Hydrology of Fractured Rocks, Dubrovnik, 1965.

3. Barbin, A.R. and Jones J.B., "Turbulent Flow in the Inlet Region of a Smooth Pipe", Trans. A.S.M.E., Journ. Basic Eng., Vol. 85, Series D, No. 1, March 1963, pp. 29-34.

4. Batchelor, G.K., "The Theory of Homogeneous Turbulence", Cambridge University Press, 1960.

5. Carper, H.J., Heilhecker, J.K. and Logan, E., "The Effects of a Change in Wall Roughness on Turbulence Intensity and Shear Stress Distribution in a Two-Dimensional Channel Flow", Developments in Mechanics, Proc. 8th Midwest. Mech. Conference, Pergamon Press, 1965, pp. 16-25.

6. Champagne, F.H., Sleicher, C.A. and Wehrmann, O.H., "Turbulence Measurements with Inclined Hot-Wires, Part 1, Heat Transfer Experiments with Inclined Hot-Wire", J. Fluid Mech., 28, Part 1, April 1967, pp. 153-175.

7. Chao, J.L. and Sandborn, V.A., "Study of Static Pressure Along a Rough Boundary", Proc. A.S.C.E., J. Hyd. Div., Vol. 91, No. HY2, March 1965, pp. 193-204.

8. Clauser, F.H., "The Turbulent Boundary Layer", Advances in Applied Mechanics, Vol. 4, Academic Press, 1956, pp. 1-51.

9. Collis, D.C. and Williams, M.J., "Two-Dimensional Convection from Heated Wires at Low Reynolds Number", J. Fluid Mech., 6, Part 3, October 1959, pp. 357-384.

10. Committee on Sedimentation, Hydraulics Division, A.S.C.E., "Sediment Transportation Mechanics: Suspension of Sediment," Proc. A.S.C.E., J. Hyd. Div., Vol. 89, No. HY5, September 1963, pp. 45-76.

11. Corcos, G.M., "Pressure Fluctuations in Shear Flows", Univ. of California, Inst. of Eng. Res. Report, Series 183, No. 2, 1962.

12. Corcos, G.M., "The Structure of the Turbulent Pressure Field in Boundary Layer Flows", J. Fluid Mech., 18, Part 3, March 1964, pp. 353-378.

13. Corrsin, S. and Kistler, A.L., "Free-Stream Boundaries of Turbulent Flows", N.A.C.A. TN 3133, 1954, also Report 1244, 1955.

14. Delleur, J.W., "Flow Direction Measurement by Hot-Wire Anemometry", Proc. A.S.C.E., J. Eng. Mech. Div., Vol. 92, No. EM4, August 1966, pp. 45-70.

15. Einstein, H.A., "The Bed-Load Function for Sediment Transport in Open Channel Flows", U.S. Department of Agriculture, Tech. Bull. 1026, 1950.

16. Fage, A., "On the Static Pressure in Fully Developed Turbulent Flow", Proc. Royal Soc. London, A, 155, 1936, pp. 576-596.

17. Flow Corporation, "X-Wire Turbulence Measurements", Bulletin 68, January 1962.

18. Gardner, S., "On Surface Pressure Fluctuations Produced by Boundary Layer Turbulence", Acustica, Vol. 16, 2, 1965-66, pp. 67-74.

19. Goldstein, S., "Modern Developments in Fluid Dynamics", Clarendon Press, 1938.

20. Hinze, J.O., "Turbulence", McGraw-Hill, 1959.

21. Hinze, J.O., "Turbulent Pipe Flow", Colloque Internatinal sur "La Mécanique de la Turbulence", Marseille, 1961, Centre National de la Recherche Scientifique, 1962, pp. 129-165.

22. Hurd, C.W., Chesky, K.P. and Shapiro, A.H., "Influence of Viscous Effects on Impact Tubes", J. Appl. Mech., Vol. 20, 2, June 1953, pp. 253-256.

23. Inoue, E., "On the Turbulent Structure of Airflow Within Crop Canopies", Journ. Meteor. Soc. of Japan, Vol. 41, 1963, pp. 317-326.

24. Kalinske, A.A., "Movement of Sediment as Bed Load in Rivers", Trans. A.G.U., Vol. 28, 1947, pp. 615-620.

25. Kistler, A.L., "The Structure of the Laminar Sublayer", Colloque International sur "La Mécanique de la Turbulence", Marseille, 1961, Centre National de la Recherche Scientifique, 1962, pp. 287-298.

26. Kovasznay, L.S.G., "Turbulence Measurements", High Speed Aerodynamics and Jet Propulsion, Vol. 9, Physical Measurements in Gas Dynamics and Combustion, Section F, Princeton University Press, 1954.

27. Laufer, J., "The Structure of Turbulence in Fully Developed Pipe Flow", N.A.C.A., Report 1174, 1954.

28. Lee, Y.W., "Statistical Theory of Communication", Wiley, 1960.

29. Leliavsky, S., "An Introduction to Fluvial Hydraulics", Constable, 1955.

30. Lettau, H.H., "A Generalized Mathematical Model of the Mean Velocity Distribution in Fully Turbulent Flow", University of Wisconsin, Department of Meteorology, Technical Report No. 3, February 1961.

31. Logan, E. and Jones, J.B., "Flow in a Pipe Following an Abrupt Increase in Surface Roughness", Trans. A.S.M.E., Journ. Basic Eng., Vol. 85, Series D, No. 1, March 1963, pp. 35-40.

32. MacMillan, F.A., "Experiments on Pitot-Tubes in Shear Flow", Great Britain Aero. Res. Council, Rep. and Mem. No. 3028, 1957.

33. Millikan, C., "A Critical Discussion of Turbulent Flows in Channels and Circular Tubes", Proc. 5th Int. Cong. Appl. Mech., Cambridge, Mass., 1938.

34. Moran, D.D., "Response of Turbulent Pipe Flow to Changes in Boundary Roughness", M.I.T. Department of Civil Eng., M.S. Thesis, 1967.

35. Morris, H.M., "Flow in Rough Conduits", Trans. A.S.C.E., Vol. 120, 1955.

36. Morris, H.M., "Design Methods for Flow in Rough Conduits", Proc. A.S.C.E., J. Hyd. Div., Vol. 85, HY7, July 1959, pp. 43-62.

37. Murray, J.D., "Viscous Damping of Gravity Waves Over a Permeable Bed", J. Geophys. Res., Vol. 70, No. 10, May 15, 1965, pp. 2325-2332.

38. Olson, R.M. and Eckert, E.R.G., "Experimental Studies of Turbulent Flow in a Porous Circular Tube with Uniform Fluid Injection Through the Tube Wall", Trans. A.S.M.E., J. Appl. Mech., Vol. 33, Series E, No. 1, March 1966, pp. 7-17.

39. Phillips, O.M., "The Irrotational Motion Outside a Free Turbulent Boundary", Proc. Cambridge Phil. Soc., Vol. 51, 1955, pp. 220-229.

40. Polubarinova-Kochina, P. Ya., "Theory of Ground Water Movement", Princeton University Press, 1962.

41. Polzin, J., "Zur Messung des Statischen Druckes an Rauhen Wänden", Ingenieur-Archiv, 10, 1939, pp. 326-338.

42. Raudkivi, A.J., "Loose Boundary Hydraulics", Pergamon Press, 1967.

43. Reichardt, H., "Vollständige Darstellung der Turbulenten Geschwindigkeitsverteilung in Glatten Leitungen", Z. Angew. Math. Mech., 31, No. 7, July 1951, pp. 208-219.

44. Robertson, J.M., Burkhart, T.H. and Martin, J.D., "A Study of Turbulent Flow in Rough Pipes", Univ. of Illinois, Theo. and Appl. Mech. Dept. Report No. 279, May 1965.

45. Robertson, J.M. and Martin, J.D., "Turbulence Structure Near Rough Surfaces", A.I.A.A. Journal, Vol. 4, No. 12, December 1966, pp. 2242-2245.

46. Rotta, J., "Das in Wandnähe Gültige Geschwindigkeitsgesetz Turbulenter Strömungen", Ingenieur-Archiv, 18, No. 4, 1950, pp. 277-280.

47. Rotta, J.C., "Turbulent Boundary Layers in Incompressible Flow", Progress in Aeronautical Sciences, Vol. 2, Pergamon Press, 1962.

48. Rumer, R.R. and Drinker, P.A., "Resistance to Laminar Flow Through Porous Media", Proc. A.S.C.E., J. Hyd. Div., Vol. 92, No. HY5, September 1966, pp. 155-164.

49. Sandborn, V.A., "Experimental Evaluation of Momentum Terms in Turbulent Pipe Flow", N.A.C.A. TN 3266, 1955.

50. Shaw, R. "The Influence of Hole Dimensions on Static Pressure Measurements", J. Fluid Mech., 7, Part 4, April 1960, pp. 550-564.

51. Sternberg, J., "A Theory for the Viscous Sublayer of a Turbulent Flow", J. Fluid Mech., 13, Part 2, June 1962, pp. 241-271.

52. Stewart, R.W., "Irrotational Motion Associated with Free Turbulent Flows", J. Fluid Mech., 1, Part 6, December 1956, pp. 593-606.

53. Townsend, A.A., "Equilibrium Layers and Wall Turbulence", J. Fluid Mech., 11, Part 1, 1961, pp. 97-120.

54. Uram, E.M., "Turbulent Boundary Layers on Rough Surfaces", Stevens Institute of Technology, Sc.D. Thesis, 1966.

55. Vanoni, V.A. and Brooks, N.H., "Laboratory Studies of the Roughness and Suspended Load of Alluvial Streams", California Institute of Tech., Sedimentation Lab., Report No. E-68, December 1957.

56. Ward, J.C., "Turbulent Flow in Porous Media", Proc. A.S.C.E., J. Hyd. Div., Vol. 90, No. HY5, September 1964, pp. 1-12.

57. Willmarth, W.W. and Wooldridge, C.E., "Measurements of the Fluctuating Pressure at the Wall Beneath a Thick Turbulent Boundary Layer", J. Fluid Mech., 14, Part 2, October 1962, pp. 187-210.

58. Yalin, S., "An Expression for Bed-Load Transportation", Proc. A.S.C.E. J. Hyd. Div., Vol. 89, No. HY3, May 1963.

APPENDIX I
LIST OF FIGURES AND TABLES

APPENDIX II

LIST OF SYMBOLS

Only the principal symbols are defined here. Symbols with limited usage within a section are defined where they first appear. An effort has been made to keep the customary notation in each field. Some repetition of symbols in inevitable, but possible ambiguities should be resolved by the context. Numbers in parenthesis refer to the equation in which the symbol first appears.

a	constant, ≈ 3 (2-30)
A	constant in law of the wall, (2-2)
A	constant in hot wire equation, (3-14)
A_o	same, for zero fluid velocity
$A(\eta)$	cross-spectral function of the wall pressure, (2-53)
B	constant in law of the wall, (2-2)
B	constant in hot wire equation, (3-14)
dB	random point function, (2-45)
c	fluctuation of the effective cooling velocity acting on hot wire
C	mean cooling velocity acting on hot wire
d	outer diameter of pitot tube or of hot wire
D	I.D. of pipe
e	turbulent energy dissipation in porous medium, (2-42)
e_L	same, integrated over one wave length, (2-41)
E	total dissipation in pipe flow, (2-43)
E	Fourier transform of the wall pressure correlation coefficient, (2-48)
E_o	Fourier transform of $A(\eta)$, (2-55)
E_u	energy spectrum for u, (4-10)
E_v	energy spectrum of v, (4-10)
f	frequency, cps
f	pipe friction factor
f'	normalized frequency, (2-58)
f_K	permeability friction factor (3-4)

h	thickness of porous layer
I	current in hot wire
$\bar{I}$	average current in hot wire
I_o	current in hot wire at zero velocity
i	fluctuation in hot wire current
i'	rms value of i
k	hot wire constant, (3-27)
k	wave number of pressure wave, $2\pi/L$
k_s	roughness height
K	permeability
K_1, K_2	constants of wires in x-array probe, (3-32)
L	length of sinusoidal wall pressure wave
ℓ	mixing length, (2-12)
ℓ_o	initial value of mixing length, (2-22)
m	exponent in a power velocity distribution, (2-56)
M	constant, function of m, (2-67)
M_1, M_2	ratio between velocity and current fluctuations in each wire of an x-array probe, (3-37)
n	porosity of the porous medium
n	exponent of the velocity in heat transfer equation for a hot wire, (3-14)
p	pressure
p'	rms value of the fluctuation p
P	amplitude of sinusoidal wall pressure wave, (2-29)
$\vec{q}$	specific discharge through the porous medium, (2-26)
q_x, q_y	components of q in directions x,y
q'_x, q'_y	rms values of the fluctuations q_x, q_y
q^2	total intensity of turbulence
Q	pipe discharge
Q_x	mean specific discharge through porous medium produced by pipe pressure gradient, (2-39)
r	radial distance

r ratio between linear and quadratic terms in modified Darcy's eq., (2-26)

R pipe radius

$R(\xi,\tau)$ correlation coefficient of the wall pressure, (2-47)

R hot wire resistance

R_B effective pipe radius, referred to origin of coordinate y_B

Re Reynolds number based on pipe diameter and average velocity

Re_K permeability Reynolds number, (3-4)

t time

T period of sinusoidal wall pressure wave

T_s integral time scale of wall pressure, (2-61)

T absolute temperature in degrees centigrades

u longitudinal component of velocity fluctuation

u' rms value of u

u_* shear velocity, $\sqrt{\tau_o/\rho}$

U local mean velocity

U_{max} maximum velocity

U_c convection velocity for the wall pressure

$\bar{U}$ average pipe velocity

ΔU displacement of mean velocity profile in rough pipes with respect to smooth pipes, (2-8)

v radial component of velocity fluctuation

v' rms value of v

w circumferential component of velocity fluctuations

w' rms value of w

x axial distance, measured from the beginning of regular roughness

y distance from wall

y_o displacement in origin of y

$y_B = y + y_o$, effective distance from wall (measured from the origin of the logarithmic velocity profile)

Y dimensionless depth in porous medium, (2-65)

α angle between hot wire and fluid velocity

β angle between wires of x-array probe

Γ partial Fourier transform of $R(\xi,\tau)$, (2-51)

ε eddy viscosity, (2-13)

κ Kármán constant

μ dynamic viscosity

ν kinematic viscosity

ξ dimensionless radial distance, r/R

ρ_a air density

ρ_w water density

σ dimensionless frequency, (2-70)

τ shear stress at distance y from wall

τ_o wall shear stress (at y = 0)

Φ time spectrum of wall pressure, (2-52)

Φ' normalized time spectrum of wall pressure, (2-58)

ϕ_u normalized spectrum of longitudinal velocity fluctuation, (4-11)

ϕ_v normalized spectrum of radial velocity fluctuation, (4-11)

ψ time spectrum of velocity in porous medium, (2-71)

ψ' normalized spectrum of velocity in porous medium, (2-71)

ω angular frequency

Ω dimensionless frequency, (2-66)

$( )^*$ complex conjugate